PROCEEDINGS

of the

Sixteenth
International Tissue Elasticity Conference™

Avignon, France
September 9 – 12, 2018

PROCEEDINGS

of the
Sixteenth International Tissue Elasticity Conference™

Avignon, France
September 9-12, 2018

Table of Contents

QUESTIONS OR COMMENTS ARE WELCOME AT ANY TIME AT <secretariat@elasticityconference.org>
Copyright © 2018 International Tissue Elasticity Conference™ All Rights Reserved
Some abstracts may have been edited by the reviewers for clarity of presentation.

Original Cover Photo by Professor JC Bamber

FOREWORD

Dear Conference Delegate:

Welcome to the Sixteenth International Tissue Elasticity Conference™ (ITEC™), and welcome to Avignon. I strongly encourage you to take the time to explore Avignon's beautiful streets, wonderful architecture, famous 12th century bridge and extraordinary palace started in 1252 as the popes' residence for the Avignon Papacy period, as well as other nearby historical buildings such as the astonishing Pont du Gard Roman aqueduct, and the surrounding spectacular Provence countryside.

When Jonathan Ophir and Kevin Parker conceived this conference series they expressed the purpose as "to advance the field of measurement and imaging of the elastic attributes of soft tissues through tutorials and scientific presentations of the state of the art in the field, within a unique and unified forum that would bring together researchers from several countries and ultimately contribute to the rapid development and clinical introduction of this new medical imaging technology". Seventeen years on, there is now wide medical acceptance of the first generation of clinical elastography systems and a long history of scientific discovery and technical innovation. We therefore feel it appropriate that the teaching role of ITEC should increase. Accordingly our program this year contains more tutorials than usual, given by internationally famous experts, making ITEC 2018 an exceptional opportunity for students and others new to the subject to learn about it. I am grateful to all of the tutorial speakers for agreeing to pass on their knowledge and experience in this way. Of course we continue to have the usual array of cutting-edge research presentations which cover all modalities and all aspects of tissue elasticity measurement and imaging, with plenty of time scheduled for the friendly discussions and networking, for which ITEC is known.

We were deeply saddened by the passing of two dear colleagues since the last ITEC. Professor Jonathan Ophir (https://www.aium.org/aboutUs/awards/2018/memorialfame2.pdf), pictured here, died on the 19th of October 2017. He had introduced the concept of ultrasound strain imaging, many other innovations and discoveries, and even the term, elastography. He was an ITEC founder and ITEC's chief organizer for 11 years. Without Jonathan's influence, the field of tissue elasticity imaging would not exist as we know it. Karen Ophir, his wife, also a driving force behind ITEC, has kindly sent her good wishes for the conference. We wish her and the entire Ophir family well, and we hope to involve Karen in the conference at some point, via Skype.

Professor David Cosgrove (https://www.bmus.org/professor-david-cosgrove/), a stalwart supporter of ITEC, died on 16th of May 2017. David took a great interest in the physics and technology of elastography whilst also conducting careful and detailed studies that explored clinical applications.

Many volunteers and colleagues have helped to bring about this conference, especially our conference secretary, Cheryl Taylor. Please join me in thanking Cheryl for, once again, working tirelessly to make the conference a success. It is a pleasure also to acknowledge contributions from administrators at the Institute of Cancer Research, especially Liam Blake and Alan Hill for assistance in financial and legal matters, and Neil Walford's team for audio-visual equipment. Finally, we are extremely grateful to all those who have participated as helpers, reviewers, session chairs, award judges and contributors, without whom the conference could not happen.

ITEC must continue to evolve if it is to persist in serving the needs of researchers and practitioners in the field of elastometry and elastography. We should be extremely grateful if you would complete the feedback forms in these Proceedings. Alternatively, please speak directly to me or Cheryl to discuss your suggestions.

May your research be inspired by the presentations and discussions during the Sixteenth ITEC, and may you make new friends, establish productive collaborations and renew old acquaintances.

Jeffrey Bamber
General Conference Organizer
Avignon, France, September 9-12, 2018

CONFERENCE-AT-A-GLANCE

Sixteenth International Tissue Elasticity Conference™

Avignon, France September 9-12, 2018

Sunday, September 9 **9:00A - 8:00P**

9.00A-12.00P		Oral Presenters load presentations (USB)	Andromède 1
		Poster Presenters set up presentations	Andromède 2
9:00A - 5:00P		Registration Desk Open	Lobby
2:00P -5:30P	**Session EEX**:	Equipment Exhibit (*during breaks & Reception*)	Andromède 2
12:00P- 2:00P	**Session TUT-1:**	**Tutorials**	Andromède 1
2:00P – 2:30P		*Coffee Break*	Lobby
2:30P – 4:30P	**Session SAS:**	**Oral Presentations of Finalists for Student Awards Session**	Andromède 1
4:30P – 5:00P		*Recess*	
5:00P – 5:30P	**Session POS:**	**Poster Session - Live Oral Summaries**	Andromède 2
6:30P – 8:00P		Opening Dinner Reception	Le Patio Restaurant

Monday, September 10 **8:30A - 10:00P**

8:30A - 4:30P		Registration Desk Open	Lobby
8:30A – 4:30P	**Session POS:**	Posters	Andromède 2
8:30A – 4:30P	**Session EEX:**	Equipment Exhibit	Andromède 2
8:45A - 9:00A		Opening Remarks	Andromède 1
9:00A - 10:15A	**Session MIP:**	**Method for Imaging Elastic Tissue Properties – I**	Andromède 1
10:15A - 11:00A		*Coffee Break*	Lobby
11:00A - 12:30P	**Session TUT-2:**	**Tutorials – II**	Andromède 1
12:45P - 2:15P		*Group Lunch*	Le Patio Restaurant
2:15P - 3:00P	**Session MMT:**	**Mechanical Measurements Techniques for Tissues**	Andromède 1
3:00P - 3:30P		*Coffee Break*	Lobby
3:30P – 4:15P	**Session INS:**	**Instrumentation including Phantoms**	Andromède 1
7:00P - 10:00P		*Conference Dinner*	Le Carré du Palais

Tuesday, September 11 **8:45A – 5:30P**

8:45A - 5:30P		Registration Desk Open	Lobby
8:45A - 5:30P	**Session POS:**	Posters	Andromède 1
8:45A - 5:30P	**Session EEX:**	Equipment Exhibit	Andromède 1
9:00A - 10:00A	**Session MIP-2:**	**Method for Imaging Elastic Tissue Properties – II**	Andromède 1
10:00A - 10:30A		*Coffee Break*	Lobby
10:30A - 10:54A	**Session OTH:**	**Other Applications of Elasticity Imaging**	Andromède 1
10:54A - 11:39A	**Session MIP-3:**	**Method for Imaging Elastic Tissue Properties – III**	Andromède 1
11.40A – 12.00P		*Discussion*	Andromède 1
12:00P - 2:00P		*Group Lunch*	Le Patio Restaurant
2:00P - 3:30P	**Session TUT-3:**	**Tutorials – III**	Andromède 1
3:30P - 4:00P		*Coffee Break*	Lobby
4:00P - 5:00P	**Session CVE:**	**Cardiovascular Elasticity**	Andromède 1
5:00P – 5:15P		*Group Photo*	TBA
5.15P		*No Conference Activities*	

Wednesday, September 12 **9:15A -7:00P**

8:30A - 4:00P	**Session POS:**	Posters	Andromède 1
8:30A - 3:30P	**Session EEX:**	Equipment Exhibit	Andromède 1
9:00A - 10:30A	**Session TUT-4:**	**Tutorials – IV**	Andromède 1
10:30A - 11:00A		*Coffee Break*	Lobby
11:00A – 11:15A	**Session FIP-:**	**Forward & Inverse Problems**	Andromède 1
11:15A – 11:30A	**Session SIP-:**	**Signal & Image Processing**	Andromède 1
11:30A - 12:15P	**Session TUT-5:**	**Tutorials – V**	Andromède 1
12:15A - 2:00P		*Group Lunch*	Le Patio Restaurant
2:00P – 3:30P	**Session CAA:**	**Clinical and Animal Applications**	Andromède 1
3:30P – 4:00P		*Coffee Break*	Lobby
4:00P – 4:30P	**Session MPT:**	**Mechanical Properties of Tissues**	Andromède 1
5:50P – 7:30P		*Closing TAPAS reception*	Le Patio Restaurant

PROGRAM

Sixteenth International Tissue Elasticity Conference™

Avignon, France

September 9-12, 2018

Sunday, September 9 9:00A - 8:00P

9:00A – 12:00P Presentation Set Up

All Oral Presenters load presentations onto Conference computers — Andromède 1
Poster Presenters set up presentation — Andromède 1
Exhibitors set up exhibits — Andromède 2

9:00A – 5:00P Registration Desk Open — Lobby

2:00P – 5:00P Session EEX: Equipment Exhibit — Andromède 2

Sunday 12:00P – 2:00P
Session TUT: Tutorials:

Chair: JC Bamber, UK *Co–Chair: S Catheline, France* — Andromède 1

12:00P – 12:45P

SHEAR WAVE ELASTOGRAPHY: AN HISTORICAL PERSPECTIVE.
M Fink[1].*
[1]Institute Langevin, ESPCI, Paris, FRANCE.

12:45P – 1:00P Discussion

1:00P – 1:45P

BREAST ELASTOGRAPHY: CLINICAL EXPERIENCE AND REQUIREMENTS.
D Amy[1].*
[1]Aix en Provence Radiologue, Aix en Provence, FRANCE.

1:45P – 2:00P Discussion

2:00P – 2:30P COFFEE BREAK — Lobby

Sunday 2:30P – 4:30P
Session SAS: Oral Presentations of Finalists for Student Awards Session

Chair: O Goksel, Switzerland *Co–Chair: BF Kennedy, Australia* — Andromède 1

Page No.

2:30P – 2:45P

007 ANISOTROPIC COMPOSITE MATERIAL PHANTOM FOR MAGNETIC RESONANCE LASTOGRAPHY. 21
M Guidetti[1], G Lorgna[2], D Klatt[1], P Vena[2], TJ Royston[1].*
[1]University of Illinois at Chicago, Chicago, Illinois, USA.2 Politecnico di Milano, ITALY.

(Session SAS continued on next page)

(Session SAS continued from previous page)

2:45P – 3:00P

016 REVERBERANT 3D OPTICAL COHERENCE ELASTOGRAPHY (REV3D-OCE): A NOVEL METHOD FOR THE 3D ELASTIC MAPPING OF LAYERS IN CORNEA. 22

F Zvietcovich[1], JP. Rolland[2], P Meemon[3], KJ Parker[1].*
[1]Department of Electrical and Computer Engineering, [2]The Institute of Optics, University of Rochester, Rochester, New York, USA. School of Physics, Suranaree University of Technology, Nakhon Ratchasima, THAILAND.

3:00P – 3:15P

021 MULTIPLE WAVE MODES INDUCED BY AORTIC VALVE CLOSURE IN THE INTERVENTRICULAR SEPTUM; AN *IN-VIVO* AND IN-SILICO STUDY. 23

LBH Keijzer[1], M Strachinaru[1], JG Bosch[1], BM van Dalen[1,3], I. Heinonen[4], MD Verweij[2,1], AFW van der Steen[1,2], N de Jong[2,1], HJ Vos[1,2]*
[1]Erasmus MC, Rotterdam, Zuid-Holland, THE NETHERLANDS; [2]Delft University of Technology, Delft, Zuid-Holland, THE NETHERLANDS; [3]Franciscus Gasthuis & Vlietland, Rotterdam, Zuid-Holland, THE NETHERLANDS; [4]University of Turku and Turku University Hospital, Turku, FINLAND.

3:15P – 3:30P

025 NONINVASIVE ESTIMATION OF MATERIAL PARAMETERS FOR *IN VIVO* SKELETAL MUSCLE USING ULTRASOUND. 24

J Dong[1], H Li[1], Y Zhang[1], WN Lee[1].*
[1]The University of Hong Kong, Pokfulam Road, Hong Kong, CHINA.

3:30P – 3:45

030 4-D PULSE WAVE IMAGING IN THE HUMAN ABDOMINAL AORTA *IN-VIVO*. 25

GM Karageorgos[1] J Grondin[1], IZ Apostolakis[1], EE Konofagou[1].*
[1]Columbia University, New York, NY, USA.

3:45P – 4:00

032 AN ULTRASOUND PROBE INDENTER FOR THE NON-LINEAR MECHANICAL CHARACTERIZATION OF SOFT TISSUES. 37

A Arulrajah[1,2], B Wach[2], L Barbé[1], D George[1], J Vappou[1], S Chatelin[1].*
1ICube, University of Strasbourg, CNRS UMR7357, 1 place de l'hôpital, Strasbourg FRANCE; 2IHU Strasbourg, Institute of Image-Guided Surgery, 1 place de l'hôpital, Strasbourg, FRANCE.

4:00P– 4:15P

037 SHEAR WAVE SPEED AND ATTENUATION ESTIMATION IN OIL-IN-GELATIN PHANTOMS USING A RHEOLOGICAL MODEL, MECHANICAL, AND ULTRASOUND MEASUREMENTS. 26

J Ormachea[1], KJ Parker[1], MG Drage[1], H Kim[1], Z Hah[2].*
[1]University of Rochester, Rochester, NY, USA; [2]Samsung Medison Co. Ltd., SungNam, SOUTH KOREA.

4:15P – 4:30P

041 MULTIDIMENSIONAL MOTION ESTIMATION WITH STOCHASTIC INTERPOLATION VIA DISJUNCTIVE KRIGING. 27

B Rebholz[1], M Almekkawy[1].*
[1]Pennsyvania State University, University Park, Pennsylvania, USA.

4:30P – 5:00P

Recess

Sunday 5:00P – 5:15P
Session POS: Poster Session – Live Oral Summaries

Chair: S Catheline, France *Co–Chair: NL Bush, UK* Andromède 2

Page No.

5:00P – 5:02P

017 GAUSSIAN SHEAR WAVE PROPAGATION IN VISCOELASTIC MEDIA: VALIDATION OF AN APPROXIMATE FORWARD MODEL. 28

F Zvietcovich[1], N Baddour[2], JP. Rolland[1], KJ Parker[1].*

[1]University of Rochester, Rochester, NY, USA; [2]University of Ottawa, Ontario, CANADA.

5:03P – 5:05P

040 AN EXPERIMENTAL AND COMPUTATIONAL INVESTIGATION OF THE RELATIONSHIP BETWEEN WAVE SHAPES AND SPACING BETWEEN INHOMOGENEITIES IN VISCOELASTIC TISSUE-LIKE PHANTOMS. 29

*H Palnitkar[1], P Lewis[2], M Hammersley[2], R Shah[2], T Royston[1], D Klatt[1].M.Guidetti[1]**

[1]University of Illinois at Chicago, Chicago, Illinois, USA; [2]Northwestern University, Chicago, Illinois, USA.

Sunday 5:30P – 8:00P
Opening Dinner Reception

Le Patio Restaurant, Novotel

Monday, September 10 9:00A - 10:00P

8:30A - 4:30P
Registration Desk Open — Lobby
8:45A - 4:30P **Session EEX:** **Equipment Exhibit** — Andromède 2
8:45A - 4:30P **Session POS:** **Posters** — Andromède 1

Monday 8:45A - 9:00A
OPENING REMARKS
JC Bamber and S Catheline — Andromède 1

Monday 9:00A – 10:15A
Session MIP: Methods for Imaging Elastic Tissue Properties – I
Chair: J Vappou, France *Co–Chair: S Aglyamov, USA* — Andromède 1

Page No.

9:00A - 9:15A
042 NATURAL SHEAR WAVES GENERATATION BY PSALMODY FOR THYROID ELASTOGRAPHY — 30
S. Beuve[1], E. Khoury[1], E.G. Simon[1], S. Callé[2], J.P. Remenieras[1].*
[1]UMR 1253, iBrain, University of Tours, Inserm, Tours, FRANCE; [2]GREMAN UMR 7347, University of Tours, CNRS, INSA, Tours, FRANCE.

9:15A - 9:30A
013 DEVELOPMENT OF NON-INVASIVE *IN VIVO* CEREBRAL ULTRASOUNDELASTOGRAPHY USING TIME-HARMONIC VIBRATION. — 31
B Kreft[1], F Schrank[1], J Bergs[1], J Braun[2], I Sack[1], H Tzschätzsch[1].*
[1]Departement of Radiology, Charité—Universitätsmedizin, Berlin, Berlin, GERMANY, [2]Institute of Medical Informatics, Charité—Universitätsmedizin, Berlin, Berlin, GERMANY.

9:30A - 9:45A
045 SURFACE WAVES OPTICAL TOMOGRAPHY: PHANTOM STUDY. — 33
A Zorgani[1] , M Lescanne[1] , A Bel-Brunon[2] , TA Ghafour[2] , S Catheline[1].*
[1]LabTAU, U1032 INSERM, Lyon, FRANCE; [2]LaMCos, INSA-Lyon, Villeurbanne, FRANCE.

9:45A - 10:00A
039 NON-CONTACT DYNAMIC OPTICAL COHERENCE ELASTOGRAPHY FOR VARIOUS BIOMEDICAL APPLICATIONS. — 34
SR Aglyamov[1], KV Larin[1,2]*
[1]University of Houston, Houston, TX, USA; [2]Baylor College of Medicine, Houston, USA.

10:00A - 10:15A
009 HIGH-SPEED PHASE-RESOLVED INTRAVASCULAR OPTICAL COHERENCE ELASTOGRAPHY. — 35
T Wang[1]*, T Pfeiffer[2], A Akyildiz[1], W Wieser[3], H van Beusekom[1], G Springeling[1], F Mastik[1], AFW van der Steen[1,4,5], R Huber[2] and G van Soest[1].
[1]Erasmus University Medical Center, Rotterdam, THE NETHERLANDS; [2]Universität zu Lübeck, Lübeck, GERMANY; [3]Optores GmbH, München, GERMANY; [4]Shenzhen Institutes of Advanced Technology Chinese Academy of Sciences, Shenzhen, CHINA; [5]Delft University of Technology, Delft, THE NETHERLANDS.

10:15A - 11:00A
COFFEE BREAK — Lobby

Monday 11:00A - 12:30P
Session TUT-2: TUTORIALS - II

Chair: L Pflugrath, USA *Co–Chair: O Goksel, Switzerland* Andromède 1

Page No.

11:00A - 11:30A

OPTICAL COHERENCE ELASTOGRAPHY: IMAGING THE MICRO-SCALE MECHANICAL PROPERTIES OF TISSUE.

*BF Kennedy[1]**

[1]University of Western Australia, Perth, AUSTRALIA.

11:30A - 11:45A **Discussion**

11:45A - 12:15P

MAGNETIC RESONANCE ELASTOGRAPHY: METHODS AND APPLICATIONS.

S Chatelin[1], J Vappou*[1]*

[1]ICube, University of Strasbourg, Strasbourg, FRANCE.

12:15P - 12:30P **Discussion**

12:45P – 2:15P

GROUP LUNCH Le Patio Restaurant

Monday 2:15P – 3:00P
Session MMT: Mechanical Measurements Techniques for Tissues

Chair: S Chatelin, France *Co–Chair: HJ Vos, the Netherlands,* Andromède 1

2:15P - 2:30P

029 HARMONIC MOTION ELASTOGRAPHY FOR THE DIFFERENTIATION BETWEEN PANCREATIC DUCTAL ADENOCARCINOMA FROM NORMAL PANCREAS IN POST-SURGICAL HUMAN SPECIMENS. 32

A Nabavizadeh[1], T Payen[1], A C Iuga[1], KP Olive[1], EE Konofagou[1].*

[1]Columbia University, New York, NY, USA.

2:30P - 2:45P

002 CELLQUAKE ELASTOGRAPHY: ULTRAFAST IMAGING OF CELL ELASTICITY. 36

P Grasland-Mongrain[1,4], A Zorgani[2], S Nakagawa[3], S Bernard[4], L Gomes Paim[3], G Fitzharris[3,5], S Catheline[2], G Cloutier[4,6,7].*

[1]Laboratoire de Physique, Ecole Normale Supérieure de Lyon, Lyon, FRANCE. [2]LabTAU, INSERM u1032, University of Lyon, Lyon, FRANCE; [3]Oocyte and Embryo Research Lab, University of Montreal Hospital Research Center, Montreal, QC, CANADA; [4]LBUM, University of Montreal Hospital Research Center, Montreal, QC, Canada; [5]Department of Obstetrics and Gynecology, University of Montreal, Montreal, QC, CANADA; [6]Department of Radiology, Radio-Oncology and Nuclear Medicine, University of Montreal, Montreal, QC, CANADA; [7]Institute of Biomedical Engineering, University of Montreal, Montreal, QC, CANADA.

2:45P - 3:00P

022 PASSIVE ELASTOGRAPHY FOR HIFU MONITORING: IN VITRO EXPERIMENTS. 38

Bruno Giammarinaro[1], Paul Greillier[1], Stefan Catheline[1], Cyril Lafon[1].*

[1]LabTAU, INSERM, Centre Léon Bérard, Université Lyon 1, Univ Lyon, , Lyon, FRANCE.

3:00P – 3:30P

COFFEE BREAK Lobby

Monday 3:30P – 4:15P
Session INS: Instrumentation including Phantoms

Chair: J Vappou, France *Co-Chair: S Aglyamov, USA* Andromède 1

3:30P – 3:45P

012 GENERATION OF SHEAR WAVES IN SOFT MEDIA BY AN ELECTROMAGNETIC ACTUATOR. 39

Z Sun[1,2,3,4], B Giammarinaro[1,2], A Birer[1,2], S Catheline[1,2].*

[1]LabTAU INSERM U1032, Lyon, France; [2]Universtité de Lyon, Lyon, France; [3]Institute of Electrical Engineering, Chinese Academy of Sciences, Beijing, CHINA; [4]University of Chinese Academy of Sciences, Beijing, CHINA.

3:45P – 4:00P

043 DEVELOPMENT OF A COMPACT HAND-HELD DEVICE FOR USE IN QUASI-STATIC ELASTOGRAPHY: A PRELIMINARY STUDY ON TISSUE-MIMICKING PHANTOM. 40

A Verma[1], AK Thittai[1].*

[1]Indian Institute of Technology Madras, Chennai, INDIA.

4:00P – 4:15P

046 TIME REVERSAL MIRROR OF SHEAR WAVE SOURCES FROM FIELD CONTROL TO SHEAR-WAVE ELASTOGRAPHY. 41

C Zemzemi[1,2], J Aichele[1,2], S Catheline[1,2].*

[1]LabTAU INSERM U1032, Lyon, FRANCE; [2]Universtité de Lyon, FRANCE.

Monday 7:00P – 10:00P
Conference Dinner,

Le Carré du Palais
1 Place du Palais, 84000 Avignon

Restaurant directions, walking from Novotel Avignon Centre:

1. Turn right from the main exit of the Novotel.
2. Walk to the Grand Hotel and cross the main road to enter the gate through the city wall.
3. Turn right once inside the city, and walk to Cours Jean Jaurés (the next main street).
4. Turn left into Cours Jean Jaurés and walk to all the way, through the town square, past the old theatre and merry-go-round, until you reach Rue Moliére and Place de l'Horloge.

Le Carré du Palais is inside the old Banque de France building in Rue Moliére and Place de l'Horloge, just to your right, as you face the way you have been walking.

An alternative entrance to the restaurant is from the square in front of the Palais des Papes.

Tuesday, September 11 9:00A – 5:15P

9:00A – 5:30P
Registration Desk Open — Lobby

9:00A – 5:30P **Session EEX: Equipment Exhibit**
Andromède 2

Tuesday 9:00A – 10:00A
Session MIP–2: Methods for Imaging Elastic Tissue Properties – II
Chair: HJ Vos,, The Netherlands *Co-Chair: EG Simon, France* Andromède 1

Page No.

9:00A – 9:15A
054 ULTRASOUND BREAST TOMOGRAPHY: AN UPDATE. 42
JC Bamber[1], J Fromageau[1], A Messa[1], S Bernard[1], A D'Aquino[1], A Ledger[1], M Schmidt[1], MJ Schoemaker[1], AJ Swerdlow[1], EAM O'Flynn[1], N Duric[2].*
[1]Institute of Cancer Research and Royal Marsden NHS Foundation Trust, London, UK; [2]Delphinus Medical Technologies and Karmanos Cancer Institute, Detroit, USA

9:15A – 9:30A
008 BREAST CHARACTERIZATION BY VELOCITY AND PROPAGATION COMPLEXITY OF SHEAR WAVE USING REAL-TIME PROPAGATION MAPPING. 43
Y Yamakoshi[1], K Taniuchi[1].*
1Gunma University, Kiryu, Gunma, JAPAN.

9:30A – 9:45A
006 ANALYSIS OF TRANSIENT SHEAR WAVE IN LOSSY MEDIA. 44
Z Hah[1], KJ Parker[2], J Ormachea[2], D Na[1].*
[1]Samsung Medison Company, Ltd., SungNam, SOUTH KOREA; [2]University of Rochester, Department of Electrical and Computer Engineering, Rochester, NY, USA.

9:45A – 10:00A
038 2D LINEAR DISPERSION SLOPE IMAGES USING A REVERBERANT SHEAR WAVE ELASTOGRAPHY FIELD: APPLICATION IN CIRS PHANTOMS AND IN VIVO LIVER TISSUE. 45
J Ormachea[1], B Castaneda[2], KJ Parker[1].*
[1]University of Rochester, Rochester, NY, USA; 2Pontificia Universidad Catolica del Peru, PERU.

10:00A – 10:30A
COFFEE BREAK — Lobby

Tuesday 10:30A – 10:54A
Session OTH: Other Application of Elasticity Imaging
Chair: HHG Hansen, The Netherlands *Co-Chair: S Chatelin, France* Andromède 1

Page No.

10:30A – 10:45A
044 IMAGING LABORATORY EARTHQUAKES WITH ULTRASOUND ELASTOGRAPHY. 46
J Aichele[1], S Catheline[1], P Roux[2.]*
[1]INSERM, Lyon, Rhone-ALpes, FRANCE; [2]Universite Grenoble Alpes, Grenoble, Rhone-alpes, FRANCE..

10:45A – 10:54A
049 PASSIVE ELASTOGRAPHY OF THE ESOPHAGUS: AN IN VITRO APPROACH. 47
V Delattre[1,2], A Zorgani[1], S Roman[1,2], S Catheline[1].*
[1]INSERM unit U1032, Lyon, FRANCE; [2]Hospices civils de Lyon, Lyon, FRANCE.

Tuesday 10:54A – 11:39A
Session MIP-3: Methods for Imaging Elastic Tissue Properties - III

Chair: HHG Hansen, The Netherlands *Co-Chair. S Chatelin, France* Andromède 1

10:54A – 11:09A

014 INFLUENCE OF PHYSIOLOGICAL ALTERATIONS TO BRAIN STIFFNESS MEASURED BY CEREBRAL TIME-HARMONIC ULTRASOUND ELASTOGRAPHY. 48
B Kreft[1], H Tzschätzsch[1], F Schrank[1], J Bergs[1], J Braun[2], I Sack[1]*
[1]Departement of Radiology, Charité-Universitätsmedizin, Berlin, Berlin, GERMANY,
[2]Institute of Medical Informatics, Charité-Universitätsmedizin, Berlin, Berlin, GERMANY.

11:09A – 11:24A

031 3D AXIAL STRAIN IMAGING FOR IMPROVED BREAST CANCER DETECTION IN VOLUMETRIC BREAST ULTRASOUND SCANNERS PRELIMINARY *IN VIVO* VALIDATION. 49
GA Hendriks[1], C Chen[1], HH Hansen[1], CL De Korte[1,2].*
[1]Radboud university medical center, Nijmegen, THE NETHERLANDS; [2]University of Twente Enschede, THE NETHERLANDS.

11:24A – 11:39P

048 3D ULTRASOUND STRAIN IMAGING OF THE PUBORECTALIS MUSCLE. 50
S Das1, HH. G. Hansen[1], F van den Noort[2], CL de Korte[1,3].*
[1]Medical UltraSound Imaging Centre (MUSIC), Department of Radiology and Nuclear Medicine, Radboud university medical centre, Nijmegen, THE NETHERLANDS; [2]Robotics and Mechatronics (RAM), University of Twente, Enschede, THE NETHERLANDS; [3]Physics of Fluids, Faculty of Science and Technology, University of Twente, Enschede, THE NETHERLANDS

11:40A – 12.00P **Discussion**

12:15P – 2:00P
GROUP LUNCH Le Patio Restaurant

Tuesday 2:00P – 3:30P
Session TUT–3: TUTORIALS - III

Chair: CL de Korte, The Netherlands *Co-Chair: S Aglyamov, USA* Andromède 1

Page No.

2:00P – 2:30P
ELASTOGRAPHY, MECHANOTRANSDUCTION AND NEW APPLICATIONS OF ULTRAFAST IMAGING.
*M Tanter[1]**
[1]Institut Langevin, ESPCI, Paris, FRANCE.

2:30P – 2:45P **Discussion**

2:45P – 3:15P
SHEAR WAVE ELASTOGRAPHY: THE INDUSTRIAL PERSPECTIVE.
*J Bercoff[1]**
[1]Supersonic Imagine, Aix-en-Provence, FRANCE.

3:15P – 3:30P **Discussion**

3:30P – 4:00P
COFFEE BREAK Lobby

Tuesday 4:00 – 5:00P
Session CVE: Cardiovascular Elasticity

Chair: M Tanter, France *Co-Chair: O Goksel, Switzerland* Andromède 1

Page No.

4:00P – 4:15P

019 ELASTIC WAVES AFTER AORTIC VALVE CLOSURE IN HYPERTROPHIC CARDIOMYOPATHY PATIENTS AND HEALTHY VOLUNTEERS. 51

M Strachinaru[1], M Michels[1], AE van den Bosch[1], JG Bosch[1], MD Verweij[2,1], AFW van der Steen[1,2,] N de Jong[1,2], ML Geleijnse1, HJ Vos[1,2].*

[1]Erasmus MC, Rotterdam, Zuid-Holland, THE NETHERLANDS; [2] Delft University of Technology, Delft, Zuid-Holland, THE NETHERLANDS.

4:15P – 4:30P

023 PHYSICS OF WAVE PROPAGATION UNDERLYING SKIN TISSUE MOTION GENERATED BY THE PRESSURE PULSE IN THE CAROTID ARTERY. 52

D Tommasin[1], A Caenen[1], B Verhegghe [1], P Segers[1].*

[1]Ghent University, Ghent, BELGUIM.

4:30P – 4:45P

020 VISUALIZING THE 2D MOTION INDUCED BY AN ACOUSTIC RADIATION FORCE PUSH IN TRANSVERSE VESSEL PHANTOM CROSS-SECTIONS USING DISPLACEMENT COMPOUNDING ON A HIGH FREQUENCY CMUT ULTRASOUND PROBE. 53

HHG Hansen, S Fekkes[1], GAGM Hendriks[1], CL de Korte[1,2].*

[1]Radboud university medical center, Nijmegen, THE NETHERLANDS; [2]University of Twente, Enschede, THE NETHERLANDS.

4:45P – 5:00P

047 A COMPARISON STUDY OF MAPPING STIFFNESS DISTRIBUTION OF PARTIALLY STIFFENED PORCINE AORTA: VASCULAR GUIDED WAVE IMAGING VERSUS PULSE WAVE IMAGING. 54

D Ran[1], YH Wang[1], WN Lee[1].*

[1]The University of Hong Kong, Hong Kong, CHINA.

5.00P – 5.15P ***Group Photograph***

After 5:15P *No Conference Activities*

Wednesday, September 12 8:30A - 7:00P

8:30A – 3:30P
Registration Desk Open — Lobby

8:00A – 3:30P **Session EEX: Equipment Exhibit** — Andromède 2

Wednesday 9:00A – 10:30A
Session TUT–4: TUTORIALS – IV

Chair: EG Simon. France *Co-Chair: BF Kennedy, Australia* — Andromède 1

Page No.

9:00A – 9:30A

VIBRATION-CONTROLLED TRANSIENT ELASTOGRAPHY: APPLICATION TO CHRONIC LIVER DISEASES.
*L Sandrin[1]**
[1]Echosens, Paris, Ile-de-France, FRANCE.

9:30A – 9:45A **Discussion**

9:45A – 10:15A

FULL-FIELD OPTICAL COHERENCE ELASTOGRAPHY.
*C Boccara[1]**
[1]Institut Langevin, ESPCI, Paris, FRANCE.

10:15A – 10:30A **Discussion**

10:30A – 11:00A
COFFEE BREAK — Lobby

Wednesday 11:00A – 11:15P
Session FIP: Forward & Inverse Problems

Chair: C Sumi, Japan *Co-Chair: S Catheline, France* — Andromède

Page No.

11:00A – 11:15A

033 ULTRASOUND AND MAGNETIC-RESONANCE HARMONIC ELASTOGRAPHY WITH HYBRID INVERSE-PROBLEM FORMULATION OF FEM VISCOELASTICITY RECONSTRUCTION. 55
CF Otesteanu[1], VV Vishnevskiy[1,2], C Guenthner[2], S Kozerke[2], O Goksel[1.]*
[1]Computer-assisted Applications in Medicine (CAiM), ETH Zurich, SWITZERLAND;
[2]Instituite for Biomedical Engineering (IBT), ETH Zurich, SWITZERLAND.

Wednesday 11:15A – 11:30A
Session SIP: Signal and Image Processing

Chair: S Catheline, France *Co-Chair: GA Hendriks, The Netherlands* — Andromède 1

Page No.

11:15A – 11:30A

015 NEW PHASE MATCHING METHOD THAT DIRETLY WORKS ON PHASE. 56
[1]C, Sumi.
[1]Sophie University, Chiyoda-ku, Tokyo, JAPAN.

Wednesday 11:30A – 12:15P
Session TUT-5: Tutorial - V

Chair: C Boccara, France *Co-Chair: L Sandrin, France* Andromède 1

Page No.

11:30A – 12:00A

POROELASTOGRAPHY.

*JC Bamber[1]**

[1]Institute of Cancer Research and Royal Marsden NHS Foundation Trust, London, UK.

12:00A – 12:15P **Discussion**

12:15P – 2:00P

GROUP LUNCH Le Patio Restaurant

Wednesday 2:00P – 3:30P
Session CAA: Clinical and Animal Applications

Chair: CL de Korte, The Netherlands *Co-Chair: NL Bush, UK* Andromède 1

Page No.

2:00P – 2:15P

018 A HANDHELD OPTICAL COHERENCE ELASTOGRAPHY PROBE FOR IMAGING BREAST CANCER. 57

Brendan F Kennedy[1,2], James Anstie[1,2], Qi Fang[1,2], Lixin Chin[1,2], Brooke Krajancich[1,2], Luke Frewer[1,2], Philip Wijesinghe[1,2], Renate Zilkens[1,3], Synn Lynn Chin[4], Ben Dessauvagie[5,6], Bruce Latham[5], Christobel Saunders[7,8].*

[1]BRITElab, Harry Perkins Institute of Medical Research, The University of Western Australia, Perth, AUSTRALIA; [2]Department of Electrical, Electronic & Computer Engineering, The University of Western Australia, Perth, AUSTRALIA; [3]School of Surgery, The University of Western Australia, Perth, AUSTRALIA; [4]Breast Centre, Sir Charles Gairdner Hospital, Perth, AUSTRALIA; [5]PathWest, Fiona Stanley Hospital, Murdoch, Western Australia, AUSTRALIA; [6]School of Pathology and Laboratory Medicine, The University of Western Australia, Perth, AUSTRALIA; [7]Breast Centre, Fiona Stanley Hospital, Murdoch, Western Australia, AUSTRALIA; [8]Breast Clinic, Royal Perth Hospital, Perth, AUSTRALIA.

2:15P – 2:30P

026 MONITORING ATRIAL FLUTTER ABLATION WITH INTRACARDIAC STRAIN IMAGING IN THE CLINIC. 58

Vincent Sayseng[1], Chris S. Grubb[2], Hasan Garan[2], Elaine Wan[2], Elisa Konofagou[1].*

[1]Columbia University, New York, NY, USA;

[2]Columbia University Medical Center, New York, NY, USA.

2:30P – 2:45P

027 CARDIAC RESYNCHRONIZATION THERAPY QUANTIFICATION AND DIRECT ASSESSMENT OF PATIENT RESPONSE WITH 3D RENDERED ELECTROMECHANICAL WAVE IMAGING. 59

L Melki[1], CS Grubb[2], H Garan[2], E Wan[2] and EE Konofagou[1].*

[1]Columbia University, New York, NY, USA; [2]Columbia University Medical Center, New York, NY, USA.

2:45P – 3:00P

028 ASSESSING TUMOR MECHANICAL PROPERTIES AND BLOOD PERFUSION WITH MRI AND CORRELATIONS WITH TUMOR PRESSURE AT DIFFERENT COMPRESSION LEVELS IN MICE. 60

G Pagé[1], M Tardieu[1], L Besret[2], B E Van Beers[1,3], P Garteiser[1].*

[1]INSERM U1149, Paris, FRANCE ; [2]Sanofi, Vitry-sur-Seine, FRANCE, [3]Beaujon University Hospital, Clichy, FRANCE.

(Session CAA continued on next page)

(Session CAA continued from previous page)

3:00P – 3:15P

034 MR ELASTOGRAPHY OF CHRONIC PANCREATITIS REVERSAL AFTER BARIATRIC SURGERY IN OBESE RATS AT MULTIPLE FREQUENCIES. 61

Philippe Garteiser[1], Vinciane Rebours[1,2], Sabrina Doblas[1], Gwenaël Pagé[1], André Bado[1], Maude Le Gall[1], Valérie Paradis[1,2], Anne Couvelard[1,3], Bernard E Van Beers[1,2].*

[1]Inserm UMR1149 Center For Research on Inflammation and Paris Diderot University, 16 rue Henri Huchard, Paris, FRANCE; [2]Beaujon Hospital, AP-HP, 100 Bd. Du Général Leclerc, Clichy, FRANCE; [3]Bichat Hospital, AP-HP, 46 rue Henri Huchard, Paris, FRANCE

3:15P – 3:30P

036 SHEAR WAVE SPEED DISPERSION ANALYSIS IN PLACENTA USING 2-D TRANSIENT ELASTOGRAPHY. 62

E.G. Simon[1], J.P. Remenieras[1], M.C. Dumoux[2], F. Patat[3], F. Perrotin[1], S. Callé[4]*

[1]UMR 1253, iBrain, University of Tours, Inserm, Tours, FRANCE; [2]Vermon SA, Tours, FRANCE; [3]CIC-IT, CIC 1415 Inserm, University Hospital Center of Tours, Tours, FRANCE; [4]GREMAN UMR 7347, University of Tours, CNRS, INSA, Tours, FRANCE.

3:30P – 4:00P

COFFEE BREAK — Lobby

Wednesday 4:00P – 4:30P

Session MPT: Mechanical Properties of Tissues

Chair: S Catheline, France *Co-Chair: JC Bamber, UK* — Andromède 1

Page No.

4:00P – 4:15P

024 CLOT ELASTICITY IS INVERSELY CORRELATED WITH RT-PA THROMBOLYTIC SUSCEPTIBILITY IN VITRO. 63

Karla P. Mercado-Shekhar[1], Robert Kleven[1], Hermes Aponte Rivera[1], Ryden Lewis[1], Kunal B. Karani[1], Hendrik J. Vos[2], Todd A. Abruzzo[1], Kevin J. Haworth[1], Christy K. Holland[1].*

University of Cincinnati, Cincinnati, Ohio, USA[1]; Erasmus Medical Center, Rotterdam, THE NETHERLANDS[2].

4:15P – 4:30P

035 A COMPARISON OF MECHANICAL PARAMETERS OF THE PORCINE LIVER OBTAINED WITH SWE IMAGING AND INDENTATION METHOD FOR MODELLING PURPOSES. 64

M. Żmudzińska[1], M. Inglot[2], E. Świątek-Najwer[1], U. Zaleska-Dorobisz[2], C. Pezowicz[1].*

[1]Wroclaw University of Science and Technology, Wroclaw, POLAND;
[2]Wroclaw Medical University, Wroclaw, POLAND.

Wednesday 5:00P – 7:00P

Closing Tapas Reception — Le Patio Restaurant

Verasonics Inc.
Redmond, WA, USA.
Verasonics®

AUTHOR INDEX

AUTHOR INDEX

ABSTRACTS

Sixteenth International Tissue Elasticity Conference

Avignon, France September 9-12, 2018

004 **TEMPORALLY REGULARIZED GLOBAL ULTRASOUND ELASTOGRAPHY.**

Md Ashikuzzaman[1], Claudine J. Gauthier[1], Hassan Rivaz.[1]*
[1]Concordia University, Montreal, QC, CANADA.

Background: Block-matching techniques have mostly been used to estimate the displacement field during tissue deformation. The interplay between spatial resolution and displacement accuracy being too dependent on window size, energy-based techniques can replace block-matching methods. GLUE [1] optimizes a spatially regularized cost function to calculate the displacements of all samples simultaneously. Though GLUE is able to produce accurate and spatially smooth displacement fields, information in the temporal domain still remains unemployed.

Aims: In this paper, we introduce a novel ultrasound elastography technique where we incorporate three consecutive Radio Frequency (RF) frames and impose temporal continuity on displacement fields. We consider information from all three RF frames to devise a non-linear cost function with data terms, spatial and temporal continuity terms. Efficient optimization of the cost function involves solving a sparse system of equations and enables us to simultaneously estimate two 2D displacement fields.

Methods: Let $I_1(i,j)$, $I_2(i,j)$, and $I_3(i,j)$ be three consecutive RF frames. Displacement prior from frame I_1 to I_2 and I_2 to I_3 are obtained from Dynamic Programming (DP) [2]. It's a common practice to calculate the subsample displacement field to refine the initial guess. To that end, we construct a cost function: $C=\sum\sum[I_2(i,j)-I_1(i-a^1_{i,j}-\Delta a^1_{i,j},\ j-l^1_{i,j}-\Delta l^1_{i,j})]^2 + [I_2(i,j)-I_3(i+a^2_{i,j}+\Delta a^2_{i,j},\ j+l^2_{i,j}+\Delta l^2_{i,j})]^2 + \alpha_1 (a^1_{i,j}+\Delta a^1_{i,j}-a^1_{i-1,j}-\Delta a^1_{i-1,j})^2 + \alpha_2 (a^1_{i,j}+\Delta a^1_{i,j}-a^1_{i,j-1}+\Delta a^1_{i,j-1})^2 + \beta_1(l^1_{i,j}+\Delta l^1_{i,j}-l^1_{i-1,j}-\Delta l^1_{i-1,j})^2 + \beta_2(l^1_{i,j}+\Delta l^1_{i,j}-l^1_{i,j-1}-\Delta l^1_{i,j-1})^2 + \alpha_1 (a^2_{i,j}+\Delta a^2_{i,j}-a^2_{i-1,j}-\Delta a^2_{i-1,j})^2 + \alpha_2 (a^2_{i,j}+\Delta a^2_{i,j}-a^2_{i,j-1}+\Delta a^2_{i,j-1})^2 + \beta_1(l^2_{i,j}+\Delta l^2_{i,j}-l^2_{i-1,j}-\Delta l^2_{i-1,j})^2 + \beta_2(l^2_{i,j}+\Delta l^2_{i,j}-l^2_{i,j-1}-\Delta l^2_{i,j-1})^2 + \alpha_3 (a^2_{i,j}+\Delta a^2_{i,j}-a^1_{i,j}-\Delta a^1_{i,j})^2 + \beta_3(l^2_{i,j}+\Delta l^2_{i,j}-l^1_{i,j}-\Delta l^1_{i,j})^2$. Here, α_1, α_2, β_1 and β_2 are spatial regularization parameters in the axial and lateral directions respectively. α_3 and β_3 are temporal regularization weights in the axial and lateral dimensions. We obtain the subsample displacement field (Δa and Δl) by minimizing the aforementioned cost function. Total displacement field is obtained by adding the subsample estimate to DP integer displacement (a and l). Since our method considers continuity in the time-domain, we refer to it as tGLUE.

Results: We validate our method with an experimental phantom and *in-vivo* liver data. In both experiments, our method performs substantially better than GLUE and a hybrid method [3], a recently proposed window-based algorithm (Figs. 1, 2 and 3).

Conclusions: In this work, instead of two, three frames are taken into account to implement temporal continuity of displacement when tissue undergoes deformation and hence the effect of signal decorrelation is minimized.

Acknowledgements: Authors thank Drs. E. Boctor, M. Choti and G. Hager for sharing the *in-vivo* data. We also thank Dr. Md Kamrul Hasan for sharing the code of the hybrid method with us.

References:

[1] Hashemi, H S. and Rivaz, H, "Global time-delay estimation in ultrasound elastography," IEEE Trans UFFC, vol. 64, no. 10, pp. 1625–1636, 2017.
[2] Rivaz, H., et al., "Ultrasound elastography: a dynamic programming approach," IEEE Trans Medical Imaging, vol. 27, no. 10, pp. 1373–1377, 2008.
[3] Nahiyan, A. and Hasan, M. K., "Hybrid algorithm for elastography to visualize both solid and fluid-filled lesions," Ultrasound in Medicine & Biology, vol. 41, no. 4, pp. 1058 – 1078, 2015.

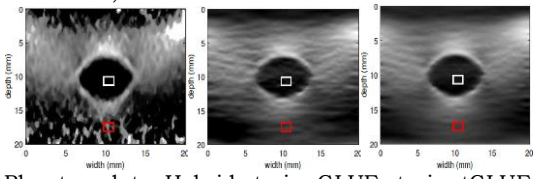

Fig. 1 Phantom data: Hybrid strain, GLUE strain, tGLUE strain

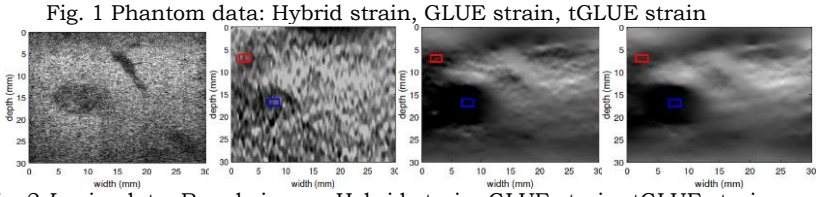

Fig. 2 *In-vivo* data: Bmode image, Hybrid strain, GLUE strain, tGLUE strain

Fig. 3 Color bar: Phantom data, GLUE and tGLUE for *in-vivo* data, Hybrid for *in-vivo* data

007 **ANISOTROPIC COMPOSITE MATERIAL PHANTOM TESTED USING MAGNETIC RESONANCE ELASTOGRAPHY**

Martina Guidetti[1], Gloria Lorgna[2], Dieter Klatt[1], Pasquale Vena[2], Thomas J. Royston[1]*
[1]University of Illinois at Chicago, Chicago, Illinois, USA; [2]Politecnico di Milano, Milan, Italy.

Background: The presence and progression of neuromuscular pathologies, including spasticity, dystrophy and hyperthyroidism, have been correlated with changes in the intrinsic mechanical properties of skeletal muscle tissue. Tools of noninvasively measuring and monitoring these properties, such as Magnetic Resonance Elastography (MRE), could benefit basic research into understanding neuromuscular pathologies, as well as translational research to develop therapies, by providing a means of assessing and tracking their efficacy. While various approaches have been proposed in the literature [1,2], there is not yet an accepted standard for the identification of the mechanical properties of anisotropic and viscoelastic tissues through MRE; advances in this technique at every step have been aided by phantom materials approximating the target tissue.

Aims: The aim of the present study was to develop and characterize a heterogeneous composite phantom design with uniform and controllable anisotropic properties comparable to skeletal muscle tissue.

Methods: A 3D printed anisotropic composite phantom, comprised of 15% w/v crosslinked gelatin fibers embedded in a 5% w/v gelatin solution for the matrix, was fabricated using a 3D-Bioplotter (EnvisionTEC). MRE experiments were performed in a 56 mm vertical bore MR scanner (Bruker 11.74 Tesla, Billerica, MA). Borosilicate glass NMR test tubes of ~9 mm inner diameter were filled with the phantom and vibrated over the frequency range from 600 to 3000 Hz in specific increments. The excitation given by the actuator on the test tube is parallel to the tube axis and this motion generates converging shear waves radially propagating from the external boundary of the sample to the central axis of the test tube. Motion was encoded in the slice direction and MREDeVIANT software was used [3]. MRE experiments were simulated through finite element (FE) methods on a composite phantom considered as a homogeneous orthotropic material with a frequency-dependent viscoelastic tensor. For computational cost reduction, Periodic Boundary Conditions (PBCs) and a symmetric cylindrical geometry were used. A homogenization procedure on a Representative Volume Element (RVE) was applied with the purpose to determine the orthotropic frequency dependent elastic parameters. All the finite element analyses were run by using Abaqus FEA (Dassault Systèmes, France) and the Hometools plugin. The properties of the two homogeneous constituent materials of the anisotropic phantom were extracted, in terms of shear storage and loss moduli for each experimental frequency. The axial displacement maps (xy plane), as encoded by the MRE experiments, and the axial displacement maps resulting from finite element simulations, were obtained.

Results: The experimental displacement maps showed elliptic wavefronts elongated in the vertical direction, formed during the propagation of the mechanical wave from the walls towards the center of the test tube [4]. This elongation means that the wavelengths are shorter in the vertical direction by a factor of about 1.5, which is consistent with a shear modulus lower in the *zy* plane than in the *zx* one. The degree of anisotropy was measured as the ratio between the long and short semi-axis of the ellipses formed in the wave images. Increasing values of the ratio with increasing frequency were obtained and the results are in line with reports in the literature on skeletal muscle anisotropy [1].

Conclusions: MRE and computational FE studies were conducted on a novel 3D-printed composite phantom design, exhibiting anisotropic heterogeneous viscoelastic properties to mimic some of the essential features of skeletal muscle tissue. There are limitations to the homogenization approach since it can be applied only if the wavelength is large enough if compared to the fiber separation distance, nominally by a ratio of at least 3 or 4; otherwise an explicit description of the fiber would be required. A comparison between computational and experimental results can improve the optimization of MRE inversion algorithms applied to viscoelastic and anisotropic media through a deeper understanding of the influence of heterogeneity, anisotropy and viscoelasticity on mechanical wave motion.

Acknowledgements: Financial support: NIH Grant # AR071162.

References: 1. Klatt D., Phys. Med. Biol., 2010,55,6445. 2. Guo J., Mag. Res. Med,2016, 75.4:1537-45.5. 3. Yasar TK, Mag. Res. Med., 2013, 70,479-89. 4. Schmidt JL., J. Biomech., 2016, 49,1042-9.

016 **REVERBERANT 3D OPTICAL COHERENCE ELASTOGRAPHY (REV3D-OCE): A NOVEL METHOD FOR THE 3D ELASTIC MAPPING OF LAYERS IN CORNEA.**

Fernando Zvietcovich[1], Jannick P. Rolland[1], Panomsak Meemon[2], Kevin J. Parker[1]*
[1]University of Rochester, Rochester, NY, USA; [2]Suranaree University of Technology, Nakhon Ratchasima, THAILAND.

Background: Measuring the elasticity of layers in cornea is fundamental to better understanding, diagnosing, and monitoring degenerative ocular diseases [1]. Current methods in optical coherence tomography (OCT) use air-puff or acoustic radio force (ARF) systems to produce the propagation of Lamb waves [2]. However, Lamb wave speed values (1) are dispersive, (2) are dependent on the boundary conditions (cornea thickness), and (3) do not provide high contrast in depth layer mapping. Therefore, the estimation of shear modulus of each corneal layer remains a challenge. Our previous work on reverberant shear wave (RevSW) fields demonstrated its application for lesion detection in breast models using ultrasound [3]. Current simulations of RevSW performed in finite element models of the cornea suggest its potential for the elastic characterization of layers.
Aims: Demonstrate the capabilities of RevSW fields applied to OCT for the 3D elastic characterization of depth-dependent corneal layers in experiments using animal models and numerical simulations. We call this novel method as reverberant 3D optical coherence elastography: Rev3D-OCE.
Methods: RevSW fields are generated in an *ex vivo* cornea by the sinusoidal steady state excitation, at 2 kHz, of a 3D printed ring actuator with eight heads touching the corneal epithelium (Fig. 1a-top). The motion was detected by Doppler phase shift detection using a custom-made spectral-domain OCT system with 1307 nm central wavelength and about 100 nm spectral width. 3D volumes of 8 × 8 × 2 mm of cornea were acquired at a line rate of 25 kHz using the MB-mode acquisition protocol described in [2]. Subsequently, complex-valued cross correlation maps extracted from reverberant volumes (Fig. 1a-bottom) are used to estimate local wave number as described in [3]. Experiments in fresh porcine corneas at controlled intraocular pressure are conducted. Regular tone burst (Lamb wave propagation) experiments were also conducted in the same samples for further comparison. Numerical simulation in Abaqus/CAE (6.14-1, Dassault Systems) were also conducted to corroborate our results.
Results: Experiments with porcine cornea reveal differentiated layers as shown in the 2D and 3D shear wave speed maps (Fig. 1b). Moreover, we found that the speed contrast of our approach is much superior than the regular Lamb wave method when a vertical depth profile was analyzed (Fig. 1c). The Rev3D-OCE speed values range from 3.4 m/s to 4.2 m/s, while Lamb wave results range from 3.73 m/s to 3.81 m/s. Numerical simulations confirmed the detection of independent layers in cornea for a four-layer model.
Conclusions: We demonstrated that Rev3D-OCE is successful in the identification of differentiated layers in *ex vivo* cornea using OCT. In addition, speed profiles (Fig. 1c) have the same tendency as results provided by Brillouin Scattering [4], and they enable the direct calculation of shear modulus.

Acknowledgements: This research benefitted from support of the II-VI Foundation, Fondo para la Innovacion, la Ciencia y la Tecnologia 097-FINCYT-BDE-2014 (Peruvian Government), Suranaree University of Technology and the Higher Education Research Promotion and National Research University Project of Thailand, and the Hajim School of Engineering and Applied Sciences at the University of Rochester.

References:

[1] C. Edmund, "Corneal elasticity and ocular rigidity in normal and keratoconic eyes," *Acta Ophthalmol.* (Copenh.) **66**(2), 134–140 (1988). [2] S. Wang, and K. V. Larin, "Noncontact depth-resolved micro-scale optical coherence elastography of the cornea," *Biomed. Opt. Express* **5**(11), 3807-3821 (2014). [3] J. P. Kevin et al., "Reverberant shear wave fields and estimation of tissue properties," *Physics in Medicine & Biology* **62**(3), 1046 (2017). [4] G. Scarcelli, R. Pineda, and S. H. Yun, "Brillouin Optical Microscopy for Corneal Biomechanics," *Investigative Ophthalmology & Visual Science* **53**(1), 185-190 (2012).

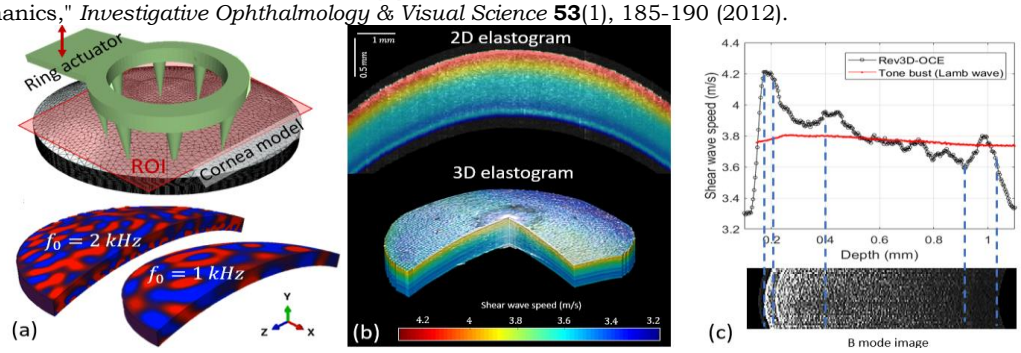

Figure 1. (a) Ring actuator and RevSW motion volumes from numerical simulations. (b) 2D and 3D elastography of porcine cornea. (c) Depth-resolved shear wave speed profile depicting differentiated corneal layers versus regular Lamb wave method.

021 **MULTIPLE WAVE MODES INDUCED BY AORTIC VALVE CLOSURE IN THE INTERVENTRICULAR SEPTUM; AN *IN-VIVO* AND IN-SILICO STUDY.**

LBH Keijzer[1], M Strachinaru[1], JG Bosch[1], BM van Dalen[1,3], I. Heinonen[4], MD Verweij[2,1], AFW van der Steen[1,2], N de Jong[2,1], HJ Vos[1,2].*

[1]Erasmus MC, Rotterdam, Zuid-Holland, THE NETHERLANDS; [2]Delft University of Technology, Delft, Zuid-Holland, THE NETHERLANDS; [3]Franciscus Gasthuis & Vlietland, Rotterdam, Zuid-Holland, THE NETHERLANDS; [4]University of Turku and Turku University Hospital, Turku, FINLAND.

Background: Lamb waves (LWs) induced by aortic valve closure (AVC) in the interventricular septum (IVS) might be used to non-invasively measure the stiffness of the heart muscle. Earlier studies used either a parasternal [1,2] or an apical view [3] to track the LWs. Since Tissue Doppler is sensitive to axial particle motion only, a parasternal view would mainly track transversal particle motion on the IVS, which is dominant in antisymmetric LWs, while an apical view would mainly track longitudinal particle motion, dominant in the symmetric mode. Symmetric LWs have higher propagation speeds than antisymmetric LWs, and thus knowing the LW mode induced enables correct translation of propagation speeds into tissue stiffness; yet, multiple modes may be present simultaneously, and even other waves might exist.

Aims: As a single mode can only have one propagation speed, we track the particle motion with high resolution in all directions and investigate the presence of multiple LW modes by analysing propagation speeds.

Methods: We tested in-vivo and in-silico. For in-silico testing, wave propagation in a homogenous plate induced by different sources was simulated in PZFlex (Weidlinger Associates, Inc, Scotland). The difference in transversal and longitudinal particle velocity was studied. For in-vivo testing, 3 pigs with open chest were scanned in long-axis parasternal and 4-chamber apical view. High-resolution high-frame rate B-mode images were recorded (Aixplorer, SSI, France; L15-4 probe in plane wave mode). Speckle-tracking was used to compute axial and lateral particle velocities. These were then converted to longitudinal and transversal particle velocity along the IVS. A Radon transform was used to obtain propagation speeds from either type of particle motion.

Results: The in-silico measurements show that depending on the source, different LW modes and different particle-velocity amplitudes in both directions could be induced. Furthermore, when both particle velocity components were dominated by an antisymmetric mode, the particle velocity was found to be largest in transversal direction. The contrary was found for the symmetric mode. The in-vivo results are shown in Figure 1. Overall, we found three ranges of propagation speeds: larger than 8m/s, with associated high variation; 4-7m/s; and 2-4m/s. As the two data points per measurement were obtained simultaneously, the different propagation speeds indicate the presence of two simultaneous waves. Furthermore, the particle-velocity amplitudes in both directions were found to be in the same range. No significant difference was found in propagation speed of the transversal particle motion in parasternal view compared to the longitudinal particle motion in apical view, which supports the finding in an earlier study [1], suggesting that the same mode can be measured in both views.

Conclusions: These preliminary results suggest that multiple modes of LWs are simultaneously induced by AVC, which would require caution when translating propagation speeds into tissue stiffness.

Acknowledgements: This work is part of a TTW – Dutch Heart Foundation partnership program with project number 14740, which is (partly) financed by the Netherlands Organization for Scientific Research (NWO).

References: [1] H. Kanai, IEEE Trans. Ultrason. Ferroelectr. Freq. Control, vol. 52, no. 11, pp. 1931–1942, 2005; [2] H. J. Vos et al, Ultrasound Med. Biol., vol. 43, no. 4, pp. 753–764, 2017; [3] B. Brekke et al., Ultrasound Med. Biol., vol. 40, no. 1, pp. 222–231, 2014.

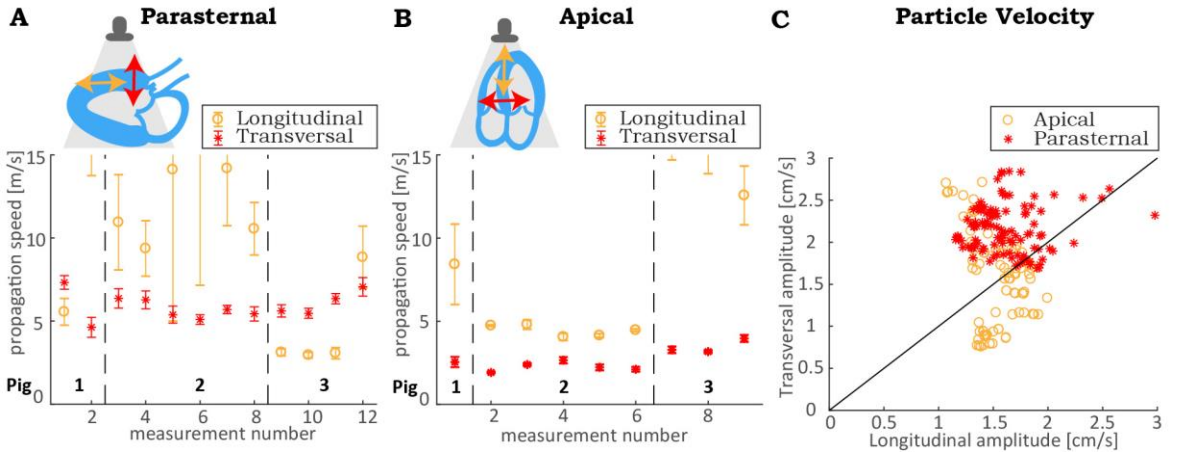

Figure 1 A+B) Mean and standard deviations of propagation speeds obtained for longitudinal and transversal particle motion in parasternal (A) and in apical view (B). For every measurement, 10 anatomical M-lines were drawn. C) Peak-to-peak amplitudes of the particle velocity in both directions.

025 **NONINVASIVE ESTIMATION OF MATERIAL PARAMETERS FOR *IN VIVO* SKELETAL MUSCLE USING ULTRASOUND.**

Jinping Dong[1], He Li[1], Yang Zhang[1], Wei-Ning Lee[1].*
[1]The University of Hong Kong, Pokfulam Road, Hong Kong, CHINA.

Background: Skeletal muscle exhibits nonlinearity and anisotropy, which can be described by several material parameters in its strain energy function. These material parameters may serve as new diagnostic indices supplementary to stiffness and viscosity and be useful for comprehensive computational modeling of the muscle. However, they have been mainly measured *ex vivo*.

Aims: In this study, acoustoelastic theory, which entails the change in elastic wave speed in a deformed medium, was realized noninvasively to estimate muscle material parameters by combining shear wave imaging (SWI) and ultrasound strain imaging (USI). *In vivo* human biceps brachii muscle was examined and regarded as a transversely isotropic soft material.

Methods: The biceps brachii muscle of a healthy human subject was passively extended by changing elbow angle φ continually from 90° to 120° using a custom-made device. During extension, shear waves were generated by acoustic radiation force (100μs, 3 foci) at 5 Hz for 20s and captured by plane wave imaging with 3 steering angles (-2°, 0°, 2°) at 8000Hz using a Verasonics Vantage system with an L7-4 probe (fc = 5.2 MHz) mounted on a rotation stage (Fig. 1(a)). The probe was rotated from 0° (i.e., muscle fiber direction) to 90° (i.e., cross-fiber direction) at a 22.5° increment to obtain shear waves propagating in various directions. Shear wave group velocities and lateral strain of the muscle were estimated by SWI [1] and USI [2], respectively. Electromyography (EMG) was also acquired to confirm the passive state of muscle. The strain energy function (eq. (1)) and the corresponding acoustoelastic equations (eq. (2)) used in this study are as follows:

$$W=\mu I_2+1/3AI_3+a_1I_4^2+a_2I_5+a_3I_2I_5+a_4I_4^3+a_5I_4I_5 \quad (1)$$

$$\rho v^2=\gamma_{13}cos^2\theta+\gamma_{23}sin^2\theta,\ \gamma_{23}=\mu+(-3\mu-1/2A+a_3)e+(5\mu+7/4A-5/2a_3)e^2$$

$$\gamma_{13}=\mu+1/2a_2+(3\mu+1/4A+2a_1+5/2a_2+a_3+1/2a_5)e+(5\mu+7/4A+5a_1+5a_2+5a_3+3a_4+15/4a_5)e^2 \quad (2)$$

where μ, A, $a_{i=1\text{-}5}$ are material parameters, μ is related to the stiffness in cross-fiber direction, a_2 is the stiffness difference between fiber and cross-fiber directions, $I_{i=1\text{-}5}$ are invariances of the Green–Lagrange strain tensor, and ρ, v, θ and e are density, shear wave speed, probe angle and elongation (i.e., lateral strain), respectively. In theory [3], $\rho v^2=f(\theta, e)$, and the average values of v and e were calculated in a region of interest (ROI)(the red rectangles in Fig. 1(b)) and used in parameter fitting.

Results: The estimated μ, A, a_1, a_2, a_3, a_4, and a_5 for *in vivo* biceps brachii muscle were reported for the first time and found to be 2.42kPa, -34.87kPa, 23.01kPa, 2.98kPa, -11.16kPa, 13.19kPa and -34.19kPa, respectively. These values were further plugged into eq. (2) to obtain the e-ρv^2 curves shown in Fig. 1(c). It is observed that during muscle extension, shear wave speed increased with lateral strain in propagation directions closer to the fiber direction but decreased in the cross-fiber direction. This phenomenon was alternatively demonstrated as the increase in fractional anisotropy with muscle extension as shown in Fig. 1(d) and in good agreement with literature [4].

Conclusions: This study demonstrated the feasibility of material parameter estimation of *in vivo* skeletal muscle by an integrated ultrasound imaging framework, which may permit a better understanding of muscle nonlinear behavior and more realistic computational modeling of skeletal muscle.

Acknowledgements: This study was supported in part by National Natural Science Foundation of China (NSFC)/Research Grants Council (RGC) Joint Research Scheme (N_HKU713_15) and the University Development Fund.

References: [1]W.-N. Lee et al., IEEE transactions on medical imaging, vol. 31, no. 3, pp. 554-562, 2012. [2]H. Li, et al, Ultrasound in medicine & biology, vol. 42, no. 10, pp. 2436-2456, 2016. [3]M. Destrade, et al, The Journal of the Acoustical Society of America, vol. 127, no. 4, pp. 2103-2106, 2010. [4]J.-L. Gennisson, et al, Ultrasound in medicine & biology, vol. 36, no. 5, pp. 789-801, 2010.

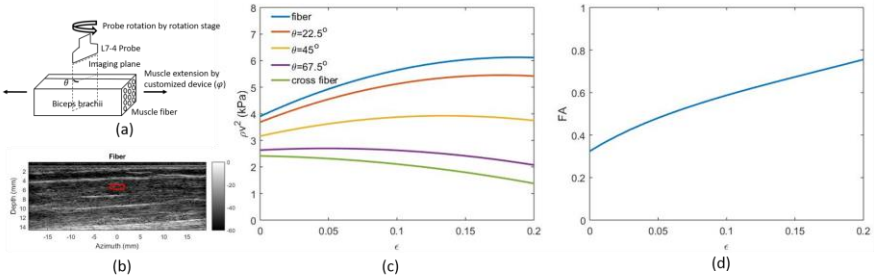

Fig.1 (a) Schematic of experimental setup; (b) B-mode image of Biceps brachii muscle in fiber direction, red rectangle is the ROI for material parameter estimation; (c) Shear wave speeds vary with muscle extension along different directions; (d) Fractional anisotropy (FA) changes with deformation, and the anisotropy increased during muscle extension.

030 **4-D PULSE WAVE IMAGING IN THE HUMAN ABDOMINAL AORTA *IN-VIVO*.**

Grigorios Marios Karageorgos[1], Julien Grondin[1], Iason Zacharias Apostolakis[1], and Elisa E. Konofagou[1]*

[1]Columbia University, PS 19-405, 6330 West 168th Street, New York, NY, USA

Background: Pulse Wave Imaging (PWI) is a non-invasive ultrasound-based method which can regionally map the pulse wave velocity (PWV) along a vessel. Recently, 4–D PWI was introduced and validated in phantoms and in common carotid arteries in-vivo, using a 16 x 16 ultrasound array. However, the limited number of piezoelectric elements and large inter-element spacing (1.4 wavelength) resulted in suboptimal image quality, while plane wave imaging restricted the field of view to the aperture dimensions, i.e., 13.6 x 13.6 mm.

Aims: The aims of the present study are to: i) improve 4-D PWI imaging quality by using an array and sequence that utilizes a larger number of elements, ii) increase the field of view by employing diverging wave imaging, iii) demonstrate the feasibility of 4-D PWI to analyze the wall dynamics of deeper and more tortuous vessels, such as the aorta.

Methods: The abdominal aortas of three healthy male volunteers (25.6 ± 2.0 y.o.) were imaged in-vivo. Two Verasonics Vantage 256 systems were synchronized to drive a 32 x 32 array (3 MHz center frequency, 50% bandwidth, 0.6 wavelength pitch). A diverging wave sequence with a 90˚ field of view was implemented at a pulse repetition frequency of 2000 Hz. Given that 512 transmit/receive channels were available on the combined systems, a 2:1 multiplexer embedded in the probe was used to alternate the activation of either of the two 32 x 16 sub-apertures of the array between consecutive transmit/receive events. The data acquired by the two sub-apertures were combined to reconstruct the entire volume using a delay-and-sum method, thus leading to an effective volume rate of 1000 vps.
After beamforming, a scan conversion process was applied to remap the scan lines in Cartesian coordinates. Displacement estimation was then performed through a 1-D cross-correlation method, and the aortic wall was manually segmented in multiple cross-sectional slices, in order to obtain the 3-D spatiotemporal map of the axial aortic wall velocities (v_{pwi}) (Fig. 1). The PWV along the propagation of the pulse wave (PW) was estimated by applying a plane fit between the time of occurrence of the 50% upstroke markers in the spatiotemporal plot and the corresponding point locations.

Results: Due to the use of diverging waves, the length of the imaged aortic segment was dependent upon the depth of the vessel in each subject, and was 35.5 ± 3.8 mm on average. The pulse wave propagation was successfully imaged in all volunteers. The average PWV along the longitudinal direction was 5.02 ± 1.29 m/s, which is in good agreement with previously reported values using 2-D PWI. The squared correlation coefficient (R^2) of the surface fit to the 50% upstroke markers was 0.91 ± 0.04, indicating a good quality of the pulse wave tracking.

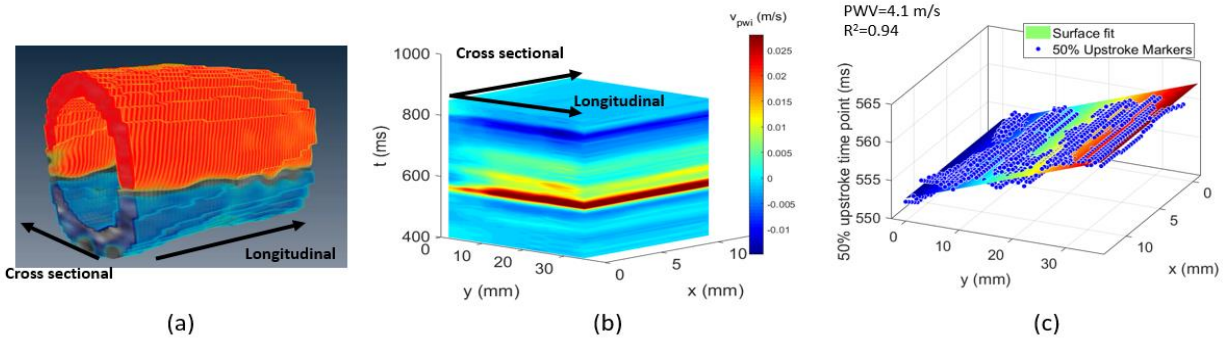

Fig. 1: (a) 3-D axial aortic wall velocities of the aortic segment overlaid onto the B-mode image at a given time point in a healthy volunteer. (b) 3-D spatiotemporal plot of v_{pwi} at manually selected points along multiple cross sectional views of the aorta. (c) 3-D plot of 50% upstroke markers along with surface fit for PWV estimation.

Conclusions: In conclusion, an improved version of 4-D PWI was presented, and its feasibility to analyze the wall dynamics of deeper vessels such as the abdominal aorta was shown in vivo for the first time, demonstrating the potential to enhance the PWI's mapping information.

Acknowledgements: Supported in part by NIH #R01HL135734

References: Li, Ronny X., et al., Physics in Medicine & Biology 58.13 (2013): 4549.

037 **SHEAR WAVE SPEED AND ATTENUATION ESTIMATION IN OIL-IN-GELATIN PHANTOMS USING A RHEOLOGICAL MODEL, MECHANICAL, AND ULTRASOUND MEASUREMENTS.**

Juvenal Ormachea[1], Kevin J. Parker[1], Michael G. Drage[1], Henry Kim[1], Zaegyoo Hah[2].*
[1]University of Rochester, Rochester, NY, USA;[2]Samsung Medison Co.Ltd., SungNam, SOUTH KOREA.

Background: Elastography can be used to characterize high grade liver fibrosis by elevated shear wave speed (SWS) estimates [1,2]. What remains unclear are the biomechanics of earlier stages of the progression of liver disease, including steatosis. The changes in rheology compared with the normal liver are not well understood. These conditions are important to understand and characterize for detection of early stages of liver diseases.

Aims: To estimate the SWS and shear wave attenuation (SWA) parameters in custom-made oil-in-gelatin phantoms using the theory reported in [3]. Then, compare these results with experimental mechanical measurements and examine them with a rheological theory model.

Methods: *Spherical particulate inclusions rheological model:* This model is presented in [4]. It shows that the new composite liver representing simple steatosis will have a shear modulus G_c related to a small volume fraction V_2 of fat with shear modulus G_2, where the normal liver is modeled as G_1. Writing the frequency dependence explicitly: $G_c=G_1(\omega)-(7.5*V_2*[G_1(\omega)-G_2(\omega)])/(4.5+3*[G_2(\omega)/G_1(\omega)])$. *Viscoelastic phantoms:* Seven different concentration of oil-in-gelatin phantoms were created by first heating a mixture of gelatin, degassed water, NaCl, and agar. The molten gelatin was then mixed with castor oil, resulting in different percent oil concentration phantoms. *Ultrasound (US) measurements:* A Samsung scanner (model RS85) was used to produce radiation force push beams and track the induced displacements. SWS and SWA were obtained using the theory reported in [3]. *Mechanical measurements:* After the US scans were completed, three small cylindrical samples were extracted for each viscoelastic phantom. For each sample, compression tests were performed using a QT/5 mechanical device (MTS Systems Co., Eden Prairie, MN, USA) to measure the stress relaxation responses and fit it with a Kelvin-Voigt fractional derivative model (KVFD) [5]. SWS and SWA parameters were obtained similarly to [5,6].

Results: SWS (group velocity) is shown in Figure 1 (left) to be decreasing as oil concentration increases. Independent values of SWS obtained from mechanical measurements, US measurements, and the rheological model using the relationship $c_p=\sqrt{G_c(\omega)/\rho}$ with ρ=1000kg/m^3 are also shown at 100 Hz (approximate spectral peak of the shear wave pulses), with reasonable agreement. The attenuation estimates are shown to be increasing as a function of oil concentration in Figure 1 (right). Independent predictions of attenuation obtained using the three different methods are shown. For mechanical measurements and the rheological model, the complex wave number k was calculated and then the imaginary part using $k=\beta+ja$, where a the shear wave attenuation coefficient.

Conclusions: An analytical model for shear wave elastography was used to extract estimates of SWS and SWA that do not depend on traditional Kelvin-Voigt or Zener model parameters. Furthermore, the US estimate results are properly bounded by independent measurements in different oil-in-gelatin phantoms. These developments may be useful in quantifying the biomechanical state of steatotic tissues.

Acknowledgements: This work was supported by the Hajim School of Engineering and Applied Sciences at the University of Rochester. We are grateful for support from Samsung Medison Co. Ltd. and for loan of the equipment. The authors are also thankful for insightful advice from Dr. R. Mattrey, Dr. D. Rubens, and Prof. K. Hoyt about the properties of the liver.

References: [1] Srinivasa BA, et al., *RadioGraphics* 36(7)1987-2006, 2016. [2] Cosgrove D, et al. *Ultraschall Med* 43(3)238-253, 2013. [3] Parker, KJ., et al. Ultrasound Med Biol, 44(7)1504-1515, 2018. [4] Parker, KJ, et al. *Phys Med Biol* 63(10)105013, 2018. [4] Parker KJ & Baddour N, *Ultrasound Med Biol* 40(4)675-684, 2014. [5] Zhang M, et al. Ultrasound Med Biol 33(10)1617-1631, 2007. [6] Ormachea J et al. *IEEE Trans Ultrason Ferroelectr Freq Control* 63(9)1351-1360, 2016.

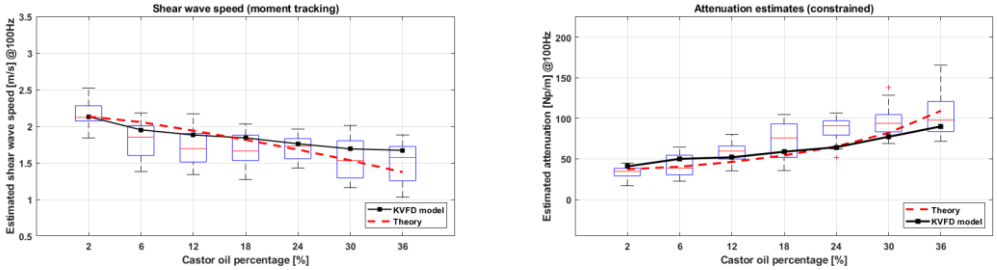

Figure1. (left) SWS vs. castor oil percentage using Samsung system. The solid line corresponds to SWS values extracted for mechanical measurements at 100 Hz using the stress relaxation data. The dashed line was derived using the real part of G_c with G_1=4kPa, η=0.11Pa•s, and a=0.025. (right) SWA coefficient vs. castor oil percentage. The solid line corresponds to attenuation values extracted for the KVFD model at 100 Hz using the mechanical stress relaxation data. The dashed line corresponds to the imaginary part of G_c using G_1 =4kPa, η=0.11Pa•s, and a=0.025.

041 **MULTIDIMENSIONAL MOTION ESTIMATION WITH STOCHASTIC INTERPOLATION Interpolation VIA DISJUNCTIVE KRIGING.**

Brandon Rebholz[1], Mohamed Almekkawy[1].*
[1]Pennsyvania State University, West Gate Building, W105, University Park, Pennsylvania, USA.

Background: Accurate motion estimates are necessary in order to estimate the elastic properties of tissue in ultrasound images [1,2]. The phase coupled algorithm has already been shown to provide accurate and robust motion estimates, and as such is the target of further improvement. The phase coupled algorithm uses lateral interpolation of the image patch cross correlation as a basis for subsample motion estimation. The interpolation methods known in geostatistics as "Kriging" [3] use the statistical properties of the structure to interpolate a value, which extends beyond the simple inverse distance weighting of the standard mathematical interpolation. In kriging techniques the correlation of the data points as a function of distance is modelled with a "correlogram", which is then used to weight the statistical likelihood that a point will influence the interpolated value. These estimates have been shown to be superior to inverse distance weighting under all tested conditions for geological data [4]. Since tissue contains different and independent structures (bone, blood vessels, muscle, fat, etc.) it is hypothesized that interpolation beyond simple mathematical weighting will provide better interpolation.

Aims: The aim is to take a motion estimator that has already been proven to be accurate and increase the estimation accuracy by any amount possible. To accomplish this stochastic interpolation schemes, known as "Kriging", are used to replace the cubic interpolation currently in use by the phase coupled algorithm. Ultimately, since displacement estimation is integral to strain calculations, the goal is to create a highly accurate estimator that can generate data for the use in further elastographic post processing.

Methods: The Disjunctive Kriging algorithm was applied into the phase coupled motion estimation algorithm to interpolate at the subsample level the correlation of the delayed signal to a patch of the original reference signal. Disjunctive Kriging is a variety of Kriging that weights the sum of independently calculated and distributed data points to generate the interpolated values [5]. Additionally, Disjunctive Kriging produces the probability that the interpolated value falls above a particular threshold, increasing the reliability of the estimate. In order to test the results on known data the Field II program was used to generate two frames of simulated blood flow. The Disjunctive Kriging method of interpolation was compared against estimates generated with a standard cubic interpolation from the "interp2" MATLAB function. The mean squared error of the estimates is then used to objectively compare the accuracy of the estimates against the ground truth values.

Results: The results of the estimation by the Disjunctive Kriging method are as expected for the majority of data points. There are some locations where the cubic interpolation value is closer to the ground truth than the Disjunctive Kriging result, however on the whole the Disjunctive Kriging result has a lower mean squared error.

Conclusions: The Disjunctive Kriging method of interpolation has clear advantages in the interpolation of data points, primarily because the accuracy of the estimates generated by the Disjunctive Kriging method is greater than that of the Cubic interpolation method. Additionally, the Disjunctive Kriging method provides further data on the quality of its own interpolation, which is highly useful in writing controls into algorithms. Disjunctive Kriging does come at the cost of an increase in execution time; however the benefits outweigh the costs involved when the final goal is an accurate elastic estimate.

References:

[1] Ophir, Jonathan, et al. "Elastography: imaging the elastic properties of soft tissues with ultrasound." Journal of medical ultrasonics 29.4 (2002): 155.
[2] O'Donnell, Matthew, et al. "Internal displacement and strain imaging using ultrasonic speckle tracking." IEEE transactions on ultrasonics, ferroelectrics, and frequency control 41.3 (1994): 314-325.
[3] Cressie, Noel. "Spatial prediction and ordinary kriging." Mathematical geology 20.4 (1988): 405-421.
[4] Zimmerman, Dale, et al. "An experimental comparison of ordinary and universal kriging and inverse distance weighting." Mathematical Geology 31.4 (1999): 375-390.
[5] Matheron, George. "A simple substitute for conditional expectation: the disjunctive kriging." Advanced geostatistics in the mining industry. Springer, Dordrecht, 1976. 221-236.

017 **GAUSSIAN SHEAR WAVE PROPAGATION IN VISCOELASTIC MEDIA: VALIDATION OF AN APPROXIMATE FORWARD MODEL.**

Fernando Zvietcovich[1], Natalie Baddour[2], Jannick P. Rolland[1], Kevin J. Parker[1]*
[1]University of Rochester, Rochester, NY, USA; [2]University of Ottawa, Ontario, CANADA.

Background: In elastography using dynamic optical coherence tomography (OCT), shear/surface waves are tracked in order to estimate speed and Young's modulus. However, for dispersive tissues, the displacement pulse is damped and distorted, reducing its propagation to the near field and diminishing the effectiveness of peak tracking models with asymptotic assumptions of attenuation [1]. Therefore, the use of a rheological model-independent approach that contemplates the initial shape of the force excitation source in space and time is needed. In that regard, propagation models have been previously proposed [1,2] at the cost of high complexity, intensive computation, and satisfying strict boundary conditions. A simplified model incorporating the general viscoelastic parameters of the media, and the initial source shape which does not require assumptions of the tissue mechanical behavior is desired.

Aims: Validate a first-order approximate forward model of near field wave propagation of a Gaussian force push in viscoelastic media using numerical simulations and experiments in phantoms.

Methods: An axisymmetric Gaussian shear wave propagation model, in radial space r and time t, is proposed for a viscoelastic medium of density ρ, complex shear modulus $\hat{\mu} = \omega^2 \rho / \hat{k}^2$, temporal frequency ω, spatial frequency ε, and complex first order approximation of wave number $\hat{k} = \omega^2 / c_0 - i|\omega|\alpha_1$, where c_0 (m/s) is the wave speed and α_1 (Np/m/rad) is the attenuation:

$$v_z(r,t) = \frac{A_0}{2}\int_0^\infty \varepsilon \cdot e^{-\sigma^2\varepsilon^2} \cdot J_0(\varepsilon r)\cos(c_0\varepsilon t)\, e^{-|\varepsilon| c_0^2 \alpha_1 t} d\varepsilon.$$

An acoustic radiation force (ARF) transducer (5 MHz, 5.01 cm focal length) was used to generate an axisymmetric Gaussian-shape (σ = 0.34 mm) force during 0.1 ms and 1 ms push durations in two viscoelastic phantoms M1 and M2, respectively. Particle velocity $v_z(r,t)$ was acquired using a phase-sensitive OCT system implemented with a swept source laser (HSL-2100-WR, Santec, Japan) of 1318 nm wavelength. Results were compared against numerical simulations (Abaqus/CAE 6.14-1) and the numerical integration of the proposed model.

Results: Figure 1 shows the comparison of spatio-temporal profiles of particle velocity calculated from numerical integration of the proposed model, numerical simulations using finite elements, and real experiments in the two phantom materials M1 and M2. c_0(m/s) and α_1(Np/m/rad) parameters are consistent with the mechanical testing of both phantoms.

Conclusions: We demonstrated the effectiveness of the proposed axisymmetric Gaussian shear wave propagation model in the near field for the viscoelastic characterization of dispersive media. Further research will concentrate on evaluating this approach in real tissue such as skin and cornea.

Acknowledgements: This research benefitted from support of the II-VI Foundation**,** Fondo para la Innovacion, la Ciencia y la Tecnologia 097-FINCYT-BDE-2014 (Peruvian Government), and the Hajim School of Engineering and Applied Sciences at the University of Rochester.

References:

[1] K. J. Parker, and N. Baddour, "The Gaussian Shear Wave in a Dispersive Medium," *Ultrasound in Medicine & Biology* **40**(4), 675-684 (2014). [2] Z. Han et al., "Optical coherence elastography assessment of corneal viscoelasticity with a modified Rayleigh-Lamb wave model," *Journal of the Mechanical Behavior of Biomedical Materials* **66**(87-94 (2017).

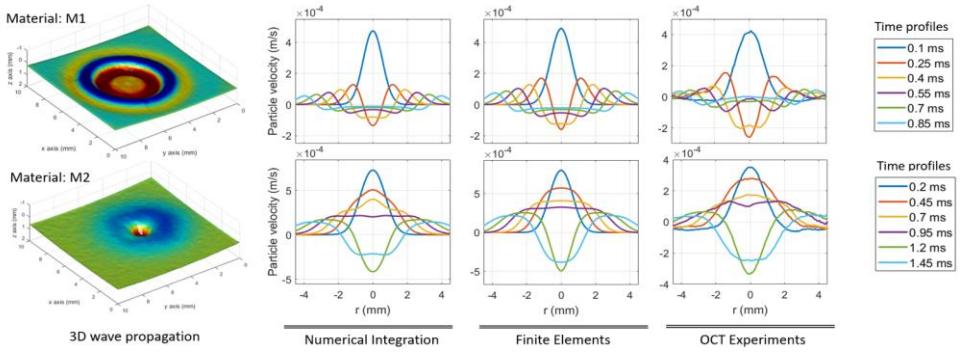

Figure 1. Comparison of wave propagation profiles during numerical integration, finite element analysis, and OCT experiments.

040 **AN EXPERIMENTAL AND COMPUTATIONAL INVESTIGATION OF THE RELATIONSHIP BETWEEN WAVE SHAPES AND SPACING BETWEEN INHOMOGENEITIES IN VISCOELASTIC TISSUE-LIKE PHANTOMS.**

Harish Palnitkar[1], Phillip Lewis[2], Margaret Hammersley[2], Ramille Shah[2], Thomas Royston[1], Dieter Klatt[1], Martina Guidetti[1].*

[1]University of Illinois at Chicago, 851 S Morgan St., Chicago, Illinois, 60607, USA; [2]Northwestern University, Chicago, Illinois, 60611, USA.

Background: The mechanical behavior of soft biological tissues such as skeletal muscle and brain white matter is inhomogeneous due to the presence of fibers. Unlike an actual biological tissue, phantoms with a known microstructure and mechanical properties enable a quantitative assessment of the influence of inhomogeneities on the nature of shear wave propagation. While prior works [1, 2] have simplified the material modeling by assuming a homogeneous medium, this approximation may not always be true, especially when significant scattering occurs at the locations of inhomogeneities.

Aims: To investigate the relationship between the wave shapes and the spacing between inhomogeneities in heterogeneous phantoms by introducing a mathematical measure, called the 1-Norm (fig. 1), and use this parameter to determine the conditions under which homogenization can be a valid approach.

Methods: Magnetic Resonance Elastography was performed on 3D printed inhomogeneous fiber phantom in order to visualize shear wave propagation. Wave front analysis (fig. 1) was used to determine the frequency spectra for the delineated contours of equal shear wave displacement, for example, zero displacement (fig. 2A, 2B), which was then used to compute the values of 1-Norm at each of the frequency. In addition, Finite Element Analysis was used as a tool to decouple the effects of anisotropy from those of inhomogeneity (fig. 2B). This was achieved by modeling inhomogeneities as uniformly spaced, symmetrically distributed spheres of diameter 0.5 mm, without fibers (fig. 2B (k-n)).

Results: From figures 2 and 3 it is observed that as the frequency of excitation increases, the value of 1-Norm increases, which points towards increasing contributions from inhomogeneity. Highest value of 1-Norm (20.2) occurs at a frequency of 5 kHz for the 3D printed fiber phantom, which indicates maximum amount of scattering at fiber intersections. It is also observed that the values of 1-Norm are significantly higher for the 3D printed phantom (in comparison to the values obtained from FEA) due to the presence of fibers that lead to a coupled scenario of anisotropy with inhomogeneity, as shown in fig. 2A (h-j).

Conclusions: 1-Norm has been proposed as a measure to quantify the amount of wave scattering in heterogeneous phantoms due to the presence of inhomogeneities. Lower values of 1-Norm indicate lower scattering implying that the wave propagation can be approximated to that of a homogeneous medium. In long term, 1-Norm may serve as a marker to determine the spatial distribution of inhomogeneities (cross-links) in engineered phantoms as well as biological tissue such as the skeletal muscle.

Acknowledgements: Support of NIH Grant AR071162 is kindly acknowledged.

References: [1] Qin, E.C., et al., Combining MR Elastography and Diffusion Tensor Imaging for the Assessment of Anisotropic Mechanical Properties: A Phantom Study. *JMRI.* 37:217–226 (2013). [2] Namani, R., et al., Anisotropic mechanical properties of magnetically aligned fibrin gels measured by magnetic resonance Elastography. *J. Biomech.* 42 (13):2047-53.

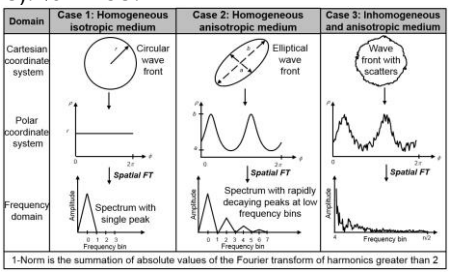

Figure 1. Wave front analysis

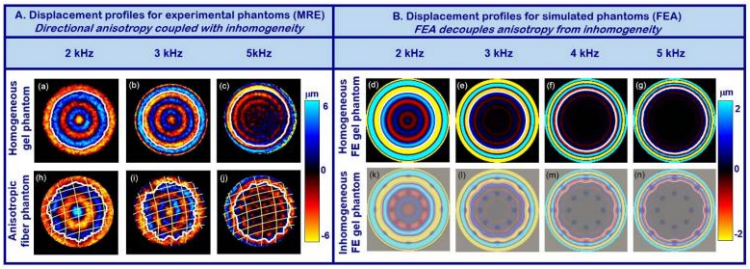

Figure 2. Contours of shear wave displacement for (A) experiments and (B) Finite Element Analysis

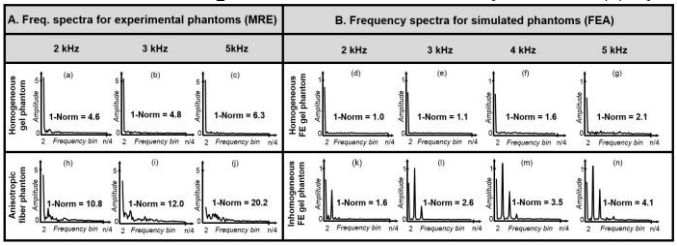

Figure 3. Frequency spectra for delineated profile of zero shear wave displacement for (A) experiments and (B) Finite Element Analysis with values of 1-Norm (inset)

042 **NATURAL SHEAR WAVES GENERATATION BY PSALMODY FOR THYROID ELASTOGRAPHY.**

S. Beuve[1], E. Khoury[1], E.G. Simon[1], S. Callé[2], J.P. Remenieras[1].*
[1]UMR 1253, iBrain, University of Tours, Inserm, Tours, FRANCE; [2]GREMAN UMR 7347, University of Tours, CNRS, INSA, Tours, FRANCE.

Background: Studies in the past few years shown direct links between some diseases and the hardness of affected organs [1]. The thyroid is a gland located in the front of the trachea and produces hormones essential for the metabolism of the body. It is accessible to the palpation process, however this exam is limited to its surface and is not quantitative. Recent time reversal methods based on noise correlation are used to determine the local value of biological tissues elasticity [2].

Aims: The aim of this project is to develop new shear wave tracking method from diffuse field naturally generated by a mono-frequency vibration of vocal cords.

Methods: In-vivo experiments were performed at 9MHz on a transverse cut of a volunteer's thyroid. The acquisition system is a programmable ultrasound scanner Verasonics Vantage equipped with a linear probe. Images are summed over those acquired using tilted plane wave emissions at 5 angles [-3°:1.5:3°] to improve image quality without degrading the frame rate. Data are recorded at 3000 frames per second after beamforming. This set of angles was repeated 400 times to build a movie of 132 ms. The probe is placed on the neck at the level of the carotid. The acoustic field is generated into the throat by singing to make vocal cords vibrate. A 150 Hz sound is played for reference on a loud speaker to emit a sound at the right frequency. An algorithm based on the ratio of autocorrelation of the particle acceleration [3] over the autocorrelation of the 2D strain rate on z was applied to calculate the elasticity map.

Results: A manually drawn mask is applied to cancel values out of the thyroid (Figure 1). Under certain boundary conditions the value of the elasticity is proportional to the square of shear wave velocity in soft tissues. The measurement of the space frequency at all location gives values of shear waves celerity between 0.3 m/s and 5 m/s. The velocity map shows in the left region of the thyroid waves travel faster suggesting it is harder. The median values are 3 m/s at the harder spot and 1.3 m/s for the soft one.

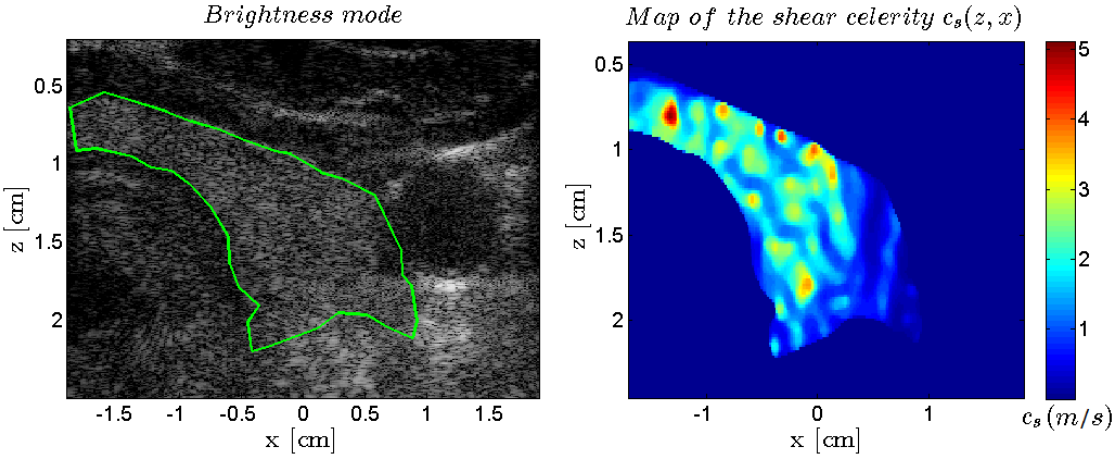

Figure 1 - Left: Image of the Thyroid - Right: 2-D celerity map

Conclusions: Our method illustrates an original way to produce an acoustic field from voice for thyroid elastography application.

Acknowledgements: This study was supported by Region Centre BRAINMUT project

References:

[1] Wuerfel J et al.Neuroimage. 49(3):2520-5, 2009
[2] Cathelin S et al. Phys Rev Lett. 100(6):064301, 2008
[3] Hoeks et al. UMB 20,pp.953-965, 1994.

013 **DEVELOPMENT OF NON-INVASIVE *IN VIVO* CEREBRAL ULTRASOUND ELASTOGRAPHY USING MULTIFREQUENCY TIME-HARMONIC VIBRATION.**

B Kreft[1], F Schrank[1], Judith Bergs[1], J Braun[2], I Sack[1] H Tzschätzsch[1]*

[1]Departement of Radiology, Charité—Universitätsmedizin, Berlin, Berlin, GERMANY; [2]Institute of Medical Informatics, Charité—Universitätsmedizin, Berlin, Berlin, GERMANY.

Background: Until now, *in vivo* information of the mechanical properties of the brain are only accessible non-invasively using time-harmonic magnetic resonance elastography (MRE) [1]. Time-harmonic tissue excitation in the low audible frequency range can generate shear waves in the entire body including the brain. Time-harmonic elastography (THE) using ultrasound was recently demonstrated in several abdominal organs [2], but has never been applied to the brain.

Aims: Developing THE for the non-invasive *in vivo* application in the human brain.

Methods: We examined the brains of 15 healthy volunteers (mean age 42 years, range 21 – 86 years). For each subject, 20 measurements were performed. To stimulate shear waves inside the cranial cavity, a patient bed with an integrated loudspeaker driven by a waveform of six superimposed frequencies in a range from 27 to 56 Hz was used. Tissue displacements were measured *in vivo* through the temporal bone window using a convex ultrasound probe (C5-2/64) operated with 2 MHz. To provide full-field-of-view maps of the shear wave speed (SWS) (figure 1) the *k*-MDEV algorithm described in Tzschätzsch *et al.* was used [2]. Inter- and intra-operator variability was tested in repeat experiments by two operators before and after volunteers were asked to stand up and move around.

Results: Cranial SWS measurements were feasible in all volunteers. Group mean SWS was measured with 1.59 ± 0.05 m/s. The test – retest experiments showed an intra- and inter-operator reproducibility of 90.8 % and 80.9 %. We also observed a significant SWS correlation with age (r = -0.76, $P = 2 \times 10^{-5}$) which corresponds to a SWS decrease of 2 % per decade as shown in figure 2.

Conclusions: Time-harmonic elastography is able to consistently measure mechanical properties of the brain tissue through an intact skull bone *in vivo*. The observed brain softening due to age may be related to intrinsic property changes as known from MRE [1,3]. Overall, our mean value of brain SWS measured by THE agrees to studies by MRE (1.48 ± 0.07 m/s). Further possible applications of cerebral THE is the non-invasive detection of intracranial pressure changes, which could lead to several applications in neurology and neurosurgery.

References:

[1] Sack I et al.: PloS ONE, 6(9), 2011
[2] Tzschätzsch H et al.: Med Image Anal, 30 1-10, 2016.
[3] Morrison J H et al., Science, 278 (5337), 412-9, 1997

Figure 1.

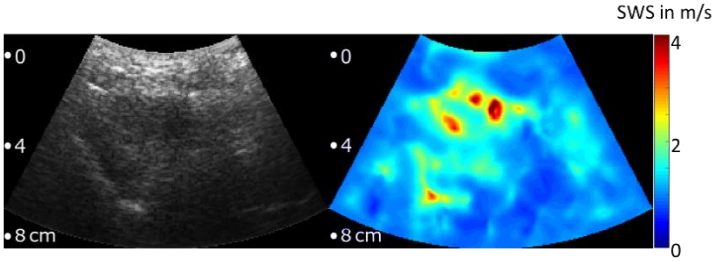

Figure 2.

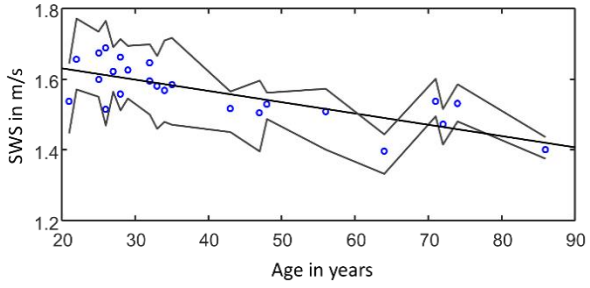

Figure 1. B-Mode of brain parenchyma (left) and corresponding elastogram (right).
Figure 2. Age related decrease of SWS observed by THE with confidence interval and linear regression.

029 **HARMONIC MOTION ELASTOGRAPHY FOR DIFFERENTIATION BETWEEN PANCREATIC DUCTAL ADENOCARCINOMA FROM THE PRELISIONAL AND NON-CANCEROUS TISSUE IN POST-SURGICAL HUMAN SPECIMENS.**

Alireza Nabavizadeh[1], Thomas Payen[1], Alina C Iuga[1], Kenneth P Olive[1], Elisa E Konofagou[1]*
[1]Columbia University, New York, NY, USA.

Background: Pancreatic Ductal Adenocarcinoma (PDA) tumors are one of the most aggressive malignancies. Until now, the best method for prolonging the survival rate is surgical resection. However, the recurrence rates are very common with poor outcomes. In addition, the margins of PDA tumors are often uncertain.

Aims: In this study, Harmonic Motion Elastography (HME) method was used to assess its capability in differentiating between the tumor, T, perilesional, P, and non-cancerous, N, part of specimens based on the Young's modulus estimation of each part.

Methods: A Focused Ultrasound (FUS) transducer (4.5 MHz) generates harmonic motion at an excitation frequency of 50Hz. while a phased array (2.5 MHz) aligned confocally with the FUS transducer acquires the radio frequency (RF) signals at frame rate of 1000 Hz. A 1-D cross correlation method with window size of 0.98 mm long and 95% overlap is applied on RF signals to estimate the local displacement. The shear wave speed can also be measured by applying a 2D directional filter on the displacement. The 2D Young's modulus (YM) value is measured based on the shear wave speed. To generate the final 2D Young's modulus map a raster scan at the step of 4 mm is performed in 2D. It should be noted that the translation of shear wave speed to Young's modulus is based on the assumptions that soft tissue are incompressible, isotropic, linear and elastic in which none of them are true in reality; however, it gives the closest estimation of stiffness using noninvasive method like HME.

Results and Discussion: HME was applied on 19 specimens with PDA tumors. Figure.1 depicts the 2D YM map using HME method on one of the specimens. Figure.2 illustrates the overall results of HME application on 19 specimens. This figure shows the estimated Young's modulus for the non-cancerous region (blue part), the tumor (red part) and perilesional tissue (green part).

Conclusion: This study shows that HME has the capability of differentiating between the tumor, the perilesional tissue and the non-cancerous region based on the Young's modulus map ex vivo.

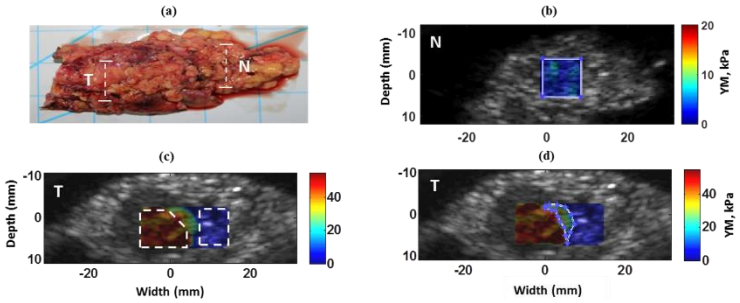

Figure 1. (a) Post-surgical pancreas specimen specified with T as tumor part and N is Non-cancerous part. (b) The overlay of 2D Young's modulus map of Non-cancerous part on its B-mode image. The estimated YM for specified region is (3.4 ± 1.1) kPa. (c) The overlay of 2D Young's modulus map of tumor , red part, along with its perilesional region, green part, and non-cancerous region, blue part on its B-mode image. The estimated YM for tumor part specified with dashed white line is (48.8 ± 9.4) kPa. and non-cancerous part specified by dashed white line is (3.8 ± 1.9) kPa. (d) Perilesional part of tumor specified by white line. The estimated Young's modulus for this part is (25.7 ± 8) kPa.

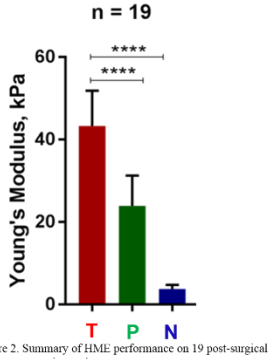

Figure 2. Summary of HME performance on 19 post-surgical human pancreatic specimens.
T: Tumor part. P: Perilesional part, N: Non-cancerous part.

045 SURFACE WAVES OPTICAL TOMOGRAPHY: PHANTOM STUDY

A Zorgani[1] , M Lescanne[1] , A Bel-Brunon[2] , T A Ghafour[2] , S Catheline[1.]*

[1]LabTAU, U1032 INSERM, Lyon, FRANCE; [2]LaMCos, INSA-Lyon, Villeurbanne, France.

Background: Using Elastography, tissue elasticity can be retrieved from shear wave speed measurement. Optical Coherence tomography (OCT) is, nowadays, an optical based technic developed in this field. This technique uses laser beam and interferometry in order to measure the wave displacement. Thus, it offers an information at a shallow depth. However, this kind of systems are sometimes very cumbersome.

Aims: The aim of the present study is to use a simplified system (only an optical ultrafast camera) to measure the speed of an induced surface waves at the surface of phantom from Particle Velocimetry Imaging (PIV) algorithms.

Methods: The experiments were conducted on a homemade gelatin phantom, the waves on the phantom surface were generated by a point- like source connected to an electrodynamic shaker. The generated signal was a single period sinusoidal burst and was trigged by the camera system. The surface of the sample was enlightened with a LED lighting system to obtain high quality images on the optical cameras. Two types of experiments were performed using a high frame rate optical camera. First, using a single camera, the displacements were measured only in a plane surface. Second, using two cameras, out of plane displacements were also captured.

Three different kinds of phantom were tested: an isotropic plane, an anisotropic plane and an isotropic dome shaped phantom. The displacement field was computed by a standard optical tracking technique.

Results: First, these experiments demonstrate the feasibility of a fully optical system to track surface wave. Second, the accuracy of surface wave speed measurement was demonstrated on two different phantom, isotropic and anisotropic. Finally, surface wave were tracked on a curved surface, and there speed wave measured.

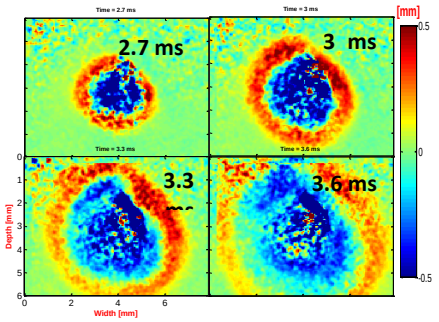

Conclusions: This feasibility study shows the feasibility of optical tomography system to detect and track surface waves. Thus, it can offers simple system for the measurement of the elasticity at the surface of organs such as the cornea or the skin.

039 **NON-CONTACT DYNAMIC OPTICAL COHERENCE ELASTOGRAPHY FOR VARIOUS BIOMEDICAL APPLICATIONS..**

Salavat R. Aglyamov[1], Kirill V. Larin[1,2]*

[1]University of Houston, Houston, TX, USA; [2]Baylor College of Medicine, Houston, USA.

Background: Optical Coherence Elastography (OCE) is a branch of elastography that uses Optical Coherence Tomography (OCT) to measure the motion of tissue in response to applied excitation. In comparison with other imaging modalities used in elastography, such as ultrasound or magnetic resonance imaging, OCT has significant advantages in terms of resolution, speed and accuracy of motion estimation, but limited by the low penetration depth of light. Therefore, OCE is an ideal imaging technique to measure biomechanical properties of ocular tissues, skin, and other superficial tissues in clinical applications, small animal models and ex-vivo studies.

Aims: In this work we review our recent results of using OCE in various biomedical applications, including characterization of ocular, cardiac and colon tissues.

Methods: The home-built OCE system was composed of a focused air-pulse delivery system or focused single element transducer and a phase-stabilized swept source optical coherence tomography (PhS-SSOCT) system. The focused air-pulse delivery system was comprised of a controller with a signal input for synchronization, a solenoid-controlled air gate, and an air-pulse port with a flat edge and diameter of ~150 μm. The system is capable of delivering a short duration focused air-pulse (≤1 ms) with a Gaussian profile. To generate the acoustic radiation force a single element ultrasound transducer at 3.7-MHz central frequency was employed in the system. The OCT systems utilized a broadband swept laser sources with a central wavelengths in the range from 810 to 1310 nm, and scan rates from 25 to 62 kHz. In the experiments we analyzed the surface wave propagation, as well as characteristics of displacement time profiles from a single localized pulsed stimulation. Mechanical properties of tissue were evaluated based on developed mathematical model of the dynamic deformation of the viscoelastic medium (Voigt model) in response to short pressure pulse. This approach was applied to evaluate the influence of the intraocular pressure (IOP) and cold cataract development on the elastic properties of the porcine crystalline lenses ex-vivo. To study corneal biomechanics we considered the effects of corneal thickness on the measured corneal biomechanical properties by experimentally altering the tissue hydration state and stiffness. In mouse model of myocardial infarction the changes in tissue biomechanics after myocardial infarction were evaluated in terms of isotropic and anisotropic elastic properties. Also, using the model of dextran sulfate sodium induced colitis in mice we measured the effect of ulcerative colitis on the stiffness of colon tissue.

Results: The results of these studies demonstrated that OCE is sensitive to the changes in the physiological tissue conditions. The crystalline lens measurements showed significant increase in the speed of the surface wave due to formation of the cold cataract. All mechanical parameters estimated in the experiments demonstrated that the stiffness of the lens increased as IOP increased, and the change in elasticity could be generally reversed by decreasing IOP. However, this effect was much less pronounced than in the cornea and sclera. Quantification of Young's modulus in corneal studies demonstrated that the cornea stiffens as it dehydrates, such that the effect of the changes in the thickness and stiffness on the speed of elastic wave propagation can be separated. In comparison with sham, the infarcted heart features a fibrotic scar region with reduced elastic wave velocity, decreased natural frequency, and less mechanical anisotropy at the tissue level at the sixth week post-myocardial infarction, suggesting lower and more isotropic stiffness. In an inflammatory bowel disease animal model OCE revealed reduced the value of the Young's modulus in diseased colon in comparison with control health tissue.

Conclusions: Dynamic OCE is a promising tool for noninvasive measurement of the tissue mechanical properties for many biomedical applications.

Acknowledgements: This study was supported by NIH grants R01EY022362, R01HL130804, and DOD CDMRP grant PR150338

009 **HIGH-SPEED PHASE-RESOLVED INTRAVASCULAR OPTICAL COHERENCE ELASTOGRAPHY.**

Tianshi Wang[1], Tom Pfeiffer[2], Ali Akyildiz[1], Wolfgang Wieser[3], Heleen van Beusekom[1], Geert Springeling[1], Frits Mastik[1], Antonius Franciscus Wilhelmus van der Steen[1,4,5], Robert Huber[2], Gijs van Soest[1].

[1]Erasmus University Medical Center, Rotterdam, THE NETHERLANDS; [2]Universität zu Lübeck, Lübeck, GERMANY; [3]Optores GmbH, München, GERMANY; [4]Shenzhen Institutes of Advanced Technology Chinese Academy of Sciences, Shenzhen, CHINA; [5]Delft University of Technology, Delft, THE NETHERLANDS

Background: Optical Coherence Elastography (OCE) is a powerful technique that can image displacement and strain of the sample, providing tissue elasticity information in addition to the conventional Optical Coherence Tomography (OCT) technique [1]. OCE measures the phase shift of each pixel at two different time points, which is associated by the tissue displacement. Such phase resolving method, however, relies heavily on accurate pixel-level co-registration, which restricts the application of OCE to bench top studies, and so far no catheter-based phase-resolved OCE has been achieved.

Aims: We aim to realize the first catheter-based phase-resolved intravascular OCE (IV-OCE) to image the strain of coronary artery and to detect atherosclerosis plaque.

Methods: The IV-OCE system consists of a 1.5 MHz Fourier Domain Mode Locked OCT engine and a motorized catheter [2,3]. The phase shift was extracted from two frames that were acquired at different intraluminal pressures. The gradient of the phase shift was further converted to strain. The intraluminal pressure was controlled by a home made infusion pump, and measured by a Combitrans disposable transducer. Fig. 1(a) shows the experiment setup, and (b) shows the frame-based phase signal processing.

Results: Imaging experiments were conducted in human coronary artery in vitro by running the system at 3000 frames/s. The IV-OCE system captured the artery wall strain when the intraluminal pressure drops from ~110 mmHg to ~20 mmHg within in 1 second. As shown in Fig. 1(c), much smaller strain was detected in the calcified plaques than that of the normal artery walls. Tissue type information is provided in addition to the conventional intensity OCT images.

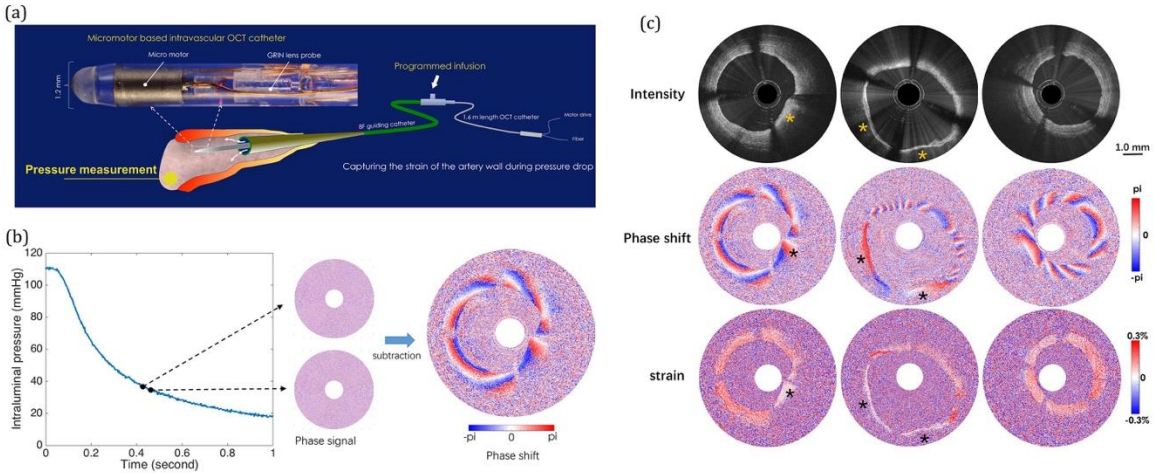

Fig. 1(a) Schematic diagram of experimental setup and photo of the motorized catheter. (b) Signal processing for the phase shift. (c) Imaging results of calcified plaques in left and middle columns and healthy artery in right column. * indicates the calcified plaques.

Conclusions: In this study, we demonstrate the first catheter-based, phase-resolved IV-OCE. It relies on a super fast phase-sensitive OCT engine and a motorized catheter. The results show that the IV-OCE can capture the artery wall strain that is induced by intraluminal pressure change. The calcified plaques can be clearly identified in the strain images due to their higher stiffness.

Acknowledgements: We acknowledge the financial support from Nederlandse Organisatie voor Wetenschappelijk (NWO) (104003006 and Veni 15940); Deutsche Forschungsgemeinschaft (DFG) (DFG—HU 1006/6); H2020 European Research Council (ERC) (ERC CoG Funding. Onderzoek ENCOMOLE-2i, 646669).

References: [1] Wang et al: 2015, Journal of Biophotonics. [2] Wang et al: 2013, Optics Letters. [2] Wang et al: 2017, Optics Letters.

002 **CELLQUAKE ELASTOGRAPHY: ULTRAFAST IMAGING OF CELL ELASTICITY.**

Pol Grasland-Mongrain[*1,4], *Ali Zorgani*[2], *Shoma Nakagawa*[3], *Simon Bernard*[4], *Lia Gomes Paim*[3], *Greg Fitzharris*[3,5], *Stefan Catheline*[2]* *and Guy Cloutier*[4,6,7].

[1]Laboratoire de Physique, Ecole Normale Supérieure de Lyon, Lyon, FRANCE; [2]LabTAU, INSERM u1032, University of Lyon, Lyon, FRANCE; [3]Oocyte and Embryo Research Lab., CRCHUM, Montreal, QC, CANADA;[4]Lab. de Biorhéologie et Ultrasons Médicaux, CRCHUM, Montreal, QC, CANADA;[5]Department of Obstetrics and Gynecology, University of Montreal, Montreal, QC, CANADA;[6]Department of Radiology, Radio-Oncology and Nuclear Medicine, University of Montreal, Montreal, QC, CANADA;[7]Institute of Biomedical Engineering, University of Montreal, Montreal, QC, CANADA.

Background Cell elasticity is mainly measured using static elastography method, i.e., by measuring the deformation following an applied force [1]. Measurements hardly make images of cell interior, and can take up to a few minutes. Shear wave elastography method, developed at the organ scale, could be adapted at the cellular level to get quick and robust measurements. It however requires high speed imaging, up to 100.000 images per second.

Aims: The cellquake elastography aims to apply the shear wave elastography technique on cells.

Methods: A 80 um diameter mouse oocyte was held by a pipette. A second pipette in contact with the oocyte was oscillating at 15 kHz with a piezoelectric actuator (piezo impact drive unit; Prime Tech Ltd, Japan). The cell was observed with a 100,000 frames/second camera (Phantom Research v2512, CA, USA) attached to a x100 microscope. Displacements were computed with a Lucas-Kanade optical flow method. Elasticity was computed using a passive elastography method [2].

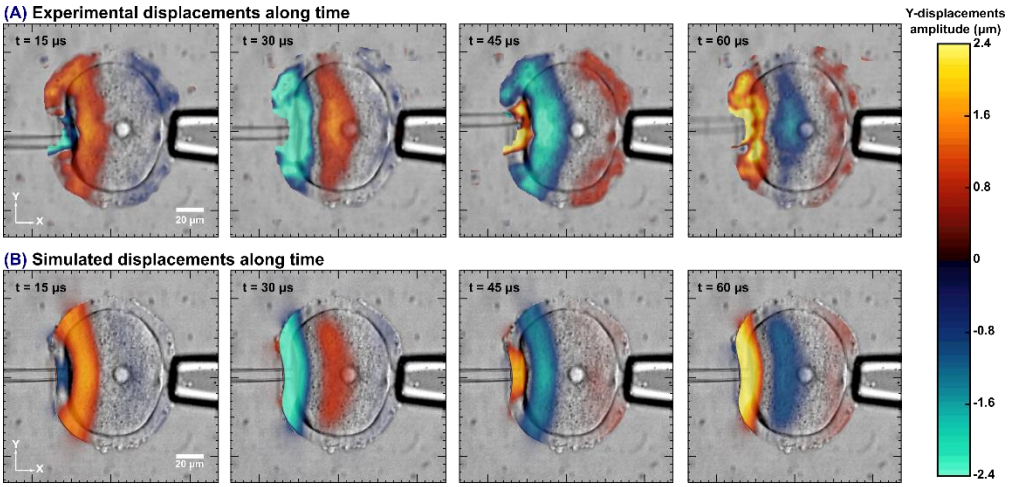

Results: Shear wave have been successfully induced in the oocyte, with a good agreement between experimental and simulated results. Elasticity images of cells have been computed. Adding cytochalasin B, a softening toxin, to the cell lead to a significant ($p<0.02$) decrease of elasticity.

Conclusions: Feasibility of the shear wave elastography technique at the cellular level has been demonstrated [3].

Acknowledgements: This work was supported by a postdoctoral fellowship award from the Natural Sciences and Engineering Research Council of Canada (NSERC) (P.G.-M.), a MEDITIS postdoctoral fellowship from NSERC provided by the Institute of Biomedical Engineering of the École Polytechnique and University of Montréal (S.B.), Fonds de Recherche du Québec – Nature et Technologies Grant PR-174387, and Canadian Institutes of Health Research Grants MOP-84358 and MOP-142334.

References: [1] Kuznetsova, T.G., Starodubtseva, M.N., Yegorenkov, N.I., Chizhik, S.A. and Zhdanov, R.I., 2007. Atomic force microscopy probing of cell elasticity. *Micron*, *38*(8), pp.824-833.
[2] Zorgani, A., Souchon, R., Dinh, A.H., Chapelon, J.Y., Ménager, J.M., Lounis, S., Rouvière, O. and Catheline, S., 2015. Brain palpation from physiological vibrations using MRI. *Proc. Nat. Acad. Sc.*, *112*(42)
[3] Grasland-Mongrain, P., Zorgani, A., Nakagawa, S., Bernard, S., Paim, L.G., Fitzharris, G., Catheline, S. and Cloutier, G., 2018. Ultrafast imaging of cell elasticity with optical microelastography. *Proc. Nat. Acad. Sc.*

032 **AN ULTRASOUND PROBE INDENTER FOR THE NON-LINEAR MECHANICAL CHARACTERIZATION OF SOFT TISSUES.**

Ajeethan Arulrajah[1,2], Benoît Wach[2], Laurent Barbé[1], Daniel George[1], Jonathan Vappou[1] and Simon Chatelin[1].*

[1]ICube, University of Strasbourg, CNRS UMR7357, 1 place de l'hôpital, Strasbourg, FRANCE; [2]IHU Strasbourg, Institute of Image-Guided Surgery, 1 place de l'hôpital, Strasbourg, FRANCE.

Background: Ultrasound elastography techniques allow measuring quantitatively the viscoelastic properties of soft tissue. Nevertheless, most of them are restricted to small deformation [1], while soft tissues exhibit strong non-linear elastic behavior under large deformation. Little work is currently available in the literature on the *in vivo* quantification of non-linear parameters of soft tissues [2]–[5].

Aims: The aim of this study is to develop a method for estimating non-linear elastic parameters of soft tissues. The method relies on the coupling between ultrasound displacement imaging and indentation. By the use of numerical model identification, the non-linear elastic parameters are non-invasively extracted.

Methods: The approach can be described in three main steps (fig 1).

i. Indentation process: a 9 MHz ultrasound linear probe (*L12-5 50mm, Philips healthcare, NL*) is used as indenter to generate large deformations (~20% of strain with maximal strain rate of 0.1 s^{-1}) in the tissue. The probe is attached to a robotized prototype and a force sensor is used to measure the force (6 axis Force/Torque sensor *Nano17, ATI Industrial Automation, NC, USA*) applied by the indenter to the tissue.
ii. Imaging part: the same ultrasound probe is used to acquire beamformed radiofrequency (RF) signals during the indentation at a frame rate of 500 Hz, using a plane wave beamforming sequence with an acquisition system (*Verasonics Inc., WA, USA*). 2D displacement fields are computed offline using a normalized cross correlation algorithm [6].
iii. Identification process: the indentation experiment is simulated numerically using a commercial finite element software (*Abaqus Simulia, Dassault Systèmes, FR*). Tissue behavior is modeled using a hyper-elastic model (Neo-Hookean) and 2D displacement maps are computed subsequently. The identification of Neo-Hookean parameters is performed through minimization of the error between the experimental and the numerical displacement fields using the simplex algorithm [7].

To validate this method, an experiment on a polyvinyl alcohol hyper-elastic cryogel was conducted. Hyper-elastic properties were compared to those obtained with rheometry tests (uniaxial compression) as the ground truth.

Results: By application on a controlled gel phantom and comparison with classical rheometry measurements, we showed that the proposed method provides a good estimation of the non-linear behavior (hyper-elastic) parameters of the soft materials.

Conclusions: The proposed method enables the characterization of the non-linear mechanical properties of soft tissues for large deformations, such as liver tissue, non-invasively. The quantitative rheological models of liver elasticity could then be used to improve the numerical liver models used in surgical simulators. While here applied for Neo-Hookean hyper-elasticity, this technique thought to be applied for the characterization of a large variety of soft tissues by specific complexifications of the identified model.

Acknowledgements: This work was supported by the IHU Strasbourg (*Institut Hospitalo-Universitaire, Institute of Image Guided Surgery, ANR-10-IAHU-02*) and under the Investissements d'Avenir program for the Labex CAMI (*Computed Assisted Medical Interventions, ANR-11-LABX-004*).

References: [1] J Vappou 2012, *Crit. Rev. Biomed. Eng.* 40(2), 121-34 **[2]** Oberai *et al.* 2009, *PMB* 54(5), 1191-207 **[3]** Hall *et al.* 2009, *Proc. EMBS IEEE Conf.* 1967–70 **[4]** Renier *et al.* 2007, *Proc. IUS IEEE* 554–7 **[5]** Bernal *et al.* 2016, *IEEE UFFC* 63(1), 101–9 **[6]** Viola *et al.* 2003, *IEEE UFFC* 50(4), 392–401 **[7]** Nelder *et al.* 1965, *Comp. J.* 7(4), 308–13.

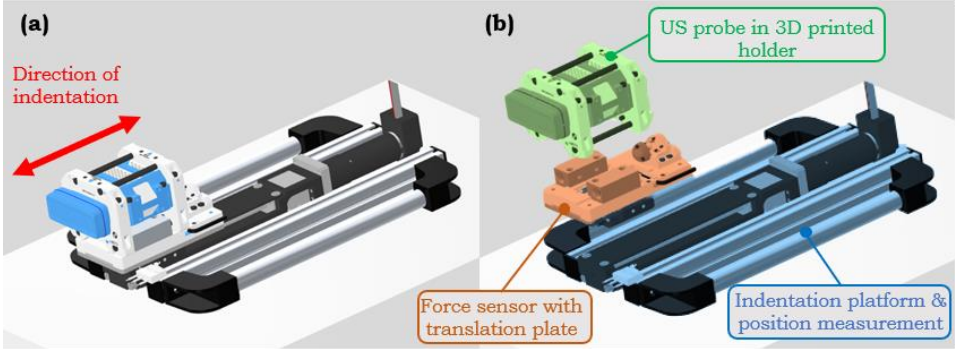

Figure 1: Indentation Prototype
(a) fully assembled view
(b) exploded view

022 **PASSIVE ELASTOGRAPHY FOR HIFU MONITORING: IN VITRO EXPERIMENTS.**

Bruno Giammarinaro[1], Paul Greillier[1], Stefan Catheline[1], Cyril Lafon[1]*
[1] LabTAU, INSERM, Centre Léon Bérard, Université Lyon 1, Univ Lyon, 151 cours Albert Thomas, F-69003, Lyon, FRANCE.

Background: High Intensity Focused Ultrasound (HIFU) methods are known to allow ablation in deep tissues. However, monitoring the treatment is required to control limitations due to ultrasound propagation. Previous studies have demonstrated that the formation of lesion can be observed as a change in tissue elasticity properties by elastography. Soft tissues elasticity is described by the shear modulus μ which is related to the shear wave velocity C and the density ρ by $\mu = \rho C^2$. Most of these studies have been performed with shear waves created by acoustic radiation force. This method presents some difficulties to obtain elasticity map in deep tissue. However, in the human body, there is a natural noise due to, for examples, cardiac activities and arterial pulsatility. Passive elastography, based on noise correlation, can estimate the shear elasticity from this diffuse wave field and it only depends on imaging techniques, allowing to measure elasticity of deep tissues.

Aims: The objective of the present study is therefore to evaluate the feasibility of the HIFU monitoring by passive elastography in soft tissues.

Methods: For that purpose, a probe composed of 5MHz 64-elements commercial imaging transducer and a 3-MHz HIFU transducer was used (Vermon, Tours). The HIFU part was a spherical transducer with a 40 mm radius of curvature, divided into 8 elements permitting a 17-55mm dynamic range. Lesions were produced *in vitro* in swine liver and heart samples with a 5 min sonication at 7 to 10.5 W/cm² acoustic intensity on the transducer surface (35% of duty cycle and 0.6 Hz of pulse repetition frequency). Imaging array was used with an ultrasound scanner (Vantage 256, Verasonics, Kirkland) which allowed high frame rate ultrasound acquisitions (700-1000Hz) to be obtained before and after lesion production using diverging wave emissions with 5 angles compounding. Sum-and-delay method was performed to beamform raw ultrasound data and speckle tracking algorithm was applied to estimate shear-wave displacements. Passive elastography maps were computed according to Catheline *et al.* [1]. Artificial shear waves were produced by an external vibrator (Model K2004E01, The Modal Shop, Cincinnati) fixed on the sample holder with frequency sweep between 50-500 Hz in order to create a diffuse wave field.

Results: Seven lesions were created and imaged. Every lesion was visible on elastography maps, showing a tissue stiffening in the targeted are. In liver samples, shear wave speed increased from 1.89±0.44m/s to 6.04±1.36m/s after sonication. In heart samples, it changed from 3.8±1.8m/s to 7.35±3.34m/s. The comparison of the lesions dimensions measured macroscopically and by elastography showed average differences of -1.2mm in length and 0.6mm in width in the imaging plane.

Conclusions: Observation of thermal lesions on macroscopic view and on shear wave velocity maps demonstrates the feasibility of monitoring HIFU treatments by passive elastography in *in vitro* tissues. *In vivo feasibility* has still to be proven. However, this could lead to a use of the natural noise in the body as in [2] for the brain in order to observe HIFU lesions.

Acknowledgements: Work supported by ANR, FUS Foundation and the Banque Publique d'Investissement (PIA, PSPC 2015).

References:

[1] Catheline S, Souchon R, Rupin M, Brum J, Dinh AH, Chapelon JY. Tomography from diffuse waves: Passive shear wave imaging using low frame rate scanners. Applied Physics Letters 2013; 103
[2] Zorgani A, Souchon R, Dinh A, Chapelon JY, Ménager JM, Lounis S, Rouvière O, Catheline S, Brain palpation from physiological vibrations using MRI. Proceedings of the National Academy of Sciences 2015; 112, p. 12917-12921

012 **GENERATION OF SHEAR WAVES IN SOFT MEDIA BY AN ELECTROMAGNETIC ACTUATOR.**

Zhishen Sun[1,2,3,4], Bruno Giammarinaro[1,2], Alain Birer[1,2], Guoqiang Liu[3,4], Stefan Catheline[1,2].*
[1]LabTAU INSERM U1032, Lyon, 69003, FRANCE; [2]Universtité de Lyon, Lyon, 69007, FRANCE; [3]Institute of Electrical Engineering, Chinese Academy of Sciences, Beijing, 100190, China; [4]University of Chinese Academy of Sciences, Beijing, 100049, CHINA.

Background: Elastography uses shear waves to measure or map the shear modulus which is one important parameter describing the elastic properties of biological tissues [1]. Electromagnetic actuators in magnetic resonance elastography are simple and inexpensive, and could work over a wide range of frequencies and produce large displacements on the order of 400 μm [2]. However, the electromagnetic actuators currently reported could only work in the MRE but not in ultrasound elastography or optical coherence elastography (OCE) because a strong static magnetic field was needed to create the Lorentz force. On the other hand, noncontact transcranial magnetic stimulation succeeded in generation of shear wave in soft biological tissues [3], but the shear wave produced by this method was too weak for clinical application—on the order of 0.5 μm. Moreover, this method required additional permanent magnets to create a static magnetic field. This article describes an electromagnetic actuator for the generation of shear waves in soft media.

Aims: This work aims to confirm the feasibility of generation of shear waves in soft media using an electromagnetic actuator.

Methods: The physics of the force acting on the actuator is explained using classical electromagnetism. The characteristics of the force acting on the actuator are studied by the displacement measurement using an interferometric laser probe (Interferometric probe SH-140, THALES LASER S.A., Orsay, France). The shear wave displacement field generated by the actuator in a polyvinyl alcohol (PVA) phantom is imaged by an ultrasound scanner (Verasonics Vantage 256TM, Washington, USA). The shear wave displacement field is also simulated using the Green function.

Results: The interferometric laser measurement confirms the characteristics of the force acting on the actuator. The actuator generates a shear wave field source of amplitude of 20 μm in the sample of PVA phantom. The shear wave fields created in the PVA phantom by experiments agrees well with that by simulation.

Conclusions: The electromagnetic actuator proves to generate strong shear wave displacement fields in a tissue-mimicking phantom, enabling more convenient ultrasound elastography.

Acknowledgements: This work is supported by the China Scholarship Council under reference 201604910849.

References: [1] Sarvazyan A. P., Rudenko O. V., Swanson S. D., Fowlkes J. B., & Emelianov S. Y. Shear wave elasticity imaging: a new ultrasonic technology of medical diagnostics. Ultrasound in Med. & Biol., 24(9), 1419, 1998.
[2] Muthupillai R., Lomas D. J., Rossman P. J., Greenleaf J. F., Manduca A., & Ehman R. L. Magnetic resonance elastography by direct visualization of propagating acoustic strain waves. Science, 269(5232), 1854, 1995.
[3] Grasland-Mongrain P., Miller-Jolicoeur E., Tang A., Catheline S., & Cloutier G. Contactless remote induction of shear waves in soft tissues using a transcranial magnetic stimulation device. Phys. Med. Biol., 61(6), 2582, 2016.

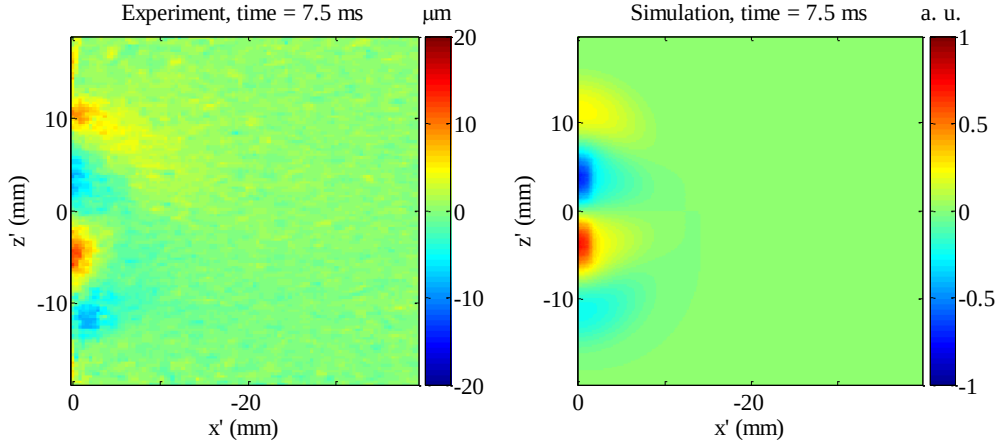

Figure 1. The longitudinal displacement field in the PVA phantom created by experiment (left) agrees well with that by simulation (right).

043 **DEVELOPMENT OF A COMPACT HAND-HELD DEVICE FOR USE IN QUASI-STATIC ELASTOGRAPHY: A PRELIMINARY STUDY ON TISSUE-MIMICKING PHANTOM.**

Abhilash Verma[1], Arun K. Thittai[1].*
[1]Indian Institute of Technology Madras, Chennai, INDIA.

Background: Quasi-static elastography is one of the prominent methods for imaging tissue elasticity distribution non-invasively. Currently, small compression to the tissue is applied using the imaging transducer itself in freehand by the operator. This leads to inter-operator variability (IOV) and inter-frame variability in the applied strain, which affects the image quality of the Axial Strain Elastograms (ASEs). Numerous studies have been done to overcome this limitation by either using a compression setup that is bulky [1] or by using a sophisticated motion controller setup, which is tailored only for a particular type of transducer [2]. Thus, there is a need to develop a compact compression device, which is versatile and can provide operator-independent and automated compression in elastography experiments.
Aims: 1. To develop a hand-held device for providing controlled and precise compression for use in quasi-static elastography. 2. Validation of the proposed device performance in elastography experiments and compare it against freehand compression method in tissue mimicking phantom.
Methods: The snapshot of the experimental setup is shown in Fig.1 (a). The major contribution of the work is the novelty in the design, where the controlled compression is achieved by moving an external compressor instead of the transducer itself; therefore our device can be attached to several US transducers irrespective of their size and weight. A spindle geared motor, position sensor, and controller manufactured by Maxon Motor AG (Sachseln, Switzerland) were used in the device to move the compressor uniaxially. SONIX TOUCH Q+® (Analogic, Peabody, MA, USA) ultrasound scanner with an L 14-5/38 transducer operating at 10 MHz center frequency was used for RF data acquisition. The proposed device was set to provide axial compression and relaxation of 3% at 1Hz on the phantom for three cycles. Two different operators were instructed to perform elastography experiments using the proposed device and freehand (i.e. using transducer itself) on the phantom. Data were acquired continuously at 15 fps in both the cases. The acquired data were synchronized with the start-frame before processing. ASEs were estimated using 2-D multi-level block matching algorithm [3] by taking consecutive frames as pre- and post- compressed RF data. The accumulated average axial strain was calculated for each frame to analyze the IOV within the cine-loop, obtained in freehand and using the proposed device.
Results: The results of accumulated average axial strain for each frame obtained from different operators by freehand and using the device are shown in Fig. 1 (b & c), respectively. Correlation coefficient between the operator performance when applying compression in freehand and by using the device was calculated as an estimate of the inter-operator agreement, which was found to be 0.39 and 0.88, respectively.

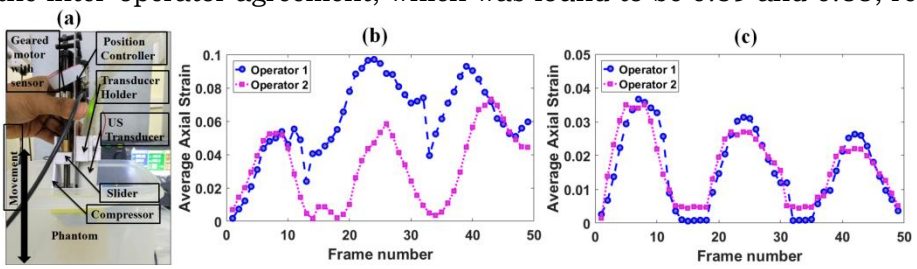

Fig.1.(a) A snapshot of experimental setup with annotations; (b & c) Plots showing the estimated accumulated average axial strain for both operators using freehand and the proposed device, respectively.

Conclusions: It can be concluded from the results that compression applied using the proposed device shows a lower IOV than when done with freehand.
Acknowledgements: This work was funded by MHRD, Government of India.
References: [1] T. Varghese, J. a Zagzebski, G. Frank, and E. L. Madsen, "Elastographic imaging using a handheld compressor," *Ultrason. Imaging*, vol. 24, no. 1, pp. 25–35, 2002.
[2] B. W. Anthony and M. W. Gilbertson, "Handheld force-controlled ultrasound probe," *J. Acoust. Soc. Am.*, vol. 134, no. 3, pp. 2377–8, 2013.
[3] A. K. Thittai et al. "Axial-shear strain distributions in an elliptical inclusion model: experimental validation and *in vivo* examples with implications to breast tumor classification." Ultra. Med. Biol., vol. 36, no. 5, pp. 814–20, 2010.

046 **TIME REVERSAL MIRROR OF SHEAR-WAVE FROM FIELD CONTROL TO SHEAR-WAVE ELASTOGRAPHY.**

C Zemzemi[12], J Aichele[12], S Catheline[12].*
[1]LabTAU INSERM U1032, Lyon, FRANCE ;[2]Universtité de Lyon, FRANCE.

Background: Improving cancer diagnostic is an important issue in oncology. Shear wave elasticity imaging techniques, known as elastography, have already shown their ability to locally retrieve the tissue elasticity and therefore suspicious cancer nodules. A method for enhancing the signal-to-noise ratio is discussed in this presentation. To characterize the tissue elasticity, most of the current technics use a single active external source to generate shear waves. This limits the use of elastography to the diagnosis of superficial (shallow) organs. In order to improve the diagnostics of deeper organs, such as prostate, spleen, we propose multiple shear wave sources and the use of time reversal in order to improve the control of the shear wave field. As in echography where the implementation of the phase array improved the imaging quality, the source array that we propose may improve the quality of shear wave imaging by enhancing the signal-noise ratio.

Aims: This work shows the use of multiple sources array for controlling the shear-wave field by time reversal and its advantages for improving shear wave imaging.

Methods: The experiments are conducted on a 5% gelatin phantom. Multiple shakers Cedrat[1] are placed around the phantom. After each stimulation, the impulse response is measured inside the phantom by a 5MHz ultrasound probe connected to an ultrafast Verasonics Vantage ultrasound scanner[2]. We use a standard phase correlation algorithm at 1000 Hz frame rate. The impulse responses are time-reversed and simultaneously sent back into the medium by their corresponding shakers.
[1] : Piezoelectric Actuators APA600MML, Cedrat technologies, Meylon, France
[2] : Vantage 256, Kirkland, USA

Results: The signal-to-noise ratio (SNR) of the beamformer improves by 10 dB compared to the use of a single source system. This is of special interest for deep organs that have so far been out of reach using elastography methods. Although still modest, the source array used perfectly controls the elastic field in space and time for multiple focal spots. This also holds true for the case where bone conduction delivers the shear waves. The time-reversal approach is adaptive, which is a great advantage, in that we can arbitrarily choose the positioning of the six-element array.

Conclusions: The use of several shear-wave sources provides improved SNR. It is our hope that this method will permit shear-wave elastography to be used to assess other mechanical parameters, such as nonlinearity and viscosity.

054 **ULTRASOUND BREAST TOMOGRAPHY: AN UPDATE.**

JC Bamber[1], J Fromageau[1], A Messa[1], S Bernard[1], A D'Aquino[1], A Ledger[1], M Schmidt[1], MJ Schoemaker[1], AJ Swerdlow[1], EAM O'Flynn[1], N Duric[2]*
[1]Institute of Cancer Research and Royal Marsden NHS Foundation Trust, London, UK;
[2]Delphinus Medical Technologies and Karmanos Cancer Institute, Detroit, USA.

Background:
Ultrasound tomography (UST) provides radiation-free, inexpensive, whole-breast, 3D, multiparametric imaging that is faster and more comfortable than MRI. The Softvue™ system (Delphinus Medical Technologies Inc., Detroit) produces images of sound speed (SS), attenuation coefficient (AC), a combination of SS and AC called stiffness, and relative reflectivity. We previously used magnetic resonance imaging (MRI) of volume-averaged water versus fat content as a reference, in a clinical study to demonstrate excellent capability of whole breast volume-averaged sound speed (VASS) obtained from UST to quantify breast density which is the single most important indicator of breast cancer risk (O'Flynn et al., 2017).

Aims:
Here, by further analysis of the data acquired during the clinical study, *in vivo* reproducibility of SS is assessed, stiffness compared with MRI, and VASS compared with mammographic density. Preliminary estimates of UST performance were obtained using phantoms.

Methods:
Forty three healthy female volunteers (age 29–59 years) underwent bilateral breast UST and 2-point Dixon MRI. A semi-automated algorithm was developed for segmenting the 3-D breast outline for VASS measurement. Left-right breast correlation was used to assess reproducibility of VASS and first-order volumetric texture properties of SS. Correlations between both VASS and stiffness, and MRI water, and (in a subset of 13) mammographic density (quantified using Cumulus™ software), were evaluated. To assess stiffness images *in vitro*, a commercial breast elastography phantom (CIRS, model 059) and a custom built gelatine phantom with solid inclusions were imaged using UST and compared with Young's modulus images provided by shear wave elastography (SWE) (Aixplorer®, Supersonic Imagine). To assess SS and AC, a custom built gelatine and agar phantoms containing inclusions filled with ethanol or castor oil, were scanned at various temperatures, and the results compared with independent measurements.

Results:
Stiffness correlated extremely well with breast composition estimated by MRI, although slightly less well than previously reported VASS with MRI. VASS correlated well with mammographic density, slightly better when the latter was estimated with craniocaudal than with mediolateral views. Good left-right breast correlation was obtained with VASS and with SS histograms of each breast, as well as with summary measures of histogram shape. In phantoms, a halo signature in the UST stiffness images signified the presence of a stiff mass on SWE. SS imaging was able to detect ethanol inclusions as small as 3 mm diameter. Accuracy of both SS and AC estimates varied, and average inclusion/background contrast decreased, with increasing inclusion size.

Conclusions:
Clinical UST provides reproducible VASS and SS volumetric texture measures. VASS and UST stiffness describe breast adipose/parenchymal composition well and hold considerable promise for breast density estimation. Preliminary evidence suggests that correlation with mammographic density may be reduced by variability in the latter. Mass stiffness in phantoms is visualized differently by UST and SWE, suggesting the need for a clinical comparison. Spatial resolution of SS imaging was good. SS and AC estimates and mass/background contrast vary with mass size. Development of the Softvue™ system has continued since this work. Therefore similar testing is now required with the latest version.

References:
O'Flynn EAM, Fromageau J, Ledger A, Messa A, D'Aquino A, Schoemaker M, Schmidt M, Duric N, Swerdlow AJ, Bamber J (2017) Ultrasound tomography evaluation of breast density: a comparison with non-contrast MRI. Investigative Radiology; 24 Jan 2017. doi: 10.1097/RLI.0000000000000347

008 **BREAST CHARACTERIZATION BY VELOCITY AND PROPAGATION COMPLEXITY OF SHEAR WAVE USING REAL-TIME PROPAGATION MAPPING.**

Y Yamakoshi[1], K Taniuchi[1].*

[1]Gunma University, 1-5-1 Tenjin, Kiryu, Gunma, JAPAN.

Background: Propagation of shear wave is affected by refraction, reflection and diffraction in breast tissue, because the shear wave velocity varies greatly among the malignant tumor, fat tissue and mammary gland. As a result, the shear wave propagates complicatedly, and a three-dimensional shear wave field is formed around the malignant tumor having a particularly high velocity. This shear wave field reduces the accuracy of the velocity measurement by two-dimensional shear wave elastography. But, the complexity of the shear wave propagation becomes a useful parameter for diagnosing the breast tissue.

Aims: To visualize the shear wave propagation in breast tissue in vivo and to characterize the breast tissue by both the propagation complexity and velocity of shear wave, real-time shear wave elastography (Color Doppler Shear Wave Imaging: CD SWI)[1] is applied.

Methods: CD SWI is a real-time visualization method of continuous shear wave's wavefront using a conventional color flow imaging (CFI). When the shear wave is excited by a small exciter attached to tissue surface, and the frequency is set to n/4 (n: odd number) times of the pulse repletion frequency of ultrasound imaging system (shear wave frequency condition: SWFC), the shear wave's wavefront appears directly on CFI as a binary pattern consisting zero and maximum flow velocities. Signal-to-noise ratio of the CFI is enhanced by introducing Fourier analysis along the time axis. The forward propagated shear wave is extracted by directional filter applied on the wave-number space. In CD SWI, the shear wave velocity, propagation direction and wavefront maps are observed. The complexity of the propagation is estimated by the standard deviation of propagation direction inside ROI. CD SWI is suited for the shear wave velocity measurement of tissues containing very stiff part like a malignant tumor, because the velocity is analytically derived from the shear wave phase map and there is no upper limit on the measurable velocity. Time required for reconstruction of shear wave maps is 4 sec.

Results: Figs.(a-1) and (a-2) are the shear wave propagation maps which are observed by CD SWI for malignant tumor and normal mammary gland, respectively. Shear wave frequency is 235.3Hz (n=3 of SWFC). In a dashed circle in fig.(a-1), the shear wave, which is refracted at the boundary of stiff lesion, propagates in the down direction while changing the propagation direction along the boundary. Low velocity shear wave also propagates in the normal direction of the boundary. We carried out finite-difference time-domain (FD-TD) simulation in order to estimate the shear wave propagation inside the heterogeneous medium. The simulation result showed almost the same result in fig.(a-1). Right figure shows a result using the complexity of the propagation direction and the velocity for the malignant tumor and normal mammary grand. Two tissues are distinguished by considering both velocity and propagation complexity.

Conclusions: Low-cost and quantitative shear wave elastography was applied to breast imaging. A problem of the method is the penetration of shear wave into deep or very stiff tissues. The penetration depth is about several cm in this experiment. In order to improve the penetration, it is considered to select the lower frequency satisfying the SWFC, for example, the frequency of n=1.

Reference: [1] Y. Yamakoshi et al. IEEE Tran. on UFFC, 64, 340 (2017).

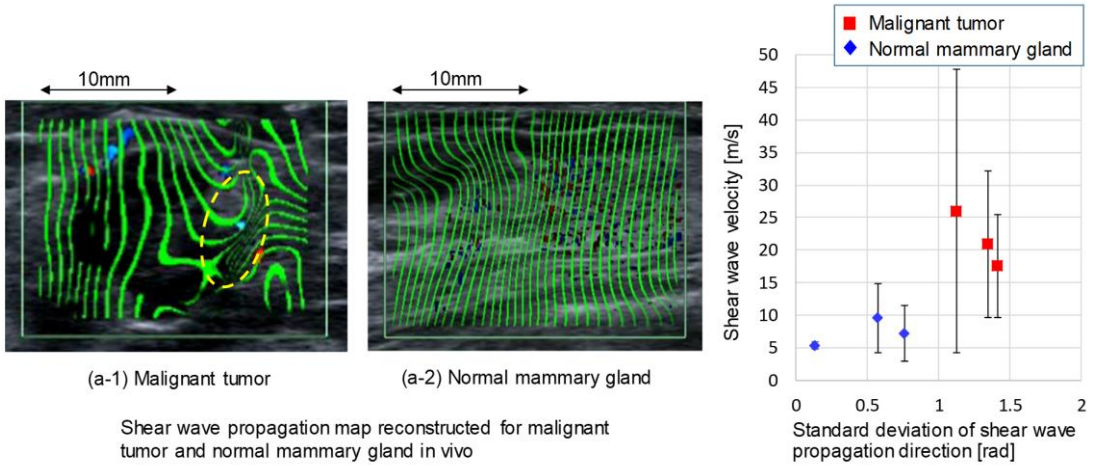

Shear wave propagation map reconstructed for malignant tumor and normal mammary gland in vivo

006 **ESTIMATES OF LOSSY MEDIA PARAMETERS.**

Zaegyoo Hah[1], Kevin J. Parker[2], Juvenal Ormachea[2], Dooyoung Na[1].*
[1]Samsung Medison Company, Ltd., SungNam, SOUTH KOREA; [2]University of Rochester, Department of Electrical and Computer Engineering, Rochester, NY, USA.

Background: Shear wave dispersion and attenuation are important characteristics of viscoelastic tissues and can be important diagnostic measures.

Aims: We extend the analytical treatment of two dimensional shear wave propagation in a biomaterial [1,2]. The approach applies integral theorems relevant to the solution of the generalized Helmholtz equation, and does not depend on a specific rheological model of the tissue's viscoelastic response.

Methods: Estimators of attenuation and shear wave speed are derived from the analytical solutions and these are applied to an elastic phantom and *in vivo* livers using a Samsung RS85 clinical ultrasound scanner.

Results: In these samples, estimated shear wave group velocities ranged from 1.0 m/s in the liver to 2.1 m/s in the viscoelastic phantom, and in phantoms these are cross-checked by independent measurements of shear velocity. Shear wave attenuation in normal livers is also estimated to be in the range of 7 dB/cm at 150 Hz.

Conclusions: Analytical models are developed that can predict the shape of shear waves produced by push pulses in viscoelastic tissues. These closed form solutions are also used to extract estimates of shear wave speed and shear wave attenuation, but do not rely on any single viscoelastic model for tissue, and so do not depend on traditional Kelvin-Voigt or Zener model parameters. Using the forward propagation model and its estimators, good agreement is found between measured and predicted waveforms. Furthermore, the model and estimator results are properly bounded by independent measurements of a phantom and liver obtained from the reverberant shear wave method. These developments may be useful in quantifying the biomechanical state of soft tissues.

Acknowledgements: We are grateful for support from Samsung Medison and for the loan of equipment.

References: [1] Parker KJ, Baddour N. The Gaussian shear wave in a dispersive medium. Ultrasound Med Biol 2014;40:675-684. [2] Parker KJ, Ormachea J, Will S, Hah Z. Analysis of transient shear wave in lossy media. Ultrasound Med Biol 2018;44:1504-1515.

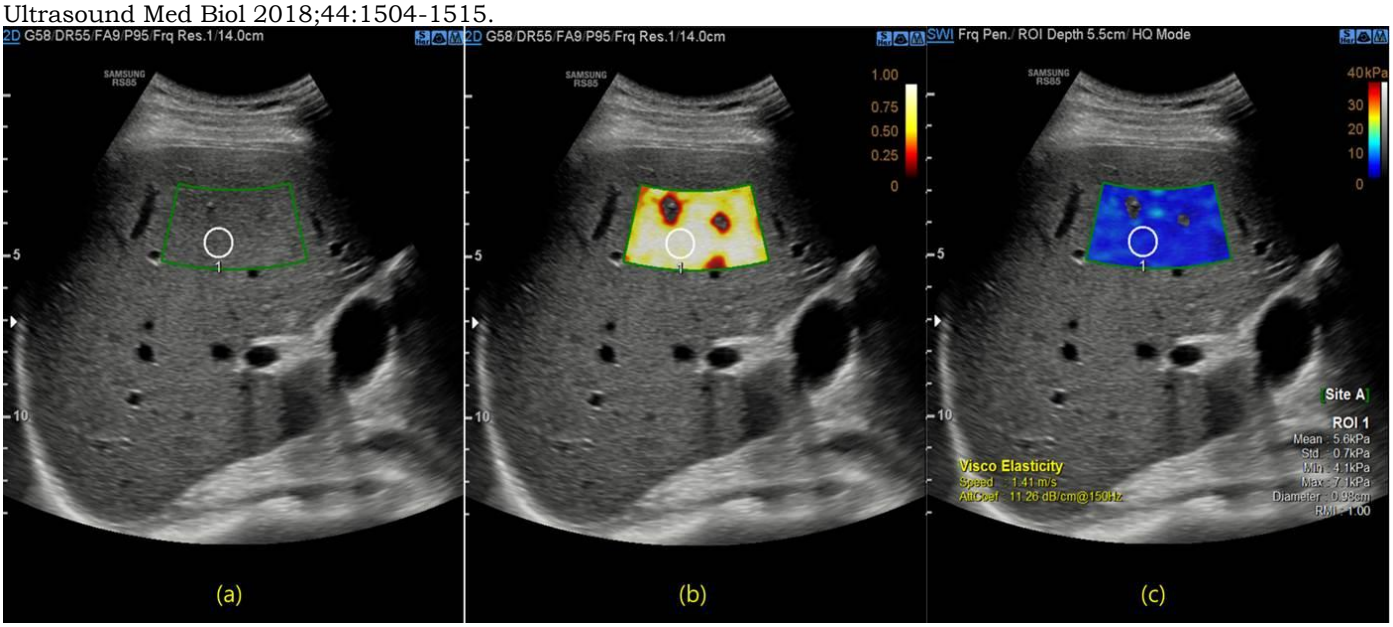

***In vivo* human liver. (a) B-scan. (b) Shear wave ROI with quality of measurement map and circle defining a local region of interest. (c) Shear wave ROI with speed map.**

038 **2D LINEAR DISPERSION SLOPE IMAGES USING A REVERBERANT SHEAR WAVE ELASTOGRAPHY FIELD: APPLICATION IN CIRS PHANTOMS AND *IN VIVO* LIVER TISSUE.**

Juvenal Ormachea[1], Benjamin Castaneda[2], Kevin J. Parker[1].*

[1]University of Rochester, Rochester, NY, USA; [2]Pontificia Universidad Catolica del Peru, PERU.

Background: Shear wave elastography estimates tissue stiffness by tracking the shear wave propagation. However, many methods assume shear wave propagation is unidirectional and aligned with the lateral imaging direction. Recently, a new method [1] was proposed to estimate tissue stiffness by creating a reverberant shear wave field propagating in all directions within the media. These reverberant conditions lead to simple solutions, facile implementation, and rapid viscoelasticity estimation of local tissue.

Aims: To obtain 2D linear dispersion slope (LDS) images using the local estimated shear wave speed (SWS) at different frequencies in CIRS phantoms and an *in vivo* human liver by applying a reverberant shear wave elastography (R-SWE) field.

Methods: Continuous harmonic reverberant shear waves were generated in a breast and a viscoelastic CIRS phantom (model 059, serial #2095.1-1, respectively) by applying vibrations using multi-frequency (80-360 Hz) external sources. A Verasonics ultrasound system was used to track the induced displacements. The SWS was estimated using the method described in [1,2], then the LDS was calculated from a chosen frequency range. A Samsung ultrasound system (model RS85, Samsung Medison, Seoul, South Korea) was used to measure the SWS for comparison purposes in the CIRS phantoms and it was considered as the reference method. Finally, the clinical feasibility of this technique was analyzed by assessing the SWS and LDS in an *in vivo* human liver under the requirements of informed consent and the University of Rochester Institutional Review Board

Results: Figure 1 shows 2D images of SWS and LDS for different cases: mean SWS of 2.49 m/s and 2.10 m/s (at 220 Hz), an accuracy error of 11.06% and 4.10% compared with Samsung system, and mean LDS of 0.25 m/s/100Hz and 0.69 m/s/100Hz were estimated using multifrequency excitations, for the breast and viscoelastic phantoms, respectively. For the *in vivo* liver, a SWS of 1.43 m/s at 200 Hz and a LDS of 0.61 m/s/100Hz were estimated.

Conclusions: It was possible to estimate the viscoelastic properties in phantom materials and *in vivo* human tissue using the R-SWE approach with consistent results in SWS and in LDS estimations. Moreover, results from the multi-frequency estimations indicate that it is not only feasible, but it can also more quickly assess frequency dependence than using single vibration frequencies, which facilitates the use of the R-SWE approach for clinical applications.

Acknowledgements: This work was supported by the Hajim School of Engineering and Applied Sciences at the University of Rochester. Juvenal Ormachea was supported by Peruvian Government scholarship 213-2014-FONDECYT. We are also grateful to Samsung Medison Co. Ltd. for loan of the equipment.

References: [1] Parker KJ, et al. "Reverberant shear wave fields and estimation of tissue properties." *Phys Med Biol* 62(3)1046-1061, 2017. [2] Ormachea J, et al. "Shear wave speed estimation using reverberant shear wave fields: implementation and feasibility studies." *Ultrasound Med Biol* 44(5)963-977, 2018.

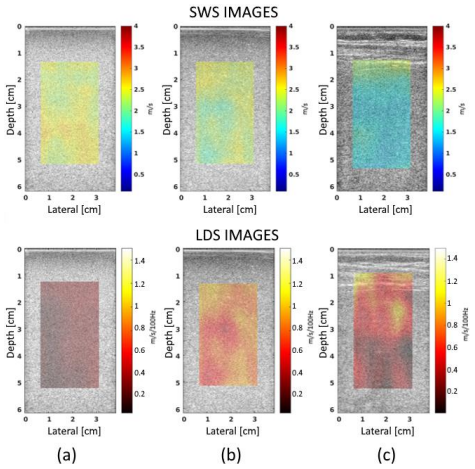

Figure1. SWS (top) and LDS (bottom) images using the R-SWE approach for (a) breast CIRS phantom, (b) viscoelastic CIRS phantom, and (c) *in vivo* human liver.

044 **IMAGING LABORATORY EARTHQUAKES WITH ULTRASOUND ELASTOGRAPHY.**

J Aichele[1], S Catheline[1], P Roux[2].*
[1]INSERM – U1032, 151 Cours Albert Thomas, Lyon, Rhone-ALpes, FRANCE; [2]Isterre, 1381 Rue de la Piscine, 38400, Saint Martin d'Hères, Rhone-alpes, FRANCE.

Background: We apply shear wave elastography, a medical imaging technique that uses ultrafast ultrasound to a geophysical research question. Earthquake ruptures are complex slip processes on a fault surface that include surface heterogeneities, friction laws and non-linear material processes. In order to better understand the nucleation of earthquakes seismologists build numerical and laboratory models and compare these to seismological observations. The imaging of the wavefield radiated by a laboratory rupture is fairly recent and to our knowledge is limited to photo-elasticity (Rosakis et al[1]) and shear wave elastography (Latour et al[2]).

Aims: In order to better understand friction and rupture processes which are responsible for earthquake nucleation, we build a laboratory experiment that reproduces the stick-slip behavior of a seismic fault for soft elastic materials. Imaging of the the wavefield by shear wave elastography allows us to characterize the rupture process.

Methods: The rupture process is generated by controlling a driving slab through a motor in synchronization with the ultrasound acquisition system. As an analog to a fault zone, a granular layer of sand or gravel constitutes the stick-slip behavior. Elastography allows us to get unique insights into shear-wave generation of rupture processes. In contrast to classical seismological methods, we are able to follow the wave propagation inside the sample and thus highly resolve the near and intermediate terms of the elastic wave-field.

Results: First results confirm the previously proven existence of super-shear or shear Mach cone as well as sub-Rayleigh rupture fronts for the in-plane shearing mode. Furthermore, the same barrier can break in different modes in one experiment. The displacements recovered from the particle velocity data indicate stress drops at regular intervals and thus the presence of repeating stick-slip events.

Conclusions: We experimentally retrieve the densely sampled shear wave field in the near source region of a rupture nucleation, a unique insight into earthquake source physics. Since our phantoms are very different from true rocks our model is however limited to an analysis of the physics. A quantitative comparison with historic earthquakes is beyond its scope. In the future, the use of passive elastography in combination with soft brittle materials could prove to be a new tool to monitor hysteresis and relaxation induced by rupture processes.

Acknowledgements: This project has received funding from the European Union's Horizon 2020 research and innovation programme under the Marie Sklodowska-Curie grant agreement No 641943 (ITN WAVES)

References: [1] Rosakis, A. J., & Coker, D. (1999). Cracks Faster than the Shear Wave Speed, 284(May), 1337–1340. [2] Latour, S., Gallot, T., Catheline, S., Voisin, C., Renard, F., Larose, E., & Campillo, M. (2011). Ultrafast ultrasonic imaging of dynamic sliding friction in soft solids: The slow slip and the super-shear regimes. EPL (Europhysics Letters), 96(January 2016), 59003. http://doi.org/10.1209/0295-5075/96/59003

049 **PASSIVE ELASTOGRAPHY OF THE ESOPHAGUS: AN IN VITRO APPROACH.**

Victor Delattre[1,2], Ali Zorgani[1], Sabine Roman[1,2], Stefan Catheline.[1]*
[1]Labtau, INSERM unit U1032, 151 Cours Albert Thomas, Lyon, 69003, FRANCE;[2] Hôpital Edouard Herriot, Hospices civils de Lyon, 5 place d'Arsonval, Lyon, 69003, FRANCE.

Aims: Numerous diseases alter the esophagus elasticity such as eosinophilic esophagitis or esophageal motility disorders like achalasia [1]. Being able to measure those modifications with minimally invasive technique is a key issue for the diagnosis of such pathologies. The ENDOFLIP is a probe that measures luminal cross sectional area of the esophagus at different points and across time. By using this commercially available device already used for clinical routine, we intend to track the propagation of shear waves naturally produced by physiological noise and compute wave length maps of the esophagus using passive elastography algorithms [2].

Methods: In order to assess the feasibility of such measurements we generated shear waves in in PVA gel tubes and compared the wavelength obtained with the ENDOFLIP to those obtained on the same gels with a high speed Chronos camera optically tracking the edges of the tube and therefore the propagation of waves. We first compared the wave length obtained on homogeneous gels with both techniques before using pairs of gels of different elasticity to investigate imaging possibilities.

Results: Although, the wave length computed with the ENDOFLIP and with the high speed camera showed some discrepancies, we were able to perform qualitative differentiation of gels when using pairs of gels with different elasticity. Using the high speed camera we measured wave speed of 1.5 m.s-1 for the hard gel versus 1 m.s-1 for the soft one. We also measured wave length of 10cm in the hard gel and 6cm in the soft gel. Using the ENDOFLIP, we were only able to measure wave length of 8cm in the hard gel and 5cm in the soft one due to poor time resolution.

Conclusions: Thus, using a commercially available device not yet used for this type of measurements, we were able to get promising results in vitro.
A study on pathologic human subjects is also being carried out and has already shown some interesting results.

References: [1] Carlson et al., Evaluation of Esophageal Motility Utilizing the Functional Lumen Imaging Probe, American Journal of Gastroanterology, 2016.
[2] Gallot et al., Passive Elastography: shear-wave tomography from physiological-noise correlation in soft tissues, IEEE Transactions on Ultrasonics, 2011.

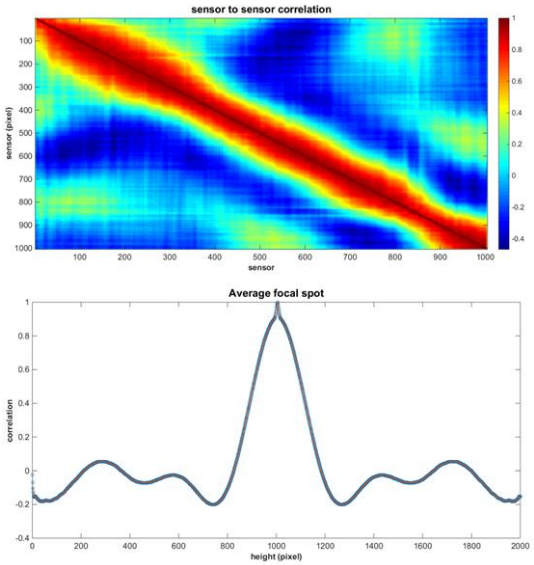

Correlation matrix of the diameter of a homogeneous gel tube and its average along the diagonal e.g. the focal spot.

014 **INFLUENCE OF PHYSIOLOGICAL ALTERATIONS TO BRAIN STIFFNESS MEASURED BY CEREBRAL TIME-HARMONIC ULTRASOUND ELASTOGRAPHY.**

B Kreft[1], H Tzschätzsch[1], F Schrank[1], Judith Bergs[1], J Braun[2], I Sack[1]*
[1]Departement of Radiology, Charité—Universitätsmedizin, Berlin, Berlin, GERMANY, [2]Institute of Medical Informatics, Charité—Universitätsmedizin, Berlin, Berlin, GERMANY.

Background: Time-harmonic ultrasound elastography (THE) has been proven sensitive to physiologically related stiffness changes of abdominal organs. It is known from magnetic resonance elastography that the mechanical properties of the brain can change at long time scales, which are age related [1]. However, also rapid changes caused by the alteration of blood flow are observable [2]. We hypothesize that THE can measure rapid stiffness changes of brain tissue due to cerebral changed blood flow as induced by the Valsalva-Maneuver or inspiration of carbogen gas.

Aims: To demonstrate the influence of physiological alterations to cerebral stiffness by *in vivo* THE.

Methods: Brain stiffness was measured by cerebral THE using the temporal bone window. The THE setup consists of a patient bed with an integrated loudspeaker for shear wave generation, a clinical ultrasound scanner (SonixMDP, Ultrasonix) for detecting tissue displacement and an elastography PC for computing the final shear wave speed (SWS) map [3]. To investigate the tissue response at a short time scale (several seconds), ten healthy subjects performed the Valsalva maneuver ten times in a row. The subjects were measured before and during each single maneuver (figure 1 b and c), so that 10 pairs of SWS values were recorded. To investigate the tissue response at longer time scales (several minutes), another group of ten healthy subjects was investigated 10 times before, 20 times during and 20 times after the inspiration of carbogen gas (95 % O_2, 5 % CO_2).

Results: While performing the Valsalva-Maneuver, each subject showed an elevated (1.60 ± 0.04 m/s vs. 1.77 ± 0.04 m/s) SWS (group mean ± standard deviation) a few seconds after the start of the maneuver (figure 2 a). Inspiration of carbogen gas yielded a continuous increase of SWS over several minutes (from 1.61 ± 0.11 m/s to 1.81 ± 0.11 m/s) with rapid return to baseline values directly after end of carbogen inhalation (figure 2 b).

Conclusions: To the best of our knowledge, our experiments demonstrate for the first time the influence of physiologically changed cerebral blood flow on *in vivo* brain stiffness. Both, the Valsalva maneuver and the inspiration of carbogen gas can result in a dilatation of brain vessels and increase in intracranial pressure, ICP [4] This might induce a mechanical pre-stress of the tissue resulting in the observed stiffening of the brain. Cerebral THE could be of potential clinical value for monitoring ICP in patients with pathological altered ICP values during therapy.

References: [1] Sack I et al.: PloS ONE, 6(9), 2011. [2] Guo J et al.: Quantification of biophysical Parameters in medical Imaging, Springer Verlag, 2018. [3] Tzschätzsch H et al.: Med Image Anal, 30 1-10, 2016. [4] Hirsch S et al.: Magnetic Resonance Elastography, Wiley-VCH, 2017

Figure 1.

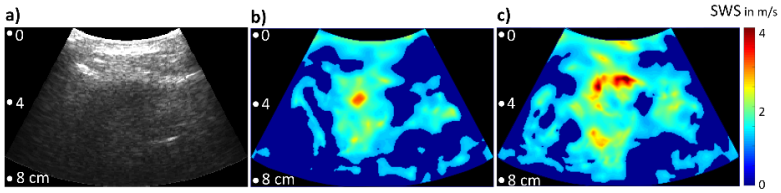

Figure 1. a) B-mode of brain parenchyma.
b) Elastogram before performing valsalva.
c) Elastogram while performing valsalva.

Figure 2. Box diagrams containing all mean values
a) of the Valsalva experiment.
b) of the Carbogen experiment.

Figure 2.

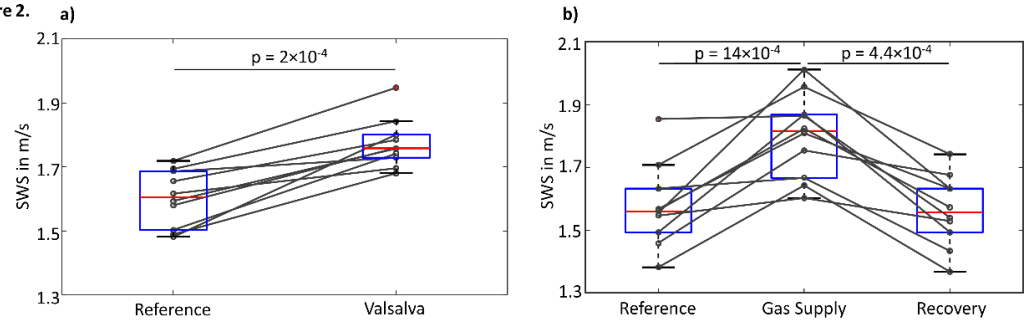

031 **3-D AXIAL STRAIN IMAGING FOR IMPROVED BREAST CANCER DETENTION IN VOLUMETRIC BREAST ULTRASOUND SCANNERS: PRELIMINARY *IN-VIVO* VALIDATION.**

GA Hendriks[1], C Chen[1], HH Hansen[1], CL De Korte[1,2]*

[1]Radboud university medical center, Medical UltraSound Imaging Center, Nijmegen, THE NETHERLANDS; [2]University of Twente, Physics of Fluids group, Enschede, THE NETHERLANDS.

Background: Mammography is the gold standard in breast cancer detection but less suitable for women with dense breast. Therefore, automated breast volume scanning (ABVS) using ultrasound was introduced as alternative. Although ABVS has high sensitivity, the specificity remains an issue resulting in high recall rates and unnecessary biopsies [1]. Strain imaging might be a solution to improve the specificity, since malignant lesions are generally stiffer than benign lesions and therefore will exhibit less strain when subjected to a similar force. In a previous study [2], we demonstrated that it was feasible to implement 3-D axial strain imaging in an ABVS-like system and validated this imaging technique in breast phantoms.

Aims: The aim of this study was to validate ABVS-based 3-D axial strain imaging *in vivo* in patients.

Methods: Female patients, who were scheduled for a breast exam in our hospital (Radboudumc, Nijmegen, The Netherlands), were imaged after providing informed consent. Next to their scheduled exam, RF data of two ultrasound breast volumes were acquired using single focus, line-by-line transmit-receive events by the ABVS (Acuson S2000, Siemens Healthineers, Issaquah, WA). In between these scans, the ABVS transducer was lifted automatically (1 mm) and during the scans (~15 seconds) the patient was asked to hold her breath. Next, displacements were calculated from the two RF data volumes using coarse-to-fine block-matching software. A least-squared strain estimator was used to calculate axial strains. If a lesion was detected during the regular breast exams, the ABVS B-mode volume was annotated and the axial strain ratio was calculated by dividing the mean background strain (same size as the lesion) by the mean strain inside the lesion. If no lesion was detected, an ellipsoid area (random size) was annotated at a random position inside the field-of-view to calculate the strain ratio.

Results: 20 patients participated in this study in which 1 invasive ductal carcinoma (IDC), 1 ductal carcinoma in situ (DCIS), 1 fibro-adenoma (FA) and 3 cysts were detected. In the remaining patients, no lesions were detected. The IDC, DCIS and FA showed strain ratios of 9.2, 0.7 and 1.5 respectively indicating that IDC has ~9 times lower strain compared to its environment and that it can be distinguished from FA. DCIS showed a strain close to its environment. An explanation for this low strain ratio might be that DCIS is often considered as a pre-cancerous lesion (pre-stadium of IDC) and therefore less stiff compared to an IDC resulting in a strain ratio close to 1. Strains in cysts were not evaluated, because strain estimation is prone to errors in such hypo-echogenic lesions. The 14 patients without detected lesions showed median strain ratio of 0.8 and interquartile range of 0.9 as expected since the annotated and background area both contained healthy tissue.

Conclusions: These initial results demonstrate that 3-D axial strain imaging in the ABVS is feasible, although the number of lesions is low and more patients will have to be included to demonstrate significant differences between groups.

Acknowledgements: This research is supported by the Dutch Technology Foundation STW (NKG 13290), which is part of the Netherlands Organization for Scientific Research (NWO), and which is partly funded by the Ministry of Economic Affairs.

References: [1] S. Wojcinski et al., BMC Medical Imaging, 13(36), 2013; [2] G.A. Hendriks et al., Physics in Medicine & Biology, 61(7), 2665-79, 2016.

048 **3D ULTRASOUND STRAIN IMAGING OF THE PUBORECTALIS MUSCLE.**

Shreya Das[1], Hendrik H. G. Hansen[1], Frieda van den Noort[2], Huub van der Vaart[3], Chris L. de Korte[1,4]*

[1]Medical UltraSound Imaging Centre (MUSIC), Department of Radiology and Nuclear Medicine, Radboud university medical centre, Nijmegen, THE NETHERLANDS; [2]Robotics and Mechatronics (RAM), University of Twente, Enschede, THE NETHERLANDS;[4]Physics of Fluids, Faculty of Science and Technology, University of Twente, Enschede, THE NETHERLANDS.

Background: The pelvic floor muscles provide support by compensating for gravity and abdominal pressure. During delivery some of them have to stretch up to three times their original length to allow for the passage of the baby. Frequently these muscles (for example, the puborectalis muscle or PRM) get damaged during childbirth, which can lead to irreversible damage. Due to this damage, women may suffer from disorders like pelvic organ prolapse or urinary and fecal incontinence [1-2]. 3D ultrasound (US) imaging can be used to image the pelvic floor muscles and detect the most severe cases of muscle damage. However, diagnosis of the damage is currently done in static images obtained from the movies, which is observer dependent and not reproducible [3]. Our hypothesis is that by US-based strain imaging the exact deformation and motion of these muscles can be quantified which will aid in diagnosing muscle failure and allow a patient specific treatment strategy.

Aims: This study explores if 3D strain estimation of the PRM is possible by following a standardized protocol in which the volunteers are asked to voluntarily relax, contract, stretch (by a Valsalva maneuver), and again relax the PRM.

Methods: Transperineal 3D ultrasound movies were obtained from female volunteers (n=9) at 12 weeks of their first pregnancy, using a curved array volume transducer connected to a GE Voluson V730 US machine at the University Medical Centre, Utrecht, The Netherlands. Volumetric DICOM US data were acquired of the PRM starting at rest and via, contraction to Valsalva, and back to rest again. Displacements were estimated in 3D using a normalized coarse-to-fine cross-correlation-based algorithm [4]. All displacements were calculated with respect to a reference frame chosen in rest just before contraction. Displacements were calculated for a region of interest (ROI) corresponding to the PRM muscle as manually segmented [5]. Finally, axial strains were calculated using a 3D Least Squares Strain Estimator (LSQSE) [4, 6].

Results: The median curve is showing a shortening during the contraction phase and a lengthening during the Valsalva phase. A maximum strain in active contraction of 4% is measured, while in Valsalva a passive lengthening of 2.5% is found. Subsequently, the strain returns to ~0% again when the PRM relaxes. The relatively low median axial strains can be explained by the fact that the muscle is oriented at an angle of ~45 degrees with respect to the axial direction.

Conclusions: These preliminary results show that strain imaging of the PRM is feasible in a pregnant volunteer. Future studies in multiple volunteers will have to explore the reproducibility of our method and investigate if strain imaging can be used to quantify damage of the PRM. Given the tilt angle of the muscle with respect to the axial direction, we recommend switching to principal strains. Real-time strain feedback during the acquisition would also be highly useful for optimal strain quality. However, these first results are promising and will hopefully lead to a new tool to classify damage of the PRM.

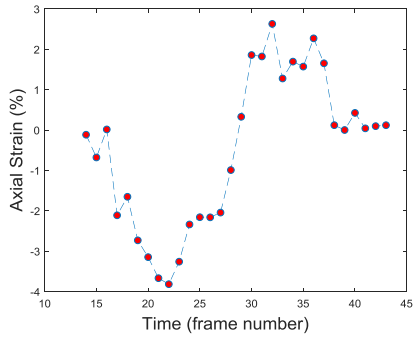

Fig. 1: Axial strain (%) in the puborectal muscle during contraction and subsequent Valsalva.

References:

[1] Bedretdinova D., et al.; Eur Urol 69(2):256-64, 2016.
[2] Dieter AA, et al.; Curr Opin Obstet Gynecol 27(5):380-4, 2015.
[3] van Veelen GA., et al.; Int Urogynecol J 25(11):1501-6, 2014.
[4] Hendriks, GAGM, et al.; Phys Med Biol 61(7):2665-79, 2016.
[5] van den Noort, F, et al.; Ultrasound Obstet Gynecol, epub ahead of print, 2017.
[6] Kallel F, et al.; Ultrason Imaging 19(3):195

019 **ELASTIC WAVES AFTER AORTIC VALVE CLOSURE IN HYPERTROPHIC CARDIOMYOPATHY PATIENTS AND HEALTHY VOLUNTEERS.**

M Strachinaru[1], M Michels[1], AE van den Bosch[1], JG Bosch[1], MD Verweij[2,1], AFW van der Steen[1,2], N de Jong[1,2], ML Geleijnse[1], HJ Vos[1,2].*

[1]Thorax Center, Erasmus MC, Rotterdam, Zuid-Holland, THE NETHERLANDS; [2]ImPhys, Delft University of Technology, Delft, Zuid-Holland, THE NETHERLANDS.

Background: Shear-like elastic waves in the heart walls are initiated by the closures of valves and can be measured with high frame rate tissue-Doppler ultrasound [1]. The propagation velocity of these waves can be used to estimate the stiffness of the myocardium [1,2]. This is important to detect early stages of e.g. hypertrophic cardiomyopathy and heart failure, where the myocardium is stiffer.

Aims: We compare elastic wave propagation velocities, originating from the aortic valve closure, on the septal wall of hypertrophic cardiomyopathy patients and normal individuals in a pilot clinical study.

Methods: Twenty known hypertrophic cardiomyopathy patients and twenty healthy volunteers matched for age and gender, were prospectively recruited and underwent a high frame rate color tissue Doppler study, synchronized to the simultaneous recording of the electrocardiogram and phonocardiogram. We used a clinical scanner (Philips IE33; Philips, Best, The Netherlands), equipped with a S5-1 probe, using a clinical tissue Doppler application achieving a frame rate over 500Hz in TDI by carefully tuning the normal system settings [3]. The slope of the shear-like elastic wave front velocity propagating in the basal interventricular septum after the closure of the aortic valve was computed along a virtual M-mode line using Philips Qlab 8 post processing software. The velocity of the shear wave induced by the closure of the aortic valve (synchronous to the onset of the 2nd heart sound) was averaged over 3 beats for every subject. We used a parasternal view to align with the particle velocity of the shear motion.

Results: Elastic waves were visible after the closure of the aortic valve, synchronous to the heart sound S2 and the ECG signal. The left figure shows a B-mode and TDI frame with the virtual M-mode line (dashed white line) on top. One heart cycle of a hypertrophic cardiomyopathy patient is shown in the middle panel, with the mean tissue Doppler velocity along the virtual M-mode line in the bottom panel. The yellow arrow points at the wave front which slope determines the propagation velocity of the wave. This velocity in the patient group was 6.25±1.10, range 4.33 to 9.33m/s. In the healthy volunteer group the velocity of the wave induced by aortic valve closure was 3.56±0.43m/s, range 3.00 to 4.66m/s.

Conclusions: The velocity range of the shear-like waves generated by the closure of the aortic valve can be measured with a clinical scanner and is significantly higher in hypertrophic cardiomyopathy patients, as compared to normal individuals. This shows that the technique is sensitive to elasticity differences.

Acknowledgements: This work is part of a TTW – Dutch Heart Foundation partnership program with project number
14740, which is (partly) financed by the Netherlands Organization for Scientific Research (NWO).

References: [1] Kanai, IEEE TUFFC 52 (11) 2005; [2] O Villemain et al., JACC: Cardiovascular Im, 2018 (in press, online pre-print available); [3] Strachinaru et al., UMB 43 (8) 2017.

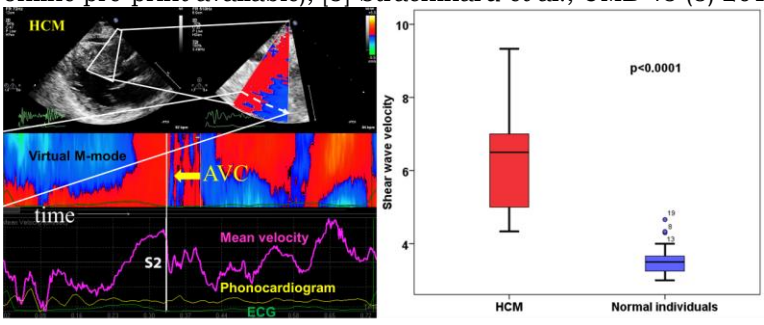

023 **PHYSICS OF WAVE PROPAGATION UNDERLYING SKIN TISSUE MOTION GENERATED BY THE PRESSURE PULSE IN THE CAROTID ARTERY.**

D Tommasin[1], A Caenen[1], B Verhegghe[1], P Segers[1].*
[1]Ghent University, Ghent, Belgium.

Background: Pulse wave velocity (PWV) is considered one of the most important clinical parameters for evaluating an individual's cardiovascular (CV) risk. Most commercial devices asses the regional PWV as the average PWV over a long CV segment. These devices are not always easy to use in clinical practice and largely ignore the most proximal and elastic section of the arterial tree. Due to an ever-increasing need and demand for novel and more efficient diagnostic tools to early detect CV diseases, innovative solutions have been explored in the direction of non-contact optical methods (e.g. Laser Doppler Vibrometry, LDV) [1]. LDV has been suggested as a potential technique to measure the local PWV of the common carotid artery (CCA) by measuring the transit time of the pulse wave between two locations along the CCA course from skin surface vibrations [2].

Aim: The objective is to numerically simulate the propagation of mechanical perturbations through soft tissues up to the skin level, in order to get a better understanding of the wave physics and explore the feasibility of non-contact optical methods for the PWV assessment.

Methods: Two CCA geometries were considered in the finite element software Abaqus: i) a straight tube (i.d. 6 mm, length 20 mm) and ii) a patient-specific CCA geometry including the bifurcation (i.d. ±6 mm, length 50 mm; see right panel of Fig 1). Models were bounded by cuboidal geometries (simulated skin surface is 10 mm above tube; 10-25 mm above carotid) representing soft tissues around the vessels. The spatial domain was discretized with hexahedral elements (C3D8R), and infinite elements (CIN3D8) were present at the lateral and bottom surface of the models to prevent wave reflection from these surfaces. A travelling pressure impulse (amplitude 40 mmHg; velocity 4 m/s), mimicking an actual arterial pulse, was imposed on the internal lumen inducing mechanical perturbations which radiate through the surrounding domain to the upper skin surface (see right panel of Fig 1). Two soft-tissue-mimicking material models were considered: i) polyvinyl alcohol (PVA, a linearly elastic material) and ii) chitosan hydrogel (hyperelastic material). The displacement perpendicular to the surface was calculated for nodes along the axis of the internal lumen and external skin surface of the models. Wave propagation velocities were subsequently derived using a time-of-flight method.

Results: Upper panels of Fig 1 show a propagation velocity of about 4 m/s for the primary wave front at the internal lumen of both geometries, agreeing with the loading conditions. This figure also depicts secondary and reflected wave fronts. On the external skin surface, the derived wave velocity of the main wave front was higher in the PVA than in the hydrogel material model: 10.8 vs. 6.6 m/s for the tube and 7.6 vs. 3.9 m/s for the carotid (see Fig 1). Additionally, the wave velocity at the external skin surface of the hydrogel carotid approached the velocity of the imposed pulse. In all cases, multiple and complex interacting wave patterns of compressional and shear waves can be observed.

Conclusions: Results show that the propagation of a short impulse inside an embedded artery leads to complex displacement patterns on the skin surface due to the interaction of different mechanical waves, leading to non-trivial relationships between PWV and skin surface vibrations.

Acknowledgements: EU Horizon 2020 programme (CARDIS, project 644798)

References: [1] Pereira T., et al., (2015) J. Med. Biol. Eng. (35) p 555–565.
[2] Li Y., et al., (2018) Optics Express (3), p 3638-3645.

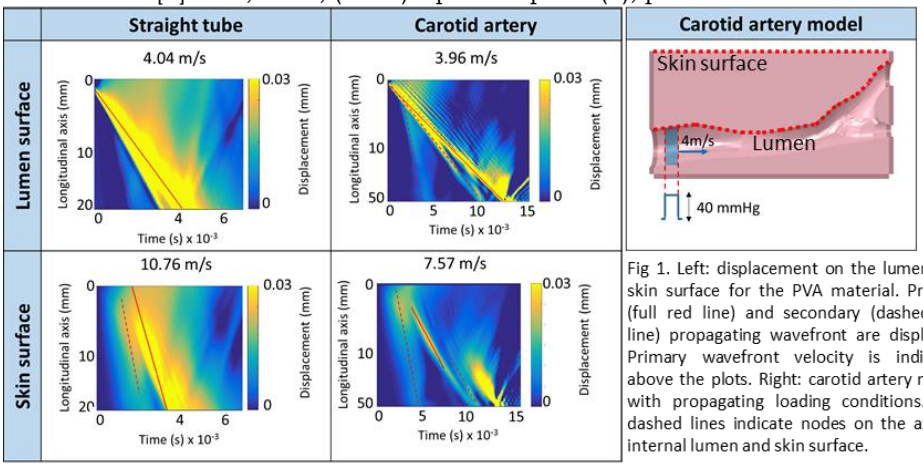

Fig 1. Left: displacement on the lumen and skin surface for the PVA material. Primary (full red line) and secondary (dashed red line) propagating wavefront are displayed. Primary wavefront velocity is indicated above the plots. Right: carotid artery model with propagating loading conditions. Red dashed lines indicate nodes on the axis of internal lumen and skin surface.

020 **VISUALIZING THE 2D MOTION INDUCED BY AN ACOUSTIC RADIATION FORCE PUSH IN CIRCULAR VESSEL PHANTOM CROSS-SECTIONS USING MULTI-ANGLE DISPLACEMENT COMPOUNDING ON A HIGH FREQUENCY CMUT ULTRASOUND PROBE.**

Hendrik HG Hansen[1], Stein Fekkes[1], Gijs AGM Hendriks[1], Chris L de Korte[1,2]*

[1]Medical UltraSound Imaging Center (MUSIC), Department of Radiology and Nuclear Medicine, Radboud university medical center, Nijmegen, THE NETHERLANDS; [2]Physics of Fluids, Faculty of Science and Technology, University of Twente, Enschede, THE NETHERLANDS.

Background: Atherosclerotic carotid artery plaque rupture is considered to initiate 20% of all strokes and transient ischemic attacks. Currently no patient-friendly imaging technique is available clinically to differentiate between lipid-rich rupture prone plaques and stable fibrous plaques. We are developing a noninvasive shear-wave ultrasound elastography technique to identify lipid-rich rupture prone plaques based on their distinct mechanical properties. Because lipid cores can be present anywhere along the circumference, the technique focusses on imaging in the transverse plane. Tracking waves induced by an acoustic radiation force impulse (ARFI) in this plane is not trivial, because the wave travels circumferentially resulting in tissue motion both in the axial and lateral direction.

Aims: This study investigates if the minute 2D motion field induced by ARFI in the circular carotid-artery-like geometry can be accurately estimated by triangulation of axial displacements (angular/displacement compounding [1,2]) derived from ultrasound data acquired with a beam-steered high frequency CMUT probe. It is also investigated what the optimal angle range should be for optimal displacement estimation accuracy and if this is possible when using only two beam-steering angles.

Methods: A Verasonics V1 equipped with an L7-4 probe (f_c = 5 MHz) was used to generate an acoustic radiation force push (200 µs, F# = 1) in the top wall of vessel-mimicking polyvinyl alcohol phantoms. The push was followed either by non-steered plane-wave acquisitions (n = 100, PRF = 10 kHz) on the L7-4 probe, or by steered plane-wave acquisitions (-20° to 20°, increment of 5°, n = 100, PRF = 10 kHz) with a high frequency L22-8v CMUT transducer (f_c = 14 MHz) connected to a Verasonics Vantage 256 system that was placed in the same plane but perpendicular to the L7-4. For each angle, axial displacements were estimated based on the phase shift in the IQ data. Least-squares displacement compounding of these angular axial displacements provided estimates of the horizontal and vertical displacement components [2]. The 0° axial L22-8v and the 0° axial L7-4 displacement estimates served as reference for the horizontal and vertical displacements, respectively. The procedure was repeated for multiple symmetric angle combinations to determine 1) the optimal angle range and 2) if steering at only two angles provided sufficiently accurate 2D motion estimates.

Results: The figure shows the estimated vertical and horizontal displacements obtained by two-angle compounding for all angle combinations next to the reference displacements. As can be observed, both displacement components can be individually obtained. The compound vertical estimates improved with increasing steering angle, whereas there seemed no dependence on angle range for the horizontal displacements. Horizontal displacements were accurate for all angle combinations.

Conclusions: The minute 2D motion induced by ARFI in a circular geometry resembling a carotid artery can be estimated from high-frequency ultrasound acquisitions obtained at two large (~20°) opposite beam-steering angles. Since the effective frame rate is reduced by a factor of two only, this approach is also expected to be feasible for clinical application. The ability to assess 2D motion will aid in understanding wave propagation in vessels and might be essential to quantify elasticity in *in vivo* arteries.

Acknowledgements: This work is part of the research programme [VICI] with project number [NKG 12122] which is (partly) financed by the Netherlands Organisation for Scientific Research (NWO).

References: [1] HHG Hansen et al., Journal of Biomechanics, 47(4), 815-23, 2014. [2] Techavipoo et al., IEEE Transactions on Medical Imaging, 23(12), 1479-89, 2004.

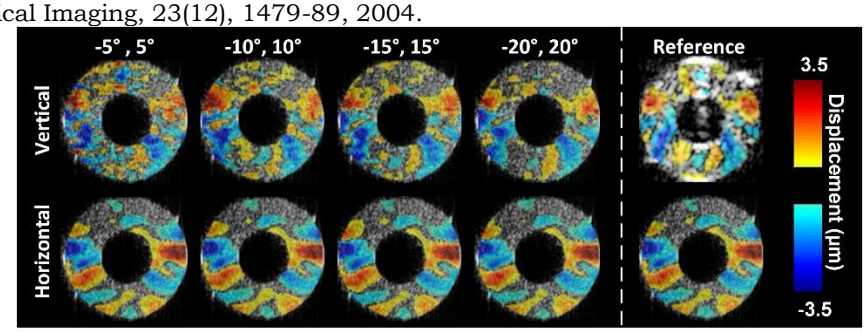

047 **A COMPARISON STUDY OF MAPPING STIFFNESS DISTRIBUTION OF PARTIALLY STIFFENED PORCINE AORTA: VASCULAR GUIDED WAVE IMAGING VERSUS PULSE WAVE IMAGING.**

Dan Ran[1], Yahua Wang[1], Wei-Ning Lee[1].*
[1]The University of Hong Kong, Pokfulam Road, Hong Kong, CHINA.

Background: Vascular guided wave imaging (VGWI) uses the guided wave induced by externally applied acoustic radiation force to estimate the vessel stiffness in the longitudinal and circumferential directions [1]; pulse wave imaging (PWI) [2] utilizes the intrinsic pulse wave generated by blood flow to estimate the average transverse stiffness within a section of the vessel wall. How sensitive and complementary the two methods are to identify the mechanical border zone between the normal and abnormal parts of the artery remains unclear.

Aims: This work aims to develop an imaging framework combining VGWI and PWI to yield the bi-directional stiffness distribution in the border zone of partially stiffened porcine aorta in an *in vitro* setting.

Methods: One excised porcine aorta (length: 130mm; average inner diameter: 12.3mm; average thickness: 1.6mm) was half immersed in formalin solution for 20 minutes to mimic atherosclerosis evolution, after which it was cyclically pressurized by an AccuFlow-Q flow pump (Shelley Medical Imaging Technologies, London, ON, Canada) with carotid flow at a rate of 15 mL/s. A Verasonics Vantage system (Verasonics, Kirkland, WA, USA) with an L7-4 probe (5.2MHz) was used to acquire VGWI and PWI data at 8000 Hz and 2100 Hz, respectively. VGWI was first performed in the longitudinal view of the hardened segment, border zone and normal region of the aorta. Piecewise group velocity of the guided wave (p-Vg) was estimated to differentiate the corresponding stiffness distribution among the three regions; PWI was then performed in the border zone. Pulse wave velocity (PWV) was estimated by linearly fitting the 50% upstroke of the pulse waveform over 10 cardiac cycles with a correlation coefficient threshold of 0.85 to derive circumferential Young's modulus (E_{T_PWI}) via a modified Moens-Korteweg equation [2]. Piecewise PWV (p-PWV) [3] was estimated with a kernel size of 19.1 mm and an overlap of 50% before it was used to compare with the p-Vg; finally, VGWI was performed in the transverse view of the aorta at two positions located at both ends of the border zone, with 12 imaging events within one cardiac cycle (1s). Dispersion analysis using a modified zero-order antisymmetric Lamb wave model was performed to derive circumferential shear modulus (μ_{T_VGWI}) [1] to compare with E_{T_PWI}.

Results: p-Vg was found to be constant in both hardened segment and normal region while showing a gradual decrease in the border zone. This indicates that p-Vg was able to identify the stiffness distribution difference among the three regions as well as the gradual stiffness change in the longitudinal direction of the border zone; p-Vg and p-PWV matched well in the border zone, where p-Vg showed a smaller variance; μ_{T_VGWI} varied with intraluminal pressure, and the maximum of $3*\mu_{T\_VGWI}$ agreed with E_{T_PWI} on the soft side of the border zone, whereas $3*\mu_{T\_VGWI}$ estimates were found smaller than E_{T_PWI} on the hard side.

Conclusions: p-Vg could depict the stiffness distribution in the longitudinal direction, and it was sensitive enough to be a supplementary index to p-PWV to identify the border zone in the artery; E_{T_PWI} combined with μ_{T_VGWI} could first reveal the circumferential stiffness distribution, then localize the regional stiffening and further assess the circumferential stiffness at the specific position in the border zone. Overall, our proposed framework was demonstrated feasible to map the stiffness distribution in bi-directions of partially stiffened porcine aorta. The statistical significance of the difference between E_{T_PWI} and $3*\mu_{T\_VGWI}$ is being studied.

Acknowledgements: This study was supported by National Natural Science Foundation of China (NSFC)/Research Grants Council (RGC) Joint Research Scheme (N_HKU713_15) and the University Development Fund.

References:

[1] Y. Guo et al., Ultrasound in medicine & biology, vol. 44, no. 4, pp. 884-896, 2018.
[2] K. Fujikura et al., Ultrasonic Imaging, vol. 35, no. 1, pp. 13-28, 2016.
[3] I. Z. Apostolakis et al., IEEE transactions on medical imaging, vol. 31, no. 3, pp. 554-562, 2012.

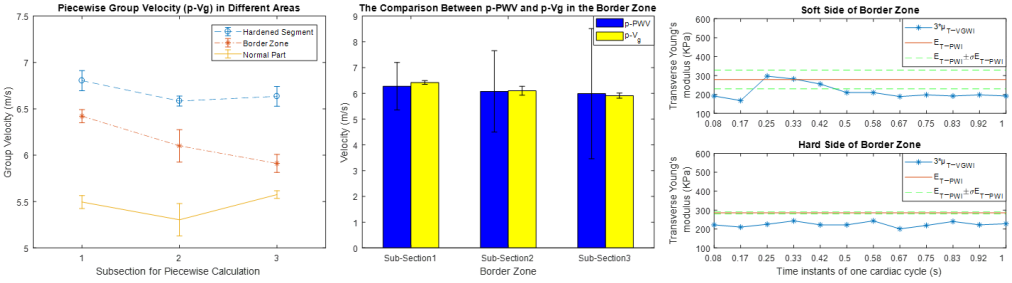

Figure 1 (Left) The piecewise group velocity (p-Vg) estimated in the hardened segment (blue), border zone (brown), and normal region (yellow) of the porcine aorta; (Middle) The comparison between piecewise pulse wave velocity (p-PWV) and piecewise group velocity (p-Vg) in the border zone of the porcine aorta; (Right) The circumferential Young's modulus estimated from PWI (E_{T_PWI}) and the temporal evolution of three times of circumferential shear moduli estimated by VGWI in the transverse plane in one cardiac cycle on the soft side (up) and the hard side (down) of the border zone. Please note that there is only one PWV value within one cardiac cycle.

033 **ULTRASOUND AND MAGNETIC-RESONANCE HARMONIC ELASTOGRAPHY WITH HYBRID INVERSE-PROBLEM FORMULATION OF FEM VISCOELASTICITY RECONSTRUCTION.**

Corin F. Otesteanu[1], Valery V. Vischnevskiy[1,2], Christian Guenthner[2], Sebastian Kozerke[2], Orcun Goksel[1]

[1]Computer-assisted Applications in Medicine (CAiM), ETH Zurich, 8092 Zurich, SWITZERLAND;
[2]Instituite for Biomedical Engineering (IBT), ETH Zurich, 8092 Zurich, SWITZERLAND.

Background: Tracked displacements during harmonic excitations can be used for reconstructing tissue viscoelastic parameters using the inverse problem (IP) formulation of the finite element method (FEM). Different IP formulations have been used in the literature [1,2] that reconstruct elasticity in a *direct* and *iterative* approach, respectively, minimizing errors in the original observation (data/displacement) and projected (e.g. force) domains. The former method may fail to generate quantitative values for lower frequency excitations while the latter is time consuming, with global convergence problems.

Aims: A hybrid method is proposed combining both approaches in one formulation to reconstruct elasticity.

Methods: We propose a novel IP formulation and viscoelasticity reconstruction method, in which both the viscoelastic parameters and the model displacements are estimated as independent parameters of an unconstrained optimization problem [3]. Total variation regularization of spatial elasticity distribution is introduced in this formulation, providing robustness to noise. We conducted numerical simulation studies, ultrasound elastography (USE) and magnetic resonance elastography (MRE) experiments.

Results: We compared the proposed method to the state of the art direct reconstruction method that uses a mixed displacement-pressure formulation. Numerical simulations were conducted on a synthetic phantom with three circular inclusions of 8, 2, and 12 kPa, in a 4 kPa background, see Fig. (a). Results show that our methods lead to an improvement of 35% RMSE and an increase in CNR of 5 dB. USE measurements were conducted on an ex-vivo bovine liver sample where a stiff inclusion was obtained by ablation. The inclusion was manually segmented in the B-mode image from Fig. (b), and reconstruction results show that with the proposed method the inclusion is well delineated and surrounding artifacts are reduced. Our method was also applied to MRE data of a CIRS phantom with a stiff circular inclusion. Results show an improvement of 4 dB in CNR of the inclusion Young's modulus (19.2 dB vs.15.4 dB) and that artifacts in the viscosity map are reduced.

Conclusions: We presented a novel FEM problem formulation that improves reconstruction accuracy and inclusion delineation compared to current IP techniques in USE and MRE.

Acknowledgements: This work was supported by the Swiss National Science Foundation.

References: [1] Honarvar, M., et al., A comparison of direct and iterative finite element inversion techniques in dynamic elastography. Phys Med Biol 61(8), 2016. [2] Fovargue, D., et al., Robust MR elastography stiffness quantification using a localized divergence free finite element reconstruction. Med. Imag. An. 44 (2018). [3] Otesteanu C.F., et al., FEM-based elasticity reconstruction using ultrasound for imaging tissue ablation. IJCARS, 2018.

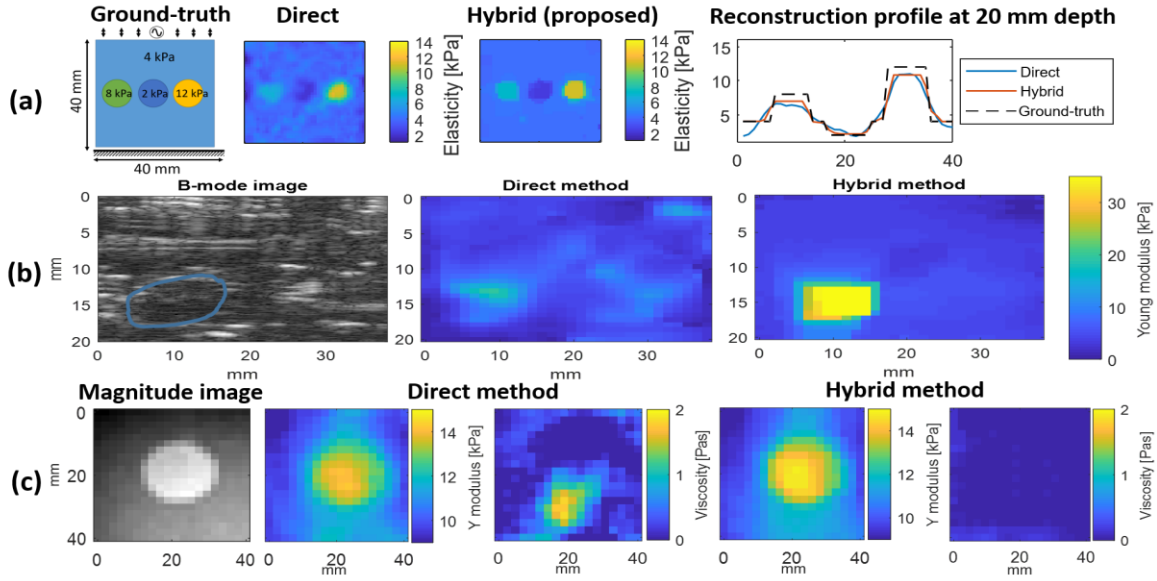

015 **NEW PHASE MATCHING METHOD THAT DIRECTLY WORK ON PHASE.**

Chikayoshi Sumi[1].*
[1]Sophia University, 4-7, Yonban-cho, Chiyoda-ku, Tokyo, JAPAN.

Summary: To allow optimizations to be performed, such as a regularized [1] or maximum *a posteriori* (MAP) estimation for ultrasonic human tissue Doppler equations directly expressed for a target displacement, the author's previously developed RF-echo phase matching method is modified. Instead of coarse and residual displacement estimates successively obtained with the multidimensional cross-correlation and autocorrelation methods, an addition is performed for the phase differences corresponding to the coarse and residual estimates. The method's feasibility and equivalence to previous methods is verified by lateral compression of an agar phantom having a high shear modulus inclusion.

Background: For elasticity measurements, the phase matching method [2,3] using the multidimensional cross-correlation method (MCCM) performs well. The contribution of the method to the ultrasonic tissue elasticity measurement field was the facilitation of *in vivo* tissue strain measurement [4]. To increase the measurement accuracy, such an optimized estimation should be performed for a lateral modulation (LM) or over-determined (OD) system obtained by generating multiple waves (MW) and/or performing spectral frequency divisions (SFD) [5,6]. However, when a target displacement distribution has components with a large variation over time and space, which is usual for deformable motion, the residual phase difference between a pair of local RF-echo signals that have been tentatively phase-matched by a coarse estimate becomes spatially discontinuous. Thus, the original phase matching method leads to erroneous estimates of the residual and target displacement distributions, if trying to perform spatially stationary statistical processing for the raw discontinuous phase data.

Aims: By performing a new phase matching method, optimizations such as regularization and MAP are enabled. Feasibility is verified through agar phantom experiments.

Methods: The new phase matching method described in the summary was applied to the 2-dimensional (2D) autocorrelation (AC) [6] and cross-spectral phase gradient (CSPG) [2,3] methods. An agar phantom having an inclusion with a high agar concentration [7] that produced a shear modulus contrast of 3.3 was compressed in the lateral direction. Displacement vector measurements including the MAP estimations were made for several lateral modulation (LM) and OD systems generated by MW or SFD.

Results: Example displacement vector measurements, for a LM system generated by $\pm 20°$ steered beams, are shown in Fig. 1, along with strain tensor measurements and shear modulus r~~econs~~tructions. Also shown are the means and standard deviations (SDs) estimated in the inclusion. The AC method provided almost the same results as those obtained by the original phase matching method [7]. The optimization substantially increased the measurement accuracy and stability for the OD systems (not shown).

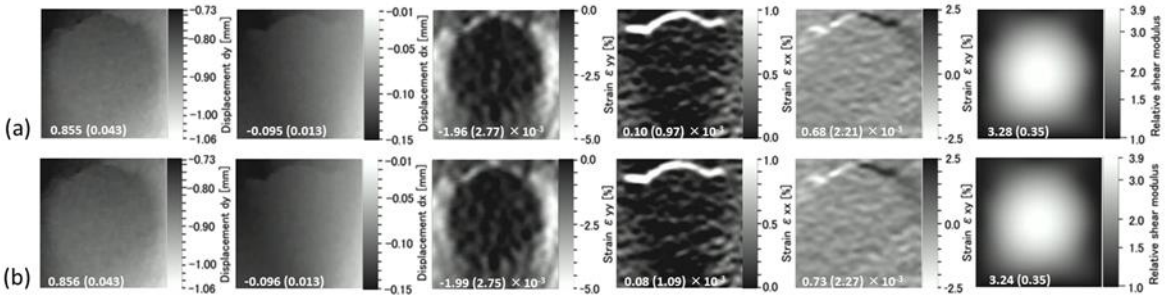

Figure 1. Measurement results obtained for lateral modulation elastography: (a) AC and (b) CSPG methods.

Conclusions: The new phase matching method worked and allowed MAP estimations on OD systems.

References: [1] IEEE Trans on UFFC **55**, 787 (2008). [2] IEEE Trans on UFFC **46**, 158 (1999). [3] IEICE Trans on Fundamental **E78-A**, 1655 (1995). [4] Jpn J Med Ultrason **22** (suppl), p. 44 (ID: 65-12) (May 1995) [in Japanese]. [5] Proc of IEEE Eng Med Biol Conf (EMBC), 2859 (Aug 2016). [6] IEEE Trans on UFFC **55**, 24 (2008). [7] IEEE Trans on UFFC **55**, 2607 (2008).

018 **A HANDHELD OPTICAL COHERENCE ELASTOGRAPHY PROBE FOR IMAGING BREAST CANCER.**

Brendan F Kennedy[1,2], James Anstie[1,2], Qi Fang[1,2], Lixin Chin[1,2], Brooke Krajancich[1,2], Luke Frewer[1,2], Philip Wijesinghe[1,2], Renate Zilkens[1,3], Synn Lynn Chin[4], Ben Dessauvagie[5,6], Bruce Latham[5], Christobel Saunders[7,8]*

[1]BRITElab, Harry Perkins Institute of Medical Research, QEII Medical Centre, Nedlands and Centre for Medical Research, The University of Western Australia, Perth, Western Australia, 6009, AUSTRALIA; [2]Department of Electrical, Electronic & Computer Engineering, School of Engineering, The University of Western Australia, 35 Stirling Highway, Perth, Western Australia, 6009, AUSTRALIA; [3]School of Surgery, The University of Western Australia, 35 Stirling Highway, Perth, Western Australia, 6009, AUSTRALIA; [4]Breast Centre, Sir Charles Gairdner Hospital, Hospital Avenue, Nedlands, Western Australia, 6009, AUSTRALIA; [5]PathWest, Fiona Stanley Hospital, 11 Robin Warren Drive, Murdoch, Western Australia, 6150, AUSTRALIA; [6]School of Pathology and Laboratory Medicine, The University of Western Australia, 35 Stirling Highway, Perth, Western Australia, 6009, AUSTRALIA; [7]Breast Centre, Fiona Stanley Hospital, 11 Robin Warren Drive, Murdoch, Western Australia, 6150, AUSTRALIA; [8]Breast Clinic, Royal Perth Hospital, 197 Wellington Street, Perth, Western Australia, 6000, AUSTRALIA.

Background: Optical coherence elastography (OCE) [1] provides elastograms with a higher spatial resolution (15-100 μm) than ultrasound elastography, albeit to an imaging depth limited to ~1 mm in dense tissue. OCE is based on the underlying imaging modality optical coherence tomography (OCT) [1]. This technique holds promise for a number of clinical and biological applications. Here, we describe our work in developing OCE for intraoperative use by surgeons to detect tumor otherwise missed using existing approaches.

Aims: Our aim is to develop a handheld imaging probe suitable for use both on excised specimens and in the breast cavity following tumor resection. Ultimately, we aim to provide surgeons with a high resolution elastography probe to more accurately resect tumor, reducing the number of patients (currently 20-30%) requiring additional surgery. Currently, there are no tools available that can provide this capability.

Methods: We have developed a compression OCE system, based on a Thorlabs OCT imaging system. Our system generates quantitative elasticity volumes (6×6×1 mm) in 1.7 s. We describe the methods and algorithms used to generate elastograms from raw OCT data. This methodology extends on our previous work [2]. We describe the phase-sensitive detection method we have developed to measure displacements as low as 2 nm in tissue. The resolution of our OCT system is 5.5 μm in the axial direction and 15 μm in the lateral directions. We estimate axial strain over 100 μm using a weighted least-squares approach. We describe our custom-build handheld imaging probe and describe novel algorithms we have developed to account for user motion that would otherwise corrupt both the spatial resolution and the mechanical load applied. In particular, we describe an algorithm we have developed that accounts for motion artefacts in the *en face* plane by co-registering OCT cross-sectional images with digital photographs simultaneously acquired with our probe.

Results: We present new and unpublished results acquired with our probe on both phantoms and freshly excised human breast tissue. Breast results are co-registered with gold-standard, post-operative histology to provide a validation of our results. For each case, we present OCT, strain and elasticity images and describe the complementary contrast provided by each image.

Conclusions: We present the first handheld OCE probe custom-designed for imaging both excised breast tissue and the tumor cavity. We describe the optical and mechanical design, the methods used to generate images and the image and signal processing algorithms we have developed. We use this probe to present OCE images of breast tissue, validated by gold-standard histology.

Acknowledgements: We acknowledge funding received from OncoRes Medical, the Australian Research Council and the Cancer Council, Western Australia.

References:

[1] Kennedy BF et al, "The emergence of optical elastography in biomedicine", Nature Photonics, v.11, pp.215-221, 2017. [2] Kennedy KM et al, "Quantitative micro-elastography: imaging tissue elasticity using compression optical coherence elastography", Scientific Reports, v.5, pp.15538, 2015.

026 **MONITORING ATRIAL FLUTTER ABLATION WITH INTRACARDIAC STRAIN IMAGING IN THE CLINIC.**

Vincent Sayseng[1], Chris S. Grubb[2], Hasan Garan[2], Elaine Wan[2], Elisa Konofagou[1]*
[1]Columbia University, PS 19-405, 6330 West 168th Street, New York, NY, 10032, USA;
[2]Columbia University Medical Center, 161 Fort Washington Avenue, Suite 648, New York, NY, 10032, USA.

Background: Atrial flutter is a heart rhythm disorder. Catheter radiofrequency (RF) ablation treats flutter by blocking the electrical pathways that initiate or maintain the arrhythmia, typically located in the cavotricuspid isthmus (CTI). However, gaps between lesions or non-transmural lesion formation may lead to treatment failure. Intracardiac Myocardial Elastography (IME) is an intracardiac echocardiography (ICE)-based strain imaging technique. Ablation lesions exhibit reduced strain compared to unablated tissue. IME can thus be used to track the progression of lesion formation in ablation procedures. Having previously shown that IME is capable of identifying lesion formation in human patients [1] with sufficient resolution to identify gaps or non-transmurality [2], IME was used to monitor ablation of the CTI in human patients in the treatment of flutter.

Aims: We demonstrate that it is possible to visualize and confirm cavotricuspid isthmus (CTI) block in patients undergoing atrial flutter ablation.

Methods: Five (n = 5) flutter patients (80.±4.9 y/o, 40% male) undergoing RF ablation of the CTI were imaged with an ICE ultrasound system transmitting a custom 600 Hz diverging wave sequence throughout the procedure (Viewmate Z, St. Jude Medical, MN, USA). The ICE ultrasound field-of-view was set to the CTI region proximal to the tricuspid valve. Cumulative displacements were estimated throughout atrial diastole via a normalized cross-correlation kernel. Axial cumulative strain was estimated using a least-squares estimator. Successful ablation (i.e. achievement of block) was confirmed via coronary sinus (CS) pacing.

Results: IME effectively tracked ablation of the CTI from start to completion. At baseline, IME observed high-magnitude (>15%) strain over atrial diastole (Fig 1a). Lesion formation was observed as regions of low-magnitude (<5%) strain; low-strain areas were visible at the tip of the catheter following ablation (Fig 2b, catheter outlined in green). Strain in the CTI was uniformly low once block was achieved and confirmed with CS pacing (Fig 2c). Among the five subjects, cumulative end-systolic strain in the CTI during atrial diastole was reduced by 29% ± 2.6% after block was achieved compared to baseline.

Conclusion: IME is a viable lesion monitoring technology for CTI ablation in humans and can accurately visualize the conduction block. Additional patients are currently being recruited for this study; potential application to other types of arrythmia, such as atrial fibrillation, are presently being explored.

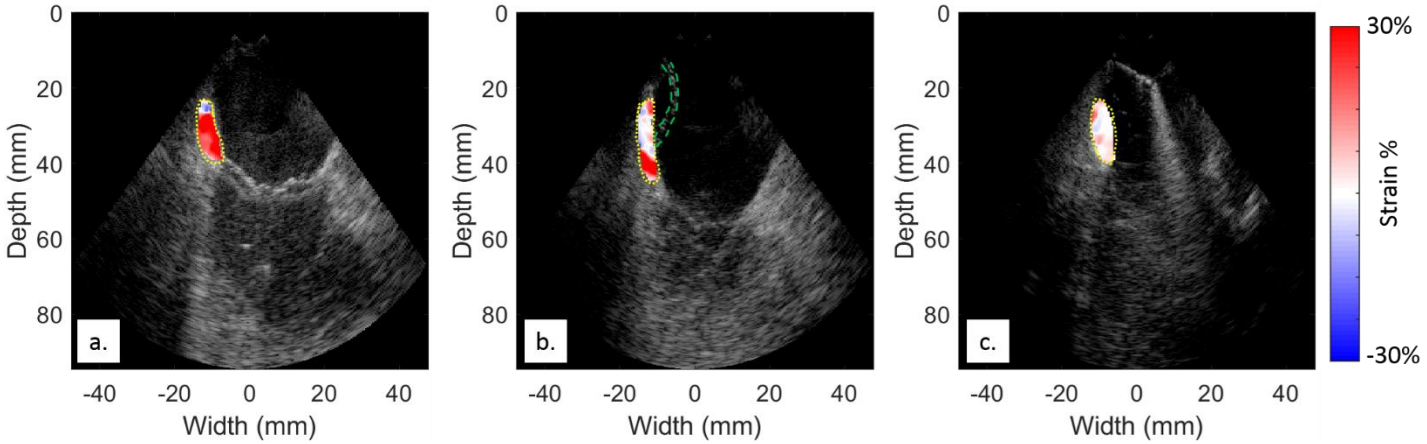

Fig 1. Monitoring ablation of the CTI region (outlined in yellow) at baseline (a), after two lesions (b), and after block was confirmed by CS pacing (c) in a human patient receiving treatment for atrial flutter. The catheter is outlined in green.

Acknowledgements: Supported in part by NIH R01 EB006042 and R01 HL140646-01, and the Wallace H. Coulter Foundation.
References: [1] Grondin et al, TUFFC Feb 2015; [2] Bunting et al, TUFFC Jan 2018

027 **CARDIAC RESYNCHRONIZATION THERAPY QUANTIFICATION AND DIRECT ASSESSMENT OF PATIENT RESPONSE WITH 3D-RENDERED ELECTROMECHANICAL WAVE IMAGING.**

Lea Melki[1], Christopher Grubb[2], Hasan Garan[2], Elaine Wan[2], Elisa Konofagou[1].*

[1]Columbia University, PS 19-405, 6330 West 168th Street, New York, NY, 10032, USA; [2]Columbia University Medical Center, 161 Fort Washington Avenue, Suite 648, New York, NY, 10032, USA.

Background: Cardiac Resynchronization Therapy (CRT) is an established treatment for Heart Failure (HF) patients with Left Bundle Branch Block and a Left Ventricular Ejection Fraction (LVEF) below 35%. Yet, a third of patients do not respond despite a narrowed QRS complex on their post implant 12-lead ECG. Electromechanical Wave Imaging (EWI) is a high frame-rate ultrasound modality capable of non-invasively mapping the electromechanical activation in all cardiac chambers in vivo [1]. In previous studies, EWI was established capable of 1) differentiating CRT responders from non-responders on 2D apical 4-chamber views a few months after their implant [2]; and 2) characterizing the 3D electromechanical activation pattern within 24 hours of their device placement and distinguishing the different biventricular (BiV) CRT pacing conditions [3].

Aims: Evaluate the feasibility of 3D-rendered EWI to quantify the amount of myocardium resynchronized (%MR) on the day of the implantation, and determine if %MR is a useful metric to predict patients response at 3- or 6- month follow up.

Methods: A 2.5 MHz diverging wave pulse excited at 2000 Hz PRF (Verasonics Inc., Kirkland, WA, USA) obtained with a P4-2 phased array (ATL/Philips, Andover, MA, USA) was used to image 17 HF patients at a depth of 20 cm, immediately after their CRT implant in four transthoracic apical echocardiographic views. The mean age was 73.6 ± 12.6 years and 88% were male. Axial displacements and strains were computed with 1D RF cross-correlation with a window size of 6.2 mm and 90% overlap, followed by a 5-mm-kernel least-squares estimator. Electromechanical activation times were defined as the timing of the first sign change of the incremental axial strain after the QRS onset. 3D rendering of the isochrones was then generated by registering the multi-2D views around the LV longitudinal symmetry axis, and performing a linear interpolation on the 2D activation times around the circumference [4]. All processing steps were performed in Matlab (Mathworks Inc., Natick, MA, USA) and the resulting 3D-rendered volume was imported and visualized in Amira 5.3.3 (Visage Imaging, Chelmsford, MA, USA). %MR was computed without and with CRT, and was defined as the percent of LV myocardium activated within 120 ms of QRS onset. The QRS duration was assessed on the clinical 12-lead ECGs without and with CRT.

Results: There was a significant increase in %MR ($\overline{\%MR_{without}}$ 70.5±14.2% vs $\overline{\%MR_{CRT}}$ 93.4±9.6%, Wilcoxon signed-rank test p<.0001), and a significant reduction in QRS duration (167±23ms without vs 140±21ms with, p=.0004) (Fig.1). Univariate logistic regression showed that $\overline{\%MR_{CRT}}$ on implant day was predictive of hospitalizations (p=0.043) and trended towards prediction of NYHA class at follow up (p=0.057). Change in QRS duration was correlated (Spearman) with EF improvement (p=0.026), while $\overline{\%MR_{CRT}}$ was correlated with hospitalizations (p=0.045).

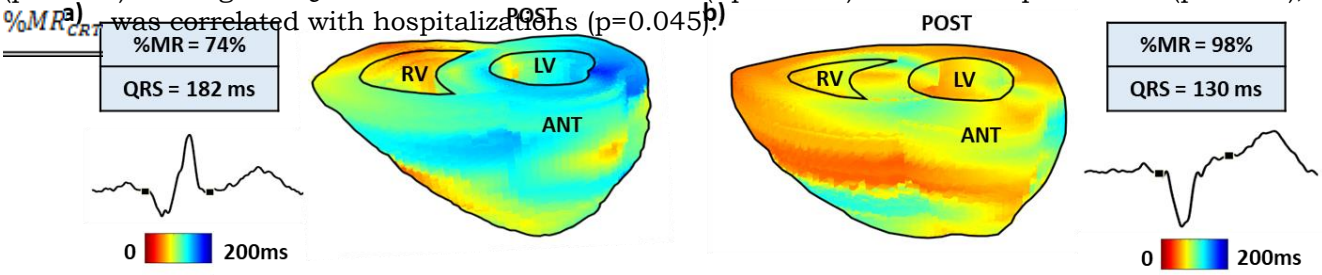

Fig.1: 3D-rendered EWI isochrones in anterior view for the same heart failure patient. a) Without CRT in his baseline: RV pacing only; b) With CRT in his optimized BiV pacing settings. Subject was a super-responder: LVEF improved from 20-25% to 40-45% at 3-month follow up and the patient endorsed an improvement in functional status. Red is the earliest activation, while blue is the latest. LV=left ventricle, RV=right ventricle, POST=posterior and ANT=anterior.

Conclusions: 3D-rendered EWI was shown capable of assessing immediate CRT response on the day of the implantation. These findings indicate that EWI could be a useful tool for CRT evaluation, complementary to the QRS duration, since it can both visualize and quantify myocardial activation, and thereby assess CRT response. In the future, we will evaluate EWI in a larger cohort, and determine if a personalized QRS threshold for %MR computation would increase clinical prediction accuracy.

Acknowledgements: Supported in part by NIH RO1 HL114358, RO1 HL140646-01 and RO1 EB006042.

References: [1] Provost et al, Proc. Natl. Acad. Sci. 2011. [2] Bunting et al, Pacing and Clinical Electrophysiology 2017. [3] Melki et al, IEEE International Ultrasonics Symposium, Washington DC, 2017. [4] Nauleau et al, Medical Physics 2017.

028 **ASSESSING TUMOR MECHANICAL PROPERTIES AND BLOOD PERFUSION WITH MRI AND CORRELATIONS WITH TUMOR PRESSURE AT DIFFERENT COMPRESSION LEVELS IN MICE.**

Gwenaël Pagé[1], Marion Tardieu[1], Laurent Bestret[2], Bernard E. Van-Beers[1,3], Philippe Garteiser[1]*
[1]INSERM U1149, Laboratory of Imaging Biomarkers, 75018, Paris, FRANCE; [2]SANOFI, 94400 Vitry-sur-Seine, FRANCE; [3]Department of Radiology, Beaujon University Hospital Paris Nord, 92110 Clichy, FRANCE.

Background: In tumors, high pressure facilitates tumor progression and hinders response to treatment [1]. Mechanical properties of tissues are influenced by their solid and liquid components [2], but the relative influence of solid and fluid stress in tumor pressure remains debated in malignant tumors [3,4].

Aims: To assess at MRI the change of mechanical properties and blood perfusion with increasing compression in xenografted tumors. The reference examination consisted in local pressure measurements with a miniaturized transducer.

Methods: MRI examinations were performed in 20 mice with subcutaneous tumors (patient derived hepatocellular carcinoma xenografts) implanted in the left flank. A 7T MRI scanner (Pharmascan, Bruker, Germany) with a volume resonator and a 20 mm diameter receiver coil was used. Mechanical vibrations were generated with a uniaxial acoustic shaker and transmitted to the tumor via a rigid carbon fiber rod linked to a 3D-printed plastic insert [5]. An inflatable balloon was placed on the tumor to apply a controlled mechanical stress. A sensor placed in the balloon chamber allowed to measure the exerted pressures. The sensor was connected to a pressure transducer (MPXV7007GP, NXP, Eindhoven, The Netherlands) interfaced to an Arduino system (Arduino.cc, 2015). MRE and MR FAIR perfusion acquisitions were performed at basal stress and at increasing stress levels. Mechanical vibrations were generated at 600 Hz and synchronized with a sinusoidal motion-encoded spin echo sequence. MRE acquisition parameters were: matrix = 87 x 67 x 9, resolution = 0.30 x 0.30 x 0.35 mm, TR/TE = 1007/18 ms and scan time of 4 min 30 s for each of three acquired spatial direction, including 4 times steps. Maps of the magnitude of the complex shear modulus (G*, kPa) were obtained by inversion of the Helmholtz wave equation [6]. MR FAIR perfusion parameters were: TR/TE = 12000/35 ms, slice selective thickness = 4.5 mm, resolution = 0.3 x 0.3 x 1.5 mm, inversion times = 30 + n × 250 ms (n = 1 … 21), acquisition time = 8 min 54 s. After MR acquisition, the total tumor pressure was measured at different strain levels using a catheter-mounted piezoelectric pressure transducer (SPR-1000 Mikro-Tip, Millar Instruments, Houston, TX, USA) in 16 mice.

Results: Figure 1 show a decrease of tumor perfusion at increasing stress (expressed as the applied balloon pressure). Both G* and tumor pressure increase and are correlated with the applied stress (Figs. 2 and 3). Finally, variations of G* in function of the applied stress were estimated as a linear slope. The resulting Figure 4 indicates a correlation between this parameter and tumor pressure in the absence of external compression.

Conclusions: This study shows that with an externally applied tumor stress, there is an increase of tumor mechanical properties and tumor pressure, and a decrease of perfusion component. This result suggests that intra-tumor pressure is generated predominantly by solid stress [7]. With a lack of correlation between tumor pressure and mechanical properties [8], our results suggest that the study of tumor mechanical properties under compression could be a good way to assess tumor pressure in-vivo.

References: [1] Jain R *et al.*, Ann. Rev of biomed Imag 16 (2014): 321-346 [2] Sinkus R *et al.*, Magn Res in Med, 58.6 (2007): 1135-1144. [3] Chauhan V P *et al,* Cancer Cell, 26.1 (2014): 14. [4] DelGiorno K E *et al.* Cancer Cell 26.1 (2014): 16. [5] Ronot M *et al.* Plos One 9.4 (2014): e94679. [6] Sinkus R *et al.,* Magn Res Imag 23.2 (2005): 159-165. [7] Dufort C C *et al.* Biophysical journal 110.9 (2016): 2106-2119. [8] Nia T *et al.*, Nat Biomed Imag 1.1 (2017): 0004.

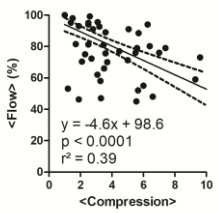

Figure 1. Evolution of normalized tumor perfusion relative to the pressure exerted by the ballon

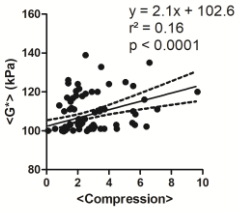

Figure 2. Evolution of normalized values of tumor G relative to the pressure exerted by the balloon*

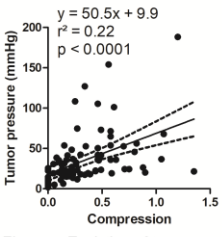

Figure 3. Evolution of tumor pressure relative to pressure exerted by the balloon

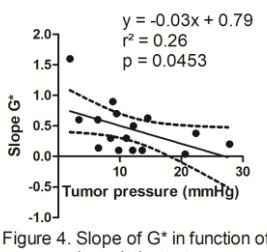

Figure 4. Slope of G* in function of the compression relative to tumor pressure

034 **MR ELASTOGRAPHY OF CHRONIC PANCREATITIS REVERSAL AFTER BARIATRIC SURGERY IN OBESE RATS AT MULTIPLE FREQUENCIES.**

Philippe Garteiser[1], Vinciane Rebours[1,2], Sabrina Doblas[1], Gwenaël Pagé[1], André Bado[1], Maude Le Gall[1], Valérie Paradis[1,2], Anne Couvelard[1,3], Bernard E Van Beers[1,2].*

[1]Inserm UMR1149 Center For Research on Inflammation and Paris Diderot University, 16 rue Henri Huchard, Paris, FRANCE; [2]Beaujon Hospital, AP-HP, 100 Bd. Du Général Leclerc, Clichy, FRANCE; [3]Bichat Hospital, AP-HP, 46 rue Henri Huchard, Paris, FRANCE.

Background: Obesity is a well-known risk factor for pancreatic diseases. In obese subjects, the pancreas contains fatty infiltration and fibrosis[1]. We have previously shown that multiparametric MRI of pancreas explants combining the assessment of mechanical properties, fat fraction and T2*, is useful in estimating the pancreatic histopathology in a rat model of obesity[2]. Bariatric surgery is one of the only treatments that can reverse diabetic symptoms[3] but its effects on pancreatic status are, however, not well known.

Aims: To determine the effect of bariatric surgery on several high frequency MR elastographic properties of pancreatic explants in a rat model of obesity.

Methods: Three groups were composed: obese rats fed with high fat diet (HFD, 6 months, n=9); rats fed with normal diet (ND, 6 months, n=6) and obese rats which underwent bariatric surgery at 3 months, followed by ND for 14 days (n=5). After MR imaging, the pancreas were analyzed with reference clinical histology techniques. MRE was performed with a 7T Bruker small animal system using a three-directional spin-echo sequence at 400Hz, 600Hz and 800Hz to accommodate the softness of pancreatic tissue[4], with 300µm isotropic resolution. Shear wave fields were obtained from phase images after unwrapping and compressional filtering by the curl operator. Viscoelastic parameters (storage modulus, G' and loss modulus, G'' at all three frequencies, and their frequency dispersion coefficient, γ) were obtained by algebraic inversion of the wave propagation equation. In addition, multiparametric MRI sequences were acquired.

Results: The storage modulus at 600Hz was significantly different between normal, obese and surgery groups (1.23[0.92-1.33]kPa, 1.71[1.27-2.06] kPa and 1.46[1.38-1.78] kPa, respectively, Kruskall-Wallis p=0.0037, figure 1). After surgery the storage modulus was not significantly different from controls. No differences in loss modulus were found between any of the groups. $\gamma_{G'}$ was significantly different between control, obese and surgical groups (1.53[1.34-1.97], 1.21[1.04-1.42] and 1.55[1.15-1.65], respectively, Kruskall-Wallis p=0.02, figure 2). After surgery, γ was not significantly different from the control group. Both G' at 600Hz and $\gamma_{G'}$ were significantly correlated to the number of fibrotic complexes (r=0.61, p=0.0059 and r=-0.52, p=0.0216, respectively, figure 3). Multiple regressions indicated that the number of endofibrotic complexes was the sole histologic factor associated to storage modulus at 600Hz.

Conclusions: Clinically accessible MR elastography results were used to assess the histological features of chronic pancreatitis in a rat model of obesity. The regression in histologic markers was accompanied with a reversion in the corresponding mechanical properties of the pancreas, demonstrating the validity of assessing the mechanical properties as surrogate for histologic results in our small animal model. This suggests that MR elastography may be used to assess not only pancreatic disease status but also to assess response to treatment after bariatric surgery.

References: 1.Rebours et al., Clinical Cancer Research 2015. 2.Garteiser et al., ISMRM procs 2016. 3.Mingrone et al., Lancet 2015. 4.Shi et al., JMRI 2015.

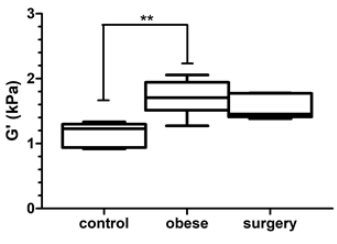

Fig. 1: Storage Modulus at 600Hz.

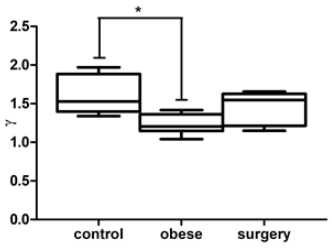

Fig. 2: Storage modulus frequency dispersion coefficient.

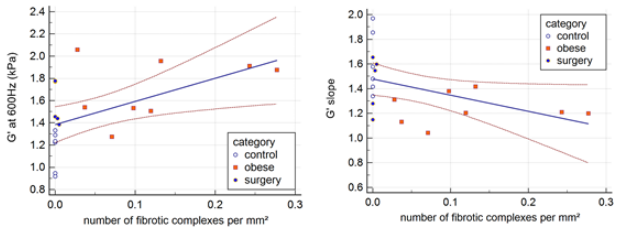

Fig. 3: Storage modulus (left) and storage modulus frequency dispersion coefficient (right) in correlation with histological markers in all groups.

036 **SHEAR WAVE VELOCITY DISPERSION ANALYSIS IN PLACENTA USING 2-D TRANSIENT ELASTOGRAPHY.**

E.G. Simon[1], J.P. Remenieras[1], M.C. Dumoux[2], F. Patat[3], F. Perrotin[1,2], S. Callé[4]*

[1]UMR 1253, iBrain, University of Tours, Inserm, Tours, FRANCE; [2]Vermon SA, Tours, FRANCE;

[3]CIC-IT, CIC 1415 Inserm, University Hospital Center of Tours, Tours, FRANCE;

[4]GREMAN UMR 7347, University of Tours, CNRS, INSA, Tours, FRANCE.

Background: In case of intra-uterine growth restriction (IUGR) or preeclampsia (PE), changes in placental tissue architecture could cause variations in elasticity. Among the ultrasound (US) elastography methods, transient elastography (TE) seems suitable for such an application.

Aims: We evaluated the interest of a frequency analysis for shear wave speed (SWS) in order to distinguish the elasticity of normal and abnormal placentas.

Methods: We developed a 2D TE system, based on the coupling of a shear wave generated by 2 vibrating rods and US images acquired at an ultrafast rate (Figure 1) [1]. Two electrodynamical exciters, decoupled from the US linear probe (128 elements centered at 2.8 MHz, Vermon), generated the vibration of the rods. Beamformed demodulated IQ data were acquired with an ultrafast US scanner (Aixplorer®, Supersonic imagine, Aix en Provence, France): acquisition at 2.8 MHz during 128ms with a PRF of 4 kHz. The particle velocity was computed using extended autocorrelation method [2]. Radiation pattern of the system is illustrated in Figure 2. Calculating the spatial FFTs of $Vz(z,\omega)$, the SWS dispersion curve was obtained between 20 Hz and 80 Hz. The experimental data obtained from TE were fitted with a fractional rheological model $G^*(i\omega)=Ge+K.[i\omega]^n$ [3]. The method has been applied *ex vivo* on 22 uncomplicated pregnancies, 9 IUGR, and 4 PE. Measurements (3 times with repositioning, 2 operators) have been performed on 2 regions, central and peripheral. Then, the experiment has been conducted *in vivo* on 2 pregnant women (normal pregnancies).

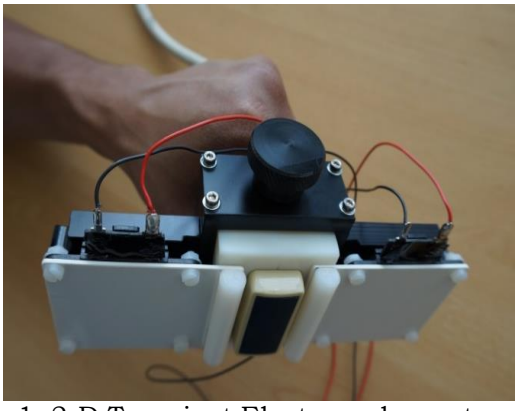

Fig 1. 2-D Transient Elastography system

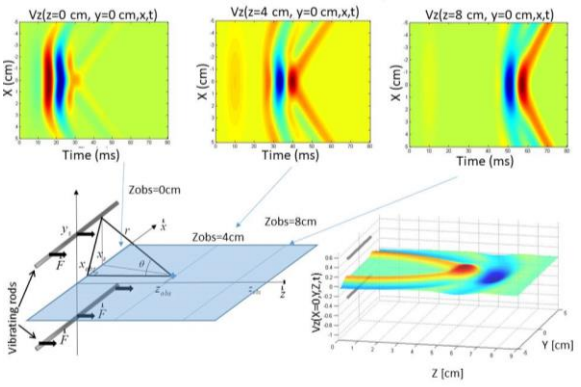

Fig 2. Radiation pattern of the system

Results: The mean SWS (at 50 Hz) was lower in case of IUGR (1.05 m/s +/-SD 0.05) than in control group (1.77 m/s +/-0.48, P<0.001) or in PE cases (1.20 m/s +/-0.22). The mean exponent n value of the model was lower in case of IUGR (1.01+/-0.24) compared to control group (1.27+/-0.11, P=0.006) or PE cases (1.18+/-0.36). We found no difference between central and peripheral regions. The optimal cutoff values of SWS and n for distinguishing normal and pathological situations were 1.37 m/s and 1.13 respectively, with AUC of 0,98 (IC 95% 0,94-1) and 0,75 (IC 95% 0,51-0,99) respectively. Intra and interobserver reproducibility was good for both SWS and n values. The *in vivo* experiments demonstrated feasibility of this method during pregnancy.

Conclusions: The frequency analysis could improve the ability of TE to distinguish normal and abnormal placentas.

References:

[1] Sandrin L, et al., Ultrason Imaging 21, pp 259- 272, 1999.
[2] Hoeks et al. UMB 20,pp.953-965, 1994.
[3] Nicolle S. et al., J. Biomechanics 43, pp 927-932, 2010.

024 **CLOT ELASTICITY IS INVERSELY CORRELATED WITH RT-PA THROMBOLYTIC SUSCEPTIBILITY IN VITRO.**

Karla P. Mercado-Shekhar[1*], Robert Kleven[1], Hermes Aponte Rivera[1], Ryden Lewis[1], Kunal B. Karani[1], Hendrik J. Vos[2], Todd A. Abruzzo[1], Kevin J. Haworth[1], Christy K. Holland[1].
[1]University of Cincinnati, College of Medicine, Cincinnati, Ohio, USA; [2]Erasmus Medical Center, Thorax Center, Rotterdam, THE NETHERLANDS.

Background: Recombinant tissue-plasminogen activator (rt-PA) is the only clinically approved thrombolytic to treat acute ischemic stroke in the United States [1]. An accepted alternative therapeutic approach is catheter-based mechanical thrombectomy. Predicting the efficacy of rt-PA treatment *a priori* could help guide the selection of treatment and avoid adverse effects from rt-PA. The composition and structure of clots was previously reported to affect elasticity and rt-PA lytic susceptibility [2, 3]. Therefore, clot elasticity could potentially serve as a predictive metric for rt-PA lytic susceptibility.

Aim: To elucidate the relationship between clot elasticity and rt-PA thrombolytic susceptibility *in vitro*.

Methods: Mildly and highly retracted human and porcine whole blood clots were fabricated in glass pipettes. The rt-PA thrombolytic efficacy was evaluated *in vitro* using the percent mass loss of clots (5 replicates per clot type) treated for 30 min with plasma and 3.15 μg/mL rt-PA [4]. A second set of clots (5 replicates per clot type) were embedded in agar phantoms prior to ultrasound elastography. The Young's modulus of each clot was estimated using single-track-location shear wave elasticity imaging, and assuming a linearly elastic and isotropic medium [5]. The imaging sequence was implemented using a Verasonics Vantage 256 scanner (Verasonics, Kirkland, WA, USA), equipped with an L7-4 linear array (5.2 MHz center frequency, Philips, Bothel, WA, USA).

Results: The percent mass loss of mildly retracted human and porcine clots (45.2±7.1% and 28.9±6.1%, respectively) were significantly higher ($p < 0.05$) than the percent mass loss of highly retracted human and porcine clots (25.5±10.0% and 10.9±2.1%, respectively). A representative composite B-mode and Young's modulus image of a highly retracted porcine clot embedded in an agar phantom (14.4±1.2 kPa) is shown in Figure 1(A). The Young's moduli of highly retracted human and porcine clots (3.2±2.0 kPa and 5.3±0.9 kPa, respectively) were significantly higher ($p < 0.05$) than those of mildly retracted human and porcine clots (0.79±0.21 kPa and 2.66±0.55 kPa, respectively). An inverse linear relationship (R^2=0.99, p=0.003) was observed between the percent clot mass loss and Young's modulus (Figure 1(B)).

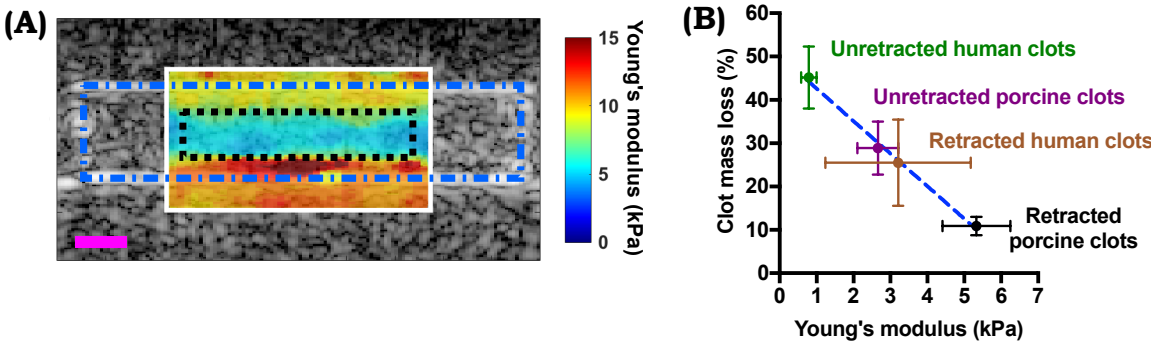

Figure 1. (A) A representative composite B-mode (gray scale, dynamic range 40 dB) and Young's modulus image of a clot. The blue dashed rectangle and black dotted rectangle represent the location of the clot and the region of interest within which the Young's modulus was estimated, respectively. Magenta scale bar = 2 mm. (B) The measured clot mass loss as a function of the Young's moduli of the different clot types (mean ± standard deviation). The blue dashed line represents a linear fit to the data.

Conclusions: This study demonstrated an inverse relationship between rt-PA thrombolytic susceptibility and clot elasticity. Highly retracted human and porcine clots were up to 4-fold and 2-fold stiffer than mildly retracted human and porcine clots, respectively. These findings represent the first step towards the development of clot elasticity as a metric for predicting the rt-PA lytic susceptibility of thromboemboli responsible for ischemic stroke.

Acknowledgements: This research was funded, in part, by the National Institute of Neurological Diseases and Disorders of the National Institutes of Health grant supplement R01 NS047603-11S1.

References: [1] Powers, W.J., et al. Stroke, 46:3020–3035, 2015. [2] Sutton, J.T., et al. Ultrasound Med Biol, 39:813–824, 2013. [3] Chueh, J.Y., et al. Am J Neuroradiol, 32:1237–1244, 2011. [4] Datta, S., et al., Ultrasound Med Biol, 34:1421-1433, 2008. [5] McAleavey et al. Ultrason Imaging, 31:217-234, 2009.

035 **A COMPARISON OF MECHANICAL PARAMETERS OF THE PORCINE LIVER OBTAINED WITH SWE IMAGING AND INDENTATION METHOD FOR MODELLING PURPOSES.**

Matylda Żmudzińska[1], Marcin Inglot[2], Ewelina Świątek-Najwer[1], Urszula Zaleska-Dorobisz[2], Celina Pezowicz[1].*

[1]Wroclaw University of Science and Technology, Faculty of Mechanics, Department of Biomedical Engineering, Mechatronics and Theory of Mechanism, Lukasiewicza Street 7/9, 50-371 Wroclaw, POLAND. [2]Wroclaw Medical University, Department of General and Pediatric Radiology, Sklodowskiej-Curie Street 68, 50-369 Wroclaw, POLAND.

Background: Insufficient information on mechanical properties of soft tissues in vivo is a serious limitation of a development of haptic laparoscopic simulations. It's been shown by Yiannakopoulou [1] that provided tactile feedback is an obstacle in surgeons training. Elastography, being a noninvasive method, gives an opportunity to obtain information on mechanical parameters in relevant conditions. However, it is necessary to compare elastographic data with classical mechanical tests, due to its limitations and assumptions in mathematical algorithms of signal processing.

Aims: The aim of this study was the comparison of mechanical parameters of porcine liver obtained with Shear Wave Elastography and with indentation test, for the assessment of application the SWE method in modelling for haptic laparoscopic simulations.

Methods: Research material consisted of 10 liver lobes, from 5 fresh porcine livers, with an assumption of equal mechanical properties of lobes [2]. First stage of experiment was a set of four SWE examinations on each lobe, with Aixplorer by SuperSonic Imagine, transducer SuperLinear™ SL10-2, ROI=15mm. A layer of ultrasound gel was kept between the sample and the transducer during the test. Subsequently, an indentation test was performed with MTS Synergie 100, spherical indenter, φ=10mm, depth of indentation 5mm. Each lobe was examined four times. Four different mathematical models (M1 - by Hayes (1972) and Zhang (1997), M2 – by Oliver and Pharr (1992), M3 – by Krouskop (1998), M4 – by Egorov (2008)) [3] were applied to calculate indentation Young's modulus (E).

Results: Obtained results are presented in table 1. Statistical analysis has shown significant differences ($p<0,05$) between SWE results and all indentation Young's moduli, as well as between $E_{M1} – E_{M2}$, $E_{M1} - E_{M4}$, $E_{M2} – E_{M3}$, and $E_{M3} – E_{M4}$.

Table 1. Mean Young's modulus (E) of SWE and mean indentation Young's moduli calculated with different models, where S - stands for indentation stiffness, a - for indenter radius, and k - for correction factor [2].

Method	SWE	E_{M1}	E_{M2}	E_{M3}	E_{M4}
Formula	-	$E = \frac{S}{2ak}$	$E = \frac{S}{2a}$	$E = \frac{S}{\pi\frac{a}{2}}$	$E = \frac{S}{\pi 2a}$
E ± SD [kPa]	10,8 ± 2,6	3,43 ± 1,1	2,4 ± 0,5	3,06 ± 0,8	2,29 ± 0,3

Conclusions: Presented results have shown that analyzed mathematical models don't correspond directly with Young's modulus obtained by SWE method. Despite this, it was observed that some of the moduli calculated with models M1-M4, correspond with each other. Furthermore, presented values are consistent with data from literature, e.g. obtained by Brunon et al. [4]. Shear Wave Elastography algorithms assume that soft tissues are linear elastic, whilst all of applied models, and majority of literature use different approaches. Viscoelastic, hyperelastic and a few other hypotheses are the most common among the authors [5]. To use the presented data for modelling purposes, further studies are needed. Firstly, for correlating values of liver mechanical parameters obtained with different methods, and secondly, for considering such variables as abdominal pressure or perfusion.

References:

[1] Yiannakoupoulou E., Nikiteas N., Perrea D., Tsigris C.. (2015). Virtual reality simulators and training in laparoscopic surgery. International Journal of Surgery. 13. 10.1016/j.ijsu.2014.11.014.

[2] Żmudzińska M., Inglot M., Świątek-Najwer E., Zaleska-Dorobisz U., Pezowicz C.. (2017). The assessment of Shear Wave Elastography (SWE) application in research of liver mechanical properties. 20-th PCBBE, Krakow. IX 2017.

[3] Delaine-Smith, R.M. & Burney, S & Balkwill, F.R. & Knight, M.M.. (2016). Experimental validation of a flat punch indentation methodology calibrated against unconfined compression tests for determination of soft tissue biomechanics. Journal of the Mechanical Behavior of Biomedical Materials. 60. 10.1016/j.jmbbm.2016.02.019.

[4] Brunon A., Bruyere-Garnier K., Coret M..Mechanical characterization of liver capsule through uniaxial quasi-static tensile tests until failure. Journal of Biomechanics. 43. 10.1016.biomech.2010.03.038.

[5] Mattei G., Ahluwalia A.. (2016) Sample, testing and analysis variables affecting liver mechanical

Please Fill Out Both Sides

Conference Evaluation and Questionnaire

OVERALL CONFERENCE

	Poor		Mid		Excellent
Overall Conference Evaluation	1	2	3	4	5
General comments:					

SCIENTIFIC PROGRAM

	Poor		Mid		Excellent
Quality of the Presentations	1	2	3	4	5
Relevance of Presentations to the Conference's Theme	1	2	3	4	5
Time Allotted for Presentations	1	2	3	4	5
Time Allotted for Discussion	1	2	3	4	5
Poster Session	1	2	3	4	5
Tutorials	1	2	3	4	5
Short presentation category	1	2	3	4	5
Student Participation	1	2	3	4	5
Equipment Exhibit	1	2	3	4	5
Additional comments/suggestions:					

CONFERENCE MATERIALS

	Poor		Mid		Excellent
Proceedings Book Online	1	2	3	4	5
Other Registration Materials	1	2	3	4	5
Additional comments/suggestions:					

CONFERENCE FACILITIES & SOCIAL PROGRAMME

	Poor		Mid		Excellent
Lecture Hall	1	2	3	4	5
Registration Desk	1	2	3	4	5
Meals: Dining facilities	1	2	3	4	5
Conference Breakfasts and Lunches	1	2	3	4	5
Conference Dinner and Entertainment	1	2	3	4	5
Coffee Breaks	1	2	3	4	5
Opening Dinner Reception	1	2	3	4	5
Closing Tapas Party	1	2	3	4	5
Audio–Visual: Screen Visibility	1	2	3	4	5
Sound Level	1	2	3	4	5
Presentation Transition	1	2	3	4	5
Internet Connectivity:	1	2	3	4	5
Additional comments:					

Please Fill Out Both Sides

Conference Evaluation and Questionnaire

VENUE AND HOTEL

	Poor		Mid		Excellent
Venue: Novotel Avignon & Environs	1	2	3	4	5
Would you return to this area?	Yes		Perhaps		No
Area Attractions	1	2	3	4	5
Hotel: Overall	1	2	3	4	5
Reservations	1	2	3	4	5
Transportation and Accessibility	1	2	3	4	5
Reception and Check–In	1	2	3	4	5
Accommodations	1	2	3	4	5
Facilities	1	2	3	4	5
Parking	1	2	3	4	5
Would you return to this hotel?	Yes		Perhaps		No
Would you like to Co-Host ITEC in the future	Yes		Perhaps		No
If yes, please state your organization name and city:					
Where would you like to see ITEC hosted?					
Additional comments:					

CONFERENCE ADMINISTRATION

	Poor		Mid		Excellent
Website	1	2	3	4	5
Registration off–site	1	2	3	4	5
Registration on–site	1	2	3	4	5
Administrative staff	1	2	3	4	5
Correspondence	1	2	3	4	5
Additional comments:					

GENERAL INFORMATION

I am a Returning Delegate	Yes		No
I plan to attend the next conference in 2019 in the USA.	Yes	Perhaps	No
and present a paper(s) / poster(s)	Yes	Perhaps	No
Other(s) from my lab would attend the next conference	Yes	Perhaps	No
and he/she / they would present a paper(s) / poster(s)	Yes	Perhaps	No
How did you learn of this conference? (Check all that apply)	☐ Email Announcement		
☐ Internet	☐ Website		
☐ Other	☐ Colleague		
Tutorial Topic Suggestions for next year:			
Additional Comments:			

If you would be willing to assist with hosting the Conference in your vicinity, please give your name to the Conference Staff.
Questions or comments are welcome at any time at secretariat@elasticityconference.org Thank you.